RMIT University

School of Aerospace, Mechanical & Manufacturing Engineering

Replication of Atmospheric Conditions for the Purpose of Testing MAVs

MAV Flight Environment Project: Final Report

Unclassified

23 December 2005

J. Milbank
B. Loxton
S. Watkins
W.H. Melbourne

USAF Project No: AOARD 05-4075
USAF Contract/Purchase Order/Agreement No: FA5209-05-P-0452

1 Acknowledgements

The authors would like to thank the United States Air Force for providing funding to complete the research covered in this report, Bacchus Marsh gliding club for the generous use of their airfield for calibration runs during on-road measurements, and the administrative and IT staff at RMIT University for their support during the project.

2 Executive Summary

This report details research performed to quantify and replicate typical flight environments for MAVs operating close to the ground. It is part of a larger program aimed to build understanding of MAV design and control that will enhance their operability in a wider range of atmospheric winds than currently possible.

The specific research goals of the work proposed here were to:

1. Provide detailed descriptions of the outdoor flight environment, including the spatial and temporal variations, experienced by MAVs (either natural or man-made) encompassing flight speeds from hovering to 10 m/s, under typical atmospheric winds
2. Determine the levels and characteristics of turbulence most relevant to MAV flight for flow simulations (which could be either CFD or EFD)
3. Reproduce typical outdoor turbulent flow environments in a wind tunnel, utilising the same probe systems and statistical parameters used to gather the outdoor data.

Measurements of atmospheric turbulence were taken using a program of on-road testing utilising four dynamically calibrated multi-hole pressure probes mounted on a mast above a test vehicle. This vehicle traversed through differing terrains and the data gathered were analysed to provide the spectral levels, turbulence intensities, length scales and pitch variation fluctuation that are relevant for typical flow environments of MAVs close to the ground. The data were analysed for both an MAV condition where its effective ground speed was 0 m/s (i.e. hovering) and the condition where its IAS was 10 m/s. These data characterise the MAV atmospheric turbulence environment for the given terrain and wind conditions, directly addressing research objectives 1 and 2, and will be valuable for future experimental and computational modelling of MAVs.

A second program of experimental testing was conducted within a large wind engineering wind tunnel in order to simulate the turbulence characteristics found during the on-road testing phase. The results showed that atmospheric turbulence characteristics for the aircraft roll inputs can be simulated within the wind tunnel for the entire relevant frequency range for 150 mm (6 inch) span MAVs, but that 1 m (40 inch) span MAVs might require additional active turbulence generation techniques. The latter would be required in order to adequately replicate the larger length scales that affect the roll inputs of the larger span MAVs. It was noted that such techniques exist and should prove effective to achieve this goal but it should also be noted that large test sections are needed to permit the turbulence generation and development. The successful replication of MAV-relevant turbulence characteristics within a wind tunnel directly addresses research objective 3.

The work to date has enabled the replication of typical unsteady flight environments in a wind tunnel for the first time. This controlled replication permits understanding and development of MAVs that offer enhanced utility in real world conditions and can be used in two main ways:

- Flight experiments of existing MAVs, in order to measure the sensitivity and controllability of man-made craft. The facility also permits study of bird and insect flight which will enable greater insights into how nature has evolved systems to permit flying in turbulent winds and;
- Measurements of flight loads and inputs from atmospheric turbulence that can be used to develop aircraft platforms to mitigate the effects of turbulence, and control systems to enable stable viewing platforms. We are currently developing a new MAV force balance to permit the direct measurements of dynamic loads on small craft.

Detailed conclusions and recommendations can be found at the end of this report regarding future avenues for extending the flight boundaries of MAVs in atmospheric winds.

3 Table of Contents

4 Background, Aims & Research Methods

4.1 Introduction

The natural world and the human constructed environment are significantly influenced by the atmospheric boundary layer (ABL). The mean (time-averaged) and turbulent effects of the atmospheric wind strongly affect the design of land-based structures and they also play a significant role in the design and operation of aircraft. In nature, the upper speed boundary of flight is set by a combination of the mean wind speed and gustiness inherent in the atmosphere. Atmospheric winds present a considerable challenge to insects and birds – with the speed at which they curtail flying set by their capability to negotiate a desired flight path and/or strength limitations on their wings. Under relatively low wind speeds the smaller flying insects remain grounded, and as the wind speed rises, increasingly larger insects, then birds, become grounded. This is despite having extremely sophisticated, interactive, control systems. A summary of flying speeds is reproduced from Tennekes (1996), and shown in Figure 1.

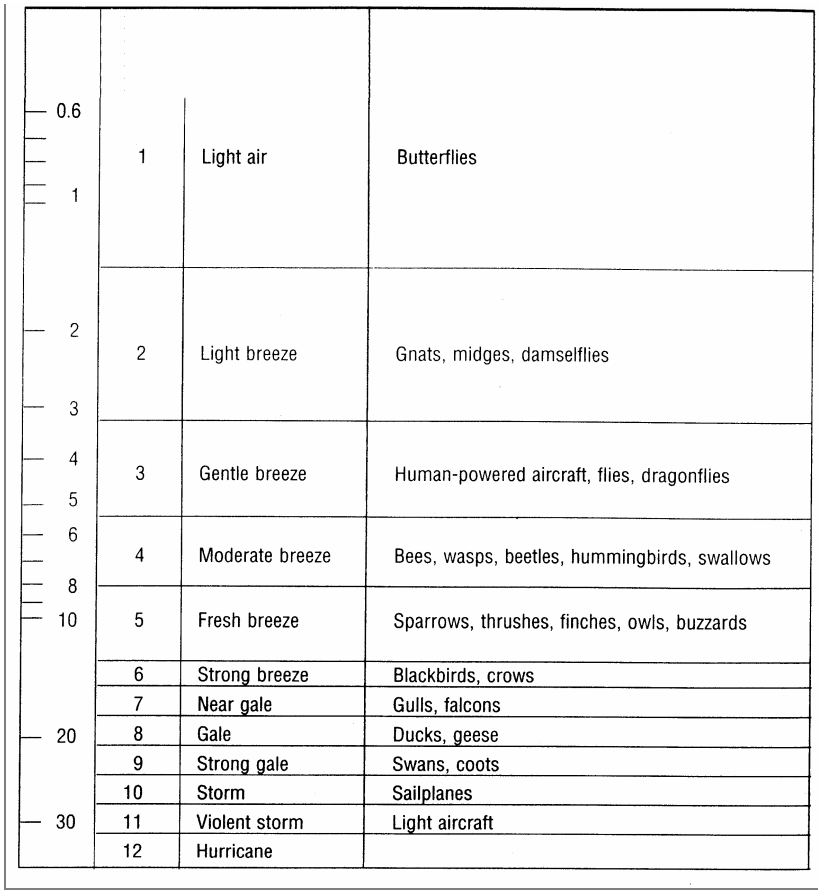

Figure 1: The flying speeds of insects, birds and aircraft (from Tennekes, 1996).

Military and the larger commercial aircraft can generally fly in all but the most extreme wind conditions (eg cyclonic), but as the size and mass of the aircraft reduces, the ability to maintain control and satisfactory forward motion reduces for any given wind condition. Much work has been done on understanding the turbulence inherent in atmospheric winds and its effects on the response of structures and aircraft; see for example Holmes (2001) and Nelson (1998). It is now the norm to provide correctly scaled models of atmospheric turbulence when undertaking both time-averaged and time-varying on buildings, masts, bridges etc. yet this is generally not done on aircraft.

Unmanned Air Vehicles (UAVs) are currently operating in a wide range of commercial and military operations Burger (2002) and Anon (1997). A recent ARPA[1] specification supporting research programs into micro air vehicles (MAVs), Wilson and Schnepf (2001), has led to many small craft being evaluated. These craft are characterised by their small dimensions (the initial DARPA specification was for a vehicle no larger than 150 x 150 mm planform[2]), lightweight (~65g) and relatively short flying duration (20 to 40 minutes).

Due to the missions envisaged for MAVs of short-range reconnaissance and surveillance, and the operational environment dictated by terrain & weather, Anon (2001), Ricketts (2001) and Sinha et al (2001). MAV operations are of relatively short flying duration and at low speed close to the ground. Thus they are 'immersed' in the lower part of the ABL. Since MAVs are to be flown 'over hillside, around street corners or up to a window for reconnaissance and surveillance' they will be operating in the 'roughness zone' where the wakes of the local surface obstructions are significant. The wind environment of cities is known to be complex and the wakes of ground-based objects can increase the turbulent energy levels. When the wind is present the operational environments of MAVs are turbulent; far more so than larger aircraft that cruise above the ABL.

Consequently the environment is emerging as a major constraint on the operations of MAVs, with an increasing vulnerability to turbulence as size and speed reduces, Spedding and Lissaman (1998). Hoover (1999) noted that flexible wings might alleviate some of the effects of turbulence, but that small gusts have extremely deleterious effects on such small craft. Investigations of the controllability of MAVs, including a 4.5-inch span MAV, were made by Jenkins et al (2001) who analysed flight control positions via reversal counting and autospectra, in order to determine the best aircraft under a range of atmospheric conditions. It was concluded that control 'workload' was unquestionably related to how often rapid (in the range 1 to 10 Hz) control movements must be made to maintain stability.

The most common role for RPVs is one of surveillance, using very low mass video and other forms of observation (see Grasmeyer and Keennon, 2001, for information on four gram video camera and telemetry instrumentation). As well as the problems associated with flight under turbulent winds, holding a stable viewing platform becomes increasingly difficult as aircraft scale reduces. In particular roll, pitch and (to a lesser extent) yaw motions have a significant influence on image sharpness, whereas the influence of vertical, lateral and fore and aft translations are minimal.

There are now several MAVs that have demonstrated outdoor flight, including Watkins (2002). In addition to the prior documentation, personal experience has shown that the largest challenge to their flight is overcoming the effects of turbulence, particularly small vortices and eddies that are inherent in atmospheric turbulence that produce seemingly random roll and pitch inputs. This seems due to the relative size of structures in atmospheric turbulence with respect to MAVs, as well as the effects of the mean atmospheric wind. It is considered that this restriction would curtail the number of possible days per year that they could be used for outdoor activities.

Little work has been done on understanding the wind environment of relatively slow flying craft close to the ground. This is in stark contrast to the aerodynamic testing of land-based structures where testing in correctly scaled atmospheric boundary layers is commonplace. There is a substantial database of wind data, generally gathered from masts at heights of 10 metres or greater for wind engineering uses.

In order to provide information on the roll and pitch disturbances encountered close to the ground for small aircraft, multi-point measurements of the velocity field are needed, including documentation of fluctuations up to the maximum frequencies of interest. Ideally a simultaneous series of measurement made at points representing the path of the aircraft through a variety of atmospheric conditions (including varying winds and "city canyon" terrains) would enable a further understanding of the disturbances.

[1] Formerly DARPA (Defence Advanced Research Projects Agency – US)

[2] Initial thinking regarding size and scale of MAVs was for them to be 'bounded' by a 150mm box, although this ARPA specification has been revised to 'manportable'.

The aims of this research program are to review the existing database of measurements close to ground level from fixed and moving perspectives and to present recent results of measurements taken from velocity probes fixed to a mast above a stationary and moving vehicle.

4.2 Current body of knowledge

4.2.1 Atmospheric data: Historical perspective, current knowledge and relevance

The ABL extends from the ground up to a height of several hundred meters. It has been studied over much of the previous century and the spatial and temporal variations of the wind (with location and height) have been documented by many workers. Information was obtained by wind engineers from relatively large anemometers on fixed masts at heights well removed from the ground (in order to predict loadings on masts, tall buildings etc.), see for example Sutton (1953), Van der Hoven (1957), Lawson (1980), Melbourne (1994) and Holmes (2001).

The variation on mean wind speed with height for locations around the world is well documented and the mean speeds can be such that forward motion of some slower flying MAVs would not be possible for some of the time. However the aim of the current review and associated work is to investigate the turbulence or fluctuating properties in the ABL, when mean flow speeds are otherwise within a suitable range for flying.

The Engineering Science Data Unit (ESDU) data sheet 74030 provides summaries of data up to 1974 and ESDU 85020 revises and summarises single point data to 1985. A third data sheet, ESDU 86010 details the variations in atmospheric turbulence in space and time for strong winds. Some multi point[3] data sets exist; however, since it is well known that the turbulence in the ABL varies strongly as a function of height from the ground (and that most wind-sensitive structures are slender in the vertical sense) the spatial separation is usually in the vertical sense. From such measurements it is known that with increasing closeness to the ground the turbulence intensity increases and changes characteristics. Above the ABL the air is relatively smooth[4]. Under all but very low wind speeds (less than about 3 m/s) or in storm conditions the turbulence in the ABL is generated by mechanical mixing, resulting from the wakes of objects on the ground. As the ground surface is approached, the vertical fluctuations are attenuated thus turbulent energy is mainly in the horizontal plane. However, there can still be significant energy in the vertical direction in the last few meters.

4.2.2 Data acquisition and atmospheric measurements

Wind data are traditionally obtained utilizing propeller, cup, dynes or ultrasonic anemometers that are placed either in isolation or located on vertical masts with inter-anemometer spacing of several metres. This reflects the interest of the building or road vehicle aerodynamics communities where the structures or vehicles are relatively large in relation to the turbulence scale. The data from the closest spacing of anemometers appears to be the work of Flay (1978), with a spacing of ~2.2 metres, which was subsequently used in ESDU 85020. The size of individual anemometers used was similar to the size of MAVs (in common with nearly all meteorological surveys) thus they cannot provide the spatial resolution needed to discriminate the turbulence characteristics relevant to MAVs. In common with meteorological measurements they were located in a vertical arrangement to primarily provide information as a function of distance from the ground surface.

Two point simultaneous measurements in the horizontal plane have been made in order to provide direct measurement on the spatial structure of turbulence as detailed in Raupach et al (1996) and some hot-wire measurements have been reported by Aylor et al (1993). These studies were taken over grass or forest canopies to further the understanding of turbulence and its effects on vegetation. To provide enhanced spatial (and frequency) resolution, some single point measurements have been

[3] Data obtained simultaneously from several anemometers displaced vertically or horizontally.

[4] At heights relevant to commercial and military aircraft operations there can be 'clear air turbulence' but this is not relevant to the current discussion.

undertaken using hot-wire anemometry which permits a resolving dimension of approximately 3mm as well as a greatly enhanced frequency response, see for example the work of Watkins (1995). Such sensors rely on very fine (5-12 micron) heated metallic wires, thus they are extremely fragile and change calibration with temperature. When operated outside the laboratory environment they prove extremely troublesome.

4.2.3 The Turbulence Environment Experienced by Moving Vehicles

The relative air velocity (defined here as the velocity experienced by the moving vehicle) is the vector sum of the velocity of the atmospheric wind and the vehicle velocity relative to the ground. Analytical frameworks that relate the turbulence characteristics for a single point on moving road vehicles to characteristics obtained from ground-based anemometers have been developed by Balzer (1977), Cooper (1984) and Watkins (1995).

To provide enhanced spatial and frequency resolution, some measurements have been undertaken using hot-wire anemometry[5] (HWA) from masts above stationary and moving vehicles, see for example the work of Watkins (1990). For vehicles moving at 100 km/h through atmospheric winds of between 1 to 9 m/s the measured longitudinal and lateral turbulence intensities were in the range 2.5% to 5% and 2% to 10%, respectively. Spectra obtained from the moving vehicle were shown to have peak energy at about 1 Hz although it varied between about 0.25 to 2.5 Hz. The work and the effects of the turbulence field on parameters of interest to passenger vehicles have been communicated in Watkins and Saunders (1998), and are used in the review paper by Howell (2000).

To define similar atmospheric parameters for MAV flight through the ABL, the techniques required are identical to those used with road vehicles, but the MAV velocities are lower. Therefore operational turbulence levels experienced by MAVs would be generally larger than that experienced by automotive vehicles and peak frequencies would be lower. However, MAV control characteristics mean that peak frequencies are not the sole parameter of interest but energy levels over a defined frequency range are also important.

4.2.4 Current state of the art in MAV design and operation

There have been recent success stories with some of the higher profile UAVs, such as Global Hawk and the Predator UAVs. There are also many very successful UAVs to come from Israel, the UK, Europe and Australia, many of which have been in service for the past few decades. Smaller UAVs however have only recently been enjoying more success, largely made possible by miniaturization of electronics and advances in propulsion and structural technology.

The most notable examples of small UAVs currently in service include the Aerosonde[6], a small 3 metre UAV designed and manufactured in Australia, and the DragonEye developed by Aerovironment[7], a small 1 metre UAV in use with the US Marine Corps for surveillance in the field. The DragonEye is one of the smallest aircraft to see active service, playing an active role in the recent Iraq operations.

On the smaller end of the scale, there are also many development efforts currently underway around the world, one example being the Black Widow[8], developed by Aerovironment, and with a wingspan of just 6 inches it is a true MAV. It was designed with DARPA funding and is capable of short flights, sending telemetry back to the ground.

[5] HWA permits a resolving dimension (spatial resolution) of approximately 3 mm, enabling enhanced spatial and frequency response. However, they are extremely fragile and change calibration with temperature.

[6] See http://www.aerosonde.com/ for information on the Aerosonde UAV

[7] See http://www.aerovironment.com/area-aircraft/unmanned.html for information on Aerovironment

[8] See http://www.aerovironment.com/news/news-archive/mav99.html for information on the Black Widow program

4.3 Program aims

The current research work aims to build towards an understanding of the transient control inputs required to hold relatively 'straight and level' flight whilst traversing real wind conditions, and to then replicate the unsteady flow environment in a large environmental wind tunnel (12m x 4m test section) extending the understanding of micro flight[9]. The specific research goals of the work proposed here are to:

4. Provide detailed descriptions of the outdoor flight environment, including the spatial and temporal variations, experienced by MAVs (either natural or man-made) encompassing flight speeds from hovering to 10 m/s, under typical atmospheric winds
5. Determine the levels and characteristics of turbulence most relevant to MAV flight for flow simulations (which could be either CFD or EFD)
6. Reproduce typical outdoor turbulent flow environments in a wind tunnel, utilizing the same probe systems and statistical parameters as used to gather the outdoor data.

It is considered that the new knowledge gained could be utilised to formulate design and control strategies for a new generation of MAVs that offer enhanced utility (e.g. increasing the number of days per year for which they can provide useful information).

4.4 Research methods

In order to achieve the aims stated above, it is proposed to utilise two phases of experimental testing: on-road measurements of atmospheric turbulence to characterise the turbulence; and wind tunnel tests to ascertain whether relevant atmospheric turbulence conditions can be replicated within a laboratory environment. Through these measurements and the associated analysis of the experimental data, the levels and characteristics of turbulence most relevant to MAV flight will be identified. The two phases of experimental testing are described in more detail below.

4.4.1 Atmospheric measurements

In order to fully understand and quantify the temporal and spatial characteristics of velocity fluctuations experienced when small craft fly through the atmosphere (i.e. perturbations associated with pitch, roll and yaw motions of MAVs) a module of four multi-hole probes will be constructed utilizing the information gained in the feasibility study. The probes will be laterally separated (i.e. positioned in the horizontal plane across the mean flow direction to document the flow across an imaginary wingspan) and the separation between the four probes will be varied, in order to measure relevant spatial locations for MAVs of differing span. Initial inter-probe separations will be 6 inches (150 mm) giving a maximum span for the four probes of 18 inches (450 mm). However, it is proposed to conduct the bulk of the testing with two-inch (50 mm) inter-probe separation in order to obtain improved spatial discrimination for MAVs of six-inch (150 mm) span. Note that the inter-probe separation can be varied to suit needs. Combinations of probe outputs will be used to determine the time histories of velocity fluctuations as a function of lateral separation at a couple of simulated flight speeds. The module will be mast-mounted at ~4 metres[10] above a vehicle and the vehicle will be driven at appropriate speeds for the collection of data relevant to MAVs. This includes tests with the vehicle stationary and aligned with the mean wind direction (which will be used to document the atmospheric wind characteristics and for providing data relevant to hovering MAVs). Checks for the proximity effect of the vehicle and support system on the measurements will be made in calibration runs. The considerable experience gained since 1983 using anemometers mounted to moving vehicles (first performed to document the flow field for truck aerodynamic add-on devices e.g. see Saunders et al, 1985) and the analytical framework summarised in Watkins et al (1995) will be utilised to gain valid and representative data and to provide a coherent analytical framework. A standard,

[9] Thus forming a sound basis for subsequent work.

[10] Road tests can provide data up to the maximum road legal height of 4.3m, provided the modified vehicle conforms to Australian Design Rules.

existing signal-processing package will be used to manipulate and process time histories to calculate velocity spectra, lateral coherence and turbulent length scales. These statistical results will be used when generating the turbulence in the physical simulation described below.

4.4.2 Wind tunnel testing

In order to provide a valid physical simulation for the development of MAVs under controlled repeatable flow conditions, it is proposed to configure a wind tunnel to simulate the turbulence levels observed on-road. The Monash University wind tunnel is ideally suited for this purpose since it has a 12 x 4 x 55m test section in the top working section that permits the generation of the general scale of turbulence required. To provide perturbations to the flow, thus generating the required turbulent structure, upstream planar grids, as well as tunnel configuration changes, will be utilised. The former is a known technique for turbulence generation for wind loads on ground-based structures (Holmes, 2001). The sensor module described above for the outdoor experiments will be used again to document the resulting flow field with similar data processing to that employed in the outdoor tests.

The rest of this report details the results of the research efforts. In Section 5 the relevant parameters for MAV flight in atmospheric turbulence are considered, including the required spatial and temporal resolution for measurements within this environment. The general requirements for the modelling of MAVs are also considered in this section. The methodology and results from the on-road and wind tunnel phases of testing are detailed in Section 6 and Section 7 respectively. Section 8 then conducts a critical comparison between the on-road measurements of atmospheric turbulence and those found within the wind tunnel environment, in order to evaluate the effectiveness of simulating atmospheric conditions. Finally, the overall conclusions and recommendations are given in Section 9.

5 MAV Flight Control Parameters

Before commencing the experimental phases of testing, it is necessary to consider what parameters must be measured in order to characterise atmospheric turbulence (Section 5.2) and in addition the spatial and temporal resolution of the instrumentation that is required (5.1). This is determined by considering general flight characteristics and typical MAV scale. Some thought is then given to how future modelling efforts may be achieved (once the experimental data is obtained) and what direction those efforts may take (Sections 5.3 and 5.4).

5.1 Relevant frequency range

In order to achieve the objectives stated in Section 4.3,it is necessary to define the temporal and spatial resolution most appropriate to MAV flight. The first of these, temporal resolution can be achieved by appropriate instrumentation frequency response. MAV characteristic length can range from approximately 150 mm up to 1 metre in wingspan, with relevant chord lengths in a similar range. The turbulent scales of most relevance to the control of MAV flight are most likely within a range of 1/10th to 10 times the wing chord/span (i.e. 15 mm to 10 m), with overall MAV relative velocities ranging between approximately 0 to 10 m/s. Assuming that the turbulence convects at the mean relative velocity (i.e. $V_r = f\lambda$)[11], the desired frequency response that will achieve an appropriate temporal resolution is within 0.1 – 700 Hz. In contrast, spatial resolution simply needs to be much smaller than the MAV characteristic length of 150 to 1000 mm.

The exact frequency range required will depend to some extent on the effective or indicated air speed that the MAV is travelling at. The above analysis can be simplified by working out the relevant wave number, essentially a normalised frequency or inverted wavelength, for MAV flight (Table 1). The wave number range is then independent of MAV indicated air speed and, as flow spectra are frequently plotted against wave number, provides a convenient point of reference.

Table 1: Relevant frequency/scale range of interest for turbulence in an MAV flight environment.

Wing span, S	$k = 1/\lambda = f/V_r$ [/m] ($\lambda = 1/10^{th}$ – 10 times S)
0.150 m (6”)	0.7 – 67
1.000 m (40”)	0.1 – 10

5.2 Relevant parameters

The turbulence in the ABL provides for some unique challenges for MAVs. These can be broadly categorised into problems of stability and control. The former refers to the inherent stability of the aircraft and how it will respond to the aerodynamic inputs generated by the turbulence, while the latter refers to the methods employed to control the aircraft in its environment, maintain a heading or flight path, or actively maintain a position. Since one of the significant mission roles for an MAV is to provide real-time imaging, maintaining a stable platform for video cameras is particularly important. Therefore the effects of atmospheric turbulence on MAV stability need to be investigated, in order to achieve a stable viewing platform and provide the clearest possible pictures.

Aircraft motion can be described as translation and rotation about the 3 aircraft axes (Figure 2). This gives a total of six degrees of freedom.

[11] Where λ is the turbulence wavelength, V_r the total relative velocity, and f the frequency.

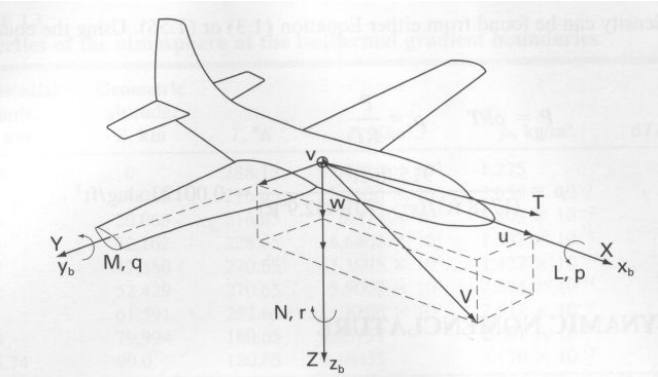

	Roll Axis x_b	Pitch Axis y_b	Yaw Axis z_b
Angular rates	p	q	r
Velocity components	u	v	w
Aerodynamic force components	X	Y	Z
Aerodynamic moment components	L	M	N
Moment of inertia about each axis	I_x	I_y	I_z
Products of inertia	I_{yz}	I_{xz}	I_{xy}

Figure 2: Definition of axis, forces, moments and velocity components in a body fixed coordinate system (from Nelson, 1998).

If we consider a camera pointing at a target some distance away, translation motions have a relatively small effect on the clarity of the image returned by the camera. Rotations about the axes have a much larger effect and are proportional to the square of the distance to the target. If the aircraft rotates a few degrees then the distance the target moves in the camera field of view can be large. In the case of movements caused by gust inputs, which can occur at a high frequency, this type of motion can render a video image useless. It is therefore of most importance to investigate this type of motion.

With regard to such rotational movements, for a camera that is required to look down on a target, then the rolling and pitching motions of the aircraft will have the greatest effect on image clarity. If the camera is pointing forward then the pitching and yawing motions have the greatest effect.

When flying through a turbulent environment, the aircraft response to gust inputs depends on its stability in a particular axis. The less stable the aircraft is in a particular axis, then the greater its response to an input. Most conventional aircraft are greatly affected by pitch and roll movements, but not so affected by yaw. This is because such aircraft are directionally stable due to the relatively large distance between the vertical fin and the aircraft centre of gravity, providing a “weathercocking” force like a weather vane and always pointing the aircraft into the direction of travel. Conventional aircraft are far less stable about the x- and y-axes and thus more susceptible to pitch and roll inputs.

The aircraft “stick fixed” response in pitch and roll (ignoring control inputs) are both attributed to the lift distribution over the main wing. If a gust front arrives at the leading edge, the wing will see an increase in velocity. If the gust front is uniform, and essentially two-dimensional, then the increase in lift will cause an increase in pitching moment and the aircraft will pitch up. As the gust leaves, the lift will reduce and the aircraft will pitch down. In this situation, it is the variation in longitudinal velocity with time, and particularly its frequency that is the important factor.

In the case of roll inputs, the gust front may be considered to be uneven along the span of the wing. As the gust front approaches the leading edge, the wing will see an increase in velocity, and therefore lift, at only certain portions of the wing relative to the rest of the wing. This local increase in lift creates an uneven lift distribution, thus causing a rolling motion. The variation in local pitch angle along the wingspan is a good measure of the possible roll inputs to an aircraft due to such a gust input.

In reality, most gusts caused by finer scale eddy motion in a turbulent flow will be more like the latter case, and much larger scale motion may approach the former two-dimensional case, although all are really three-dimensional in nature. In the case of turbulence structures with very large scales, the effects may even be considered quasi-static, where the changes occur over such a large timescale that their effects are experienced slowly and are easily compensated for.

From this discussion it is apparent that the two more important parameters to investigate are those of velocity and pitch variation, in both time and lateral spatial separation. Pitch variations in time and space are involved in both pitch and roll inputs to an MAV platform and are therefore particularly significant. Two of the authors also have significant experience in flying model aircraft and have noted that it is often the significant roll inputs that are the hardest to cope with when flying small aircraft in the atmospheric boundary layer. As these are caused by local variations in pitch angle along the aircraft wingspan, this parameter is crucial to both MAV flight control and providing a stable platform for imaging purposes. Therefore spatial variations in pitch angle are focussed on in this research, with velocity variations occupying a lesser role.

5.3 Determining MAV stability and development of MAV control systems

Once the environment is understood, we move into the problem of understanding the dynamics of the aircraft themselves, in particular how they respond to the turbulent structures in the ABL, and what methods can be employed to control the aircraft more effectively in such an environment.

To determine the response to the different turbulence environments identified during this study, we can either make models and put them in the wind tunnel, which is expensive and time consuming. Another way is to do it computationally, which will allow a much larger number of configurations to be tested in a shorter time ant a fraction of the cost of running a wind tunnel.

In reality both methods are needed, simulations are useful tools for rapid prototyping designs, however they have a number of limitation, so wind tunnels are used for more detailed design work. This is especially true when attempting to simulate very complex systems sues as real turbulent flows as inevitable assumptions and simplifications must be made.

The expected outcomes of the further study are to determine exactly how MAVs are affected by the turbulent ABL, and what aspects, or frequency bands in the ABL do the most harm. In addition by investigation a wide range of MAV designs and concepts, we will be able to determine what aspects of design have the greatest effect on the stability and controllability of MAV flight. Once these two areas are understood, methods can be designed to overcome these effects with the ultimate goal of achieving stable, controllable flight in a wide range of weather conditions.

5.4 Development of a response model

There are several methods for computationally predicting the forces acting on a body by a fluid. These rage form simple 2D approximations, to 3D lifting line methods, Vortex lattice methods and the most complex systems use Navier-Stokes solvers, such as those found in the commercial computational fluid dynamic (CFD) packages. As the complexity of the solver goes up, so does the computation time and power required. Since we are interested in an application which requires the investigation of a dynamic response, we need to be able to recalculate the entire system over and over for each point in time, many times a second. This limits us to reasonably simple solvers, however with some good approximations reasonably accurate predictions can be made.

There are two main methods that lend themselves to this application. The first is by the use of force and moment coefficients, and is employed in most commercial flight simulation software, and in some aircraft models in MATLAB. The second is an element breakdown method, which breaks the model into a number of elements and then calculated the force on each element.

As we are interested in the effect of atmospheric inputs that are varying in both time and space in more then one dimension, we need a model that is capable of simulating the effect of spatially varying inputs along the wingspan of the model at each step in time. This in effect rules out the first type of

model and really lends its self to the element breakdown method, since here the individual forces on each element can be calculated at each moment in time and summed to give the overall response.

While this method is not new, the use of spatially separated and varying aerodynamic inputs across the wing of a MAV is new, with almost all models found commercially of this type assuming a steady smooth flow. The simulation of turbulent flow will form the biggest challenge of any response model, although the work already done in this research provides valuable information on the inputs required for such a model.

Whilst the area of computer simulation of the environment and the MAVs that will fly in it are items for future work, by considering them from the start we can ensure that the data we collect now has direct relevance later on, and we can lay the groundwork on which this framework for development will be built.

6 Atmospheric Turbulence Conditions: On-Road Testing

In order to achieve the first of the research aims detailed in Section 4.3, a program of experimental testing was undertaken. This was intended to provide detailed descriptions of the outdoor flight environment experienced by MAVs, at heights low in the atmospheric boundary layer and encompassing flight speeds from hovering to 10 m/s. Because it was envisaged that critical MAV flight would occur close to ground level, the measurements were also required to be taken close to ground level[12], and for this purpose on-road testing was chosen.

The use of on-road testing for characterisation of atmospheric measurements has already been discussed in 4.2.3. It was proposed to use similar techniques to that used in Watkins (1990) and commonly used in vehicle aerodynamics and aeroacoustics testing. This involved configuring a vehicle with appropriate instrumentation, in such as a way as to be safe and comply with all road laws, and using the vast network of available public roads as the testing ground. For the purposes of characterising the MAV flight environment, this is suitable because many of the possible MAV applications involve flight in and around population areas for surveillance, reconnaissance and disaster management purposes.

On-road testing involves assessment and selection of suitable test locations, calibration of the instrumentation in order to determine both alignment offsets and any possible proximity effects due to the presence of the vehicle, conduction of the test runs in order to minimise possible disturbances due to traffic, and then processing and analysis of the collected data. These functions are described in the sections below.

6.1 Methodology

In order to measure the turbulence levels and scale in the atmospheric boundary layer, a laterally spaced instrumentation configuration was utilised. The lateral spacing specifically enabled the examination of parameters that affect the effective roll inputs of an MAV platform, as discussed in Section 5.2, while still allowing parameters that affect the effective pitch inputs to be examined if required.

The configuration consisted of four multi-hole pressure probes, or Cobra Probes, mounted on an aerodynamically faired bracket and equi-spaced in the lateral direction. The Cobra Probes are able to measure all three velocity components and static pressure with a frequency response up to ~1000 Hz (see Appendix A, Section 11.1 for further details). The bracket with probes was then mounted on a mast on top of a vehicle (Figure 3), ~4 metres above the ground, and measurements were taken in different terrains and wind conditions. Appendix A, Section 11.3, details the configuration used, and Section 11.2 defines the relevant terminology and variables.

The effective measurement points were at the probe heads, which were situated 3.9 metres above the ground thus removing the proximity effects of the vehicle on the flow. Although the probes and bracket were approximately aligned with the centreline of the vehicle, and therefore its direction of travel, the small offsets due to the differences in their individual and overall alignments with the centreline were accounted for by conducting calibration runs at various vehicle speeds, in very calm conditions on a smooth, horizontal surface[13]. Once the offsets were determined, they were subsequently removed from all data measured using the probes, thus ensuring that the data collected from all four probes was aligned with the vehicles direction of travel, i.e. in calm conditions the measured u-component velocity was aligned with the direction of travel. Therefore any flow angles

[12] The characteristics of turbulence within the atmospheric boundary layer vary with height, with high turbulence levels occurring close to ground level in comparison to the relatively much smoother flow found at higher altitudes at the edges of the atmospheric boundary layer.

[13] The smooth tarmac of an airfield was found to be perfect for this purpose. The exceptionally smooth surface ensured that bumps and undulations did not interfere with the calibration measurements, and the very smooth, open terrain along with calm wind conditions ensured that very little in the way of atmospheric disturbances was encountered.

measured by the probes were solely due to the ambient wind characteristics, and not the alignment of the probe array.

Figure 3: Cobra Probes mounted on a bracket on top of a vehicle-mounted mast.

Using the vehicle-mounted probe array, two types of measurements were taken.

- Moving measurements: while the vehicle was moving at constant speed, in a straight line, on a particular stretch of road.
- Stationary measurements: occasional measurements taken with the vehicle stationary and pointing into the prevailing wind.

The former measurements were typically of the order of 60-90 seconds in length, depending on the available stretch of road, traffic conditions and the vehicle speed. Vehicle speed was itself determined by the road conditions and also the prevailing traffic conditions, but was typically 20 or 50 km/h. The latter measurements were of 10 minutes duration and were only able to be taken where the ambient wind speed was high enough to limit the fluctuating flow angles to within the Cobra Probes' cone of acceptance of ±45° (see Appendix A, Section 11.1 for further details). This also meant that stationary measurements could not typically be taken in very built-up environments, such as metropolitan and some suburban terrains, where high flow angle fluctuations also occurred.

The stationary measurements were taken to provide extra long data samples for the purposes of validating some of the data processing techniques used with the vehicle-moving measurements. They were also required to enable reasonable estimates of atmospheric turbulence length scales, which typically require very long time samples in order to be determined with any degree of accuracy.

The reason that, in the same wind conditions, moving measurements are not subject to as greater range of flow angles as stationary measurements are examined in more detail in Section 8.1. But it is this feature, as well as the fact that moving measurements effectively compress a greater 'length' of convecting turbulent structures into a given time sample, that make them a particularly effective way of gathering data.

Measurement runs were typically conducted in light or no traffic as far as possible, in order to avoid the effects of wakes from other vehicles. The exception to this was the very built-up, metropolitan terrains where it was not possible to completely avoid traffic. In these conditions the vehicle was driven within significant gaps in the traffic and at the prevailing traffic speed, in order to avoid passing or being passed by other vehicles. Runs significantly affected by traffic, alterations in vehicle speed or direction, or bumps and significant undulations in the road surface were discarded and the measurements repeated in better conditions.

6.1.1 Data processing

Measurement samples were acquired at 5 kHz and then filtered and down sampled to 1.25 kHz to avoid aliasing effects. The raw data then had the calibration offsets applied, and a correction was performed to account for the fact that with a given flow yaw angle, turbulence structures would arrive at the 4 probes at slightly different times. This was accounted for by using the mean flow yaw angle to

calculate the time difference and time shift the data from the downwind probes an appropriate amount. The mean flow yaw angle was then removed, while retaining the overall relative flow velocity and pitch angle, thus simulating measurements taken with a true head-on orientation. At this point the main data processing was commenced.

The main data processing was done in three stages, at each of which certain parameters were calculated. The three stages consisted of:

1. the original data as measured by the Cobra Probes, and therefore including a component of vehicle speed;
2. the original data minus the vehicle speed component, thus giving the ambient wind characteristics occurring during the measurement;
3. the data from stage 2 with a mean u-component velocity added back in order to bring the total mean relative velocity (including the ambient wind) up to 10 m/s.

At each stage, calculations of the relevant statistics (mean values, standard deviations and turbulence intensity), followed by the power spectral density versus wave number ($k = f/V_r$), pitch variation fluctuation and pitch angle coherence between probes were all carried out (relevant equations are given in Appendix B, Section 12.1). This gave a total of three complete sets of data (see Appendix B, Section 12.6, for a summary of the data processing steps).

The three stages of data processing were required in order to derive the ambient wind conditions from the vehicle-moving measurements (stage 2), and to then standardise the data for an equivalent indicated air speed of 10 m/s (stage 3). As the vehicle-moving measurements were taken at varying vehicle speeds, which combined with varying ambient wind conditions caused varying relative flow speeds, standardisation was required in order to allow direct comparisons between the turbulence characteristics in different terrains.

The resulting calculated variables at stages 2 and 3 thus simulated two main MAV flight situations: stage 2 gave the turbulence characteristics for an MAV with zero ground speed, i.e. an MAV that is effectively holding its position into an ambient wind; while stage 3 gave the turbulence characteristics for an MAV flying through these ambient conditions at an equivalent indicated air speed of 10 m/s. Data from both stages 2 and 3 are used later in Section 8 to evaluate whether or not atmospheric conditions relevant to the flight of MAVs can be replicated in a wind tunnel.

6.2 Test conditions

6.2.1 Terrain types (test locations)

In taking measurements in the atmospheric boundary layer, it is necessary to classify the terrain within which the measurements are taken, as the terrain properties directly affect the boundary layer and turbulence properties. The two main parameters to classify are the terrain roughness (a measure of the number, size and spacing of obstacles on the ground at the measurement location and for several kilometres upstream) and the terrain undulation (a measure of the amount of undulation of the ground for several kilometres upstream).

The most common roughness classification scheme is that of the International Standards Organisation (ISO), ISO/CD 4354. However, as its categories are fairly broad, the classification scheme of Davenport (1960) was therefore chosen (Table 2).

As no existing reference to classification on terrain undulation or “hilliness” was found, one was therefore constructed. It separates the many different types of terrain found around the world into six very broad classifications, which can be used to describe a particular site (Table 3).

Before the commencement of testing, scouting runs were conducted at various locations in and around Melbourne, up to 100 km from the city centre. This was done in order to identify suitable locations for testing, to classify them, and take preliminary measurements. Each suitable location was given a classification by combining the appropriate category number from the roughness and undulation into a single descriptor:

terrain category = roughness-undulation, e.g. 4-2.

Table 2: Classification of effective terrain roughness, after Davenport (1960).

No.	Class Name	Roughness length (m)	Landscape description (H: obstacle height, x: obstacle separation)	ISO Categories
1	Sea	0.0002	Open water, featureless flat plain, fetch > 3 km	2
2	Smooth	0.005	Obstacle-free land with negligible vegetation, marsh, ridge-free ice	
3	Open	0.03	Flat open grass, tundra, airport runway, isolated obstacles separated by >50 H;	
4	Roughly Open	0.10	Low crops or plant cover, occasional obstacles separated by ≥ 20 H	3
5	Rough	0.25	Crops of varying height, scattered obstacles with separation x ≈ 12-15 H if porous (shelterbelts) and x ≈ 8-12 H if solid (buildings)	
6	Very Rough	0.5	Intensively cultivated landscape with large farms, orchards, bush land, x ≈ 8 H; low well-spaced buildings and no high trees, x ≈ 3-7 H	
7	Skimming	1.0	Full similar-height obstacle cover, x ≈ H, e.g. mature forests, densely-built town area	4
8	Chaotic	≥2	Irregular distribution of very large elements: high-rise city centre, big irregular forest with large clearings	

Table 3: Classification of terrain undulations.

No.	Class Name	Hill height (ft)	Description
1	Flat	0	Flat open plain, such as salt lake or sandy desert
2	Slight undulation	0 to < 50	Paddock or plain, slight undulation of a few meters in height with a long period
3	Undulating terrain	50 to < 100	Very common country, farming type terrain
4	Hilly	100 to < 500	Hilly terrain
5	Steep	500 to 5000	Steep mountainous terrain
6	Alpine	> 5000	High mountains, valleys and steep cliffs

6.2.2 Wind conditions

Ambient or atmospheric wind speed also affects the turbulence properties within the atmospheric boundary layer, and therefore a wind speed classification system was also chosen. The Beaufort wind scale (Table 4) has been around for many decades, and is well understood by meteorologists and wind engineers. It was originally derived for nautical use, but is just as applicable to inland use, although some of the higher categories are less common inland.

In terms of the testing conducted for this research, wind speeds of interest are between force 0 and force 5. Winds stronger then force 5 are outside the operational capabilities of the aircraft and are therefore not of immediate interest. For this reason, testing was limited to wind speeds less than 10

m/s at a particular test location. This encompasses the majority of wind conditions encountered on a day-to-day basis for most inland locations, which also, because of their particular terrain, usually have a lower local wind speed compared to that found over open water or featureless plain.

Table 4: Beaufort wind scale.

Force	Equivalent Speed 10 m above ground		Description
	(m/s)	(knots)	
0	0 - 0.5	0 - 1	**Calm** - smoke rises vertically.
1	0.5 - 1.5	1 - 3	**Light air** - Direction of wind shown by smoke drift, but not by wind vanes.
2	2 - 3	4 - 6	**Light Breeze** -Wind felt on face; leaves rustle; ordinary vanes moved by wind.
3	3.5 - 5	7 - 10	**Gentle Breeze** - Leaves and small twigs in constant motion; wind extends light flag.
4	5.5 - 8	11 - 16	**Moderate Breeze** - Raises dust and loose paper small branches are moved.
5	8.5 - 10.5	17 - 21	**Fresh Breeze** - Small trees in leaf begin to sway; crested wavelets form on inland waters.
6	11 - 14	22 - 27	**Strong Breeze** - Large branches in motion, whistling heard in telegraph wires; umbrellas used with difficulty.
7	14.5 - 17	28 - 33	**Near Gale** - Whole trees in motion, inconvenience felt when walking against the wind.
8	17.5 - 20.5	34 - 40	**Gale** - Breaks twigs off trees, generally impedes progress.
9	21 - 24	41 - 47	**Severe Gale** - Slight structural damage occurs (chimney-pots and slates removed).
10	24.5 - 28	48 - 55	**Storm** - Seldom experienced inland; trees uprooted; considerable structural damage occurs.
11	28.5 - 32.5	56 - 63	**Violent Storm** - Very rarely experienced; accompanied by widespread damage.
12	33 - 36.5	64 - 71	**Hurricane**

6.2.3 Experiment matrix

Category 4 - 6 undulations were impractical for the on-road testing conducted for this research as such roads were generally not in reasonable proximity to the test base, and there are also problems with the fact that such roads are usually not straight. This is not to say, however, that they are inaccessible for MAVs and perhaps could be considered for future work where test data could be gathered by means other than vehicle testing.

Category 1 undulations were also not in reasonable proximity to the test base, and so were also not covered in this test program. Terrain roughness categories between 1 and 3, extremely open flat terrain, were not covered due to both availability and the fact that the more challenging terrain for MAV flight is encompassed by a terrain roughness of 4 and above[14]. With ambient wind speeds also generally less than 10 m/s, all the above factors resulted in a test matrix as shown in Table 5.

[14] The calibration runs were performed in a terrain roughness of 3, as very smooth, flat, open terrain is preferred for determining the probe alignment offsets.

Table 5: Test matrix for on-road measurements within the atmospheric boundary layer.

Terrain	Wind strength (force)					
Roughness-undulation	0 (0-0.5 m/s)	1 (0.5-1.5 m/s)	2 (2-3 m/s)	3 (3.5-5 m/s)	4 (5.5-8 m/s)	5 (8.5-10.5 m/s)
4-2			X	X	X	X
5-2			X	X		
6-2				X	X	
7-2				X		
8-2						
4-3						
5-3				X	X	
6-3					X	
7-3						
8-3						

The darker shaded cells with crosses indicate the terrain-wind combinations where measurements were taken. They encompass a reasonable range of open to built-up terrains, mostly in slightly undulating terrain, reflecting the available wind conditions for the time of year, and both the availability of terrains around the test base and the practicality of testing in those terrains. As good measurements need to be of the order of 60 seconds, a straight, reasonably flat, sufficiently long stretch of road within the designated terrain needs to be available, with suitable speed restrictions so that 60 seconds of data can be taken without either interfering with or unduly encountering other traffic.

Several of the terrain-wind combinations were encountered in multiple locations, and so measurements were taken in all of them. In addition to this, measurements were often taken in a particular location on multiple occasions, and each test session consisted of at least 2-3 repeat measurements, often at two different vehicle speeds. It was thought that this would provide enough data to characterise the atmospheric environment that MAVs are likely to fly through in the majority of open to moderately built-up terrains.

6.3 Results

In this section, the results of testing within the atmospheric boundary layer, ~4 metres above the ground in various terrains and wind conditions, are summarised using selected results. The results are plotted as energy spectra or power spectral density[15] of the u-component velocity versus frequency, *f*, and the plots below cover terrain type 4-2. Results for all terrains, plotted versus wave number, are shown in Appendix C. Results for terrain 4-2 are shown for the v- and w- components in Appendix C, in order to illustrate the relative magnitudes of v and w fluctuations. However, in the interests of brevity, all other terrain results are only shown as u-component and pitch angle spectra. For a full listing of ambient wind conditions, turbulence intensities and length scales also see Appendix C.

Figure 4 and Figure 5 show the u-component velocity spectra for terrain type 4-2 for the ambient wind conditions and an MAV equivalent indicated air speed (IAS) of 10 m/s respectively. Both plots include

[15] Energy spectra or power spectral densities show the magnitude of the flow fluctuations versus their frequency. Typically in turbulence, the lowest frequency (larger length scale) turbulent structures will have the highest magnitude and the higher frequencies will have progressively lower magnitudes. The exception to this is where there are specific disturbances such as resonance or vortex shedding within a flow.

all the results from all measurements in terrain 4-2, and have the spectra plotted according to the ambient wind conditions during the measurement.

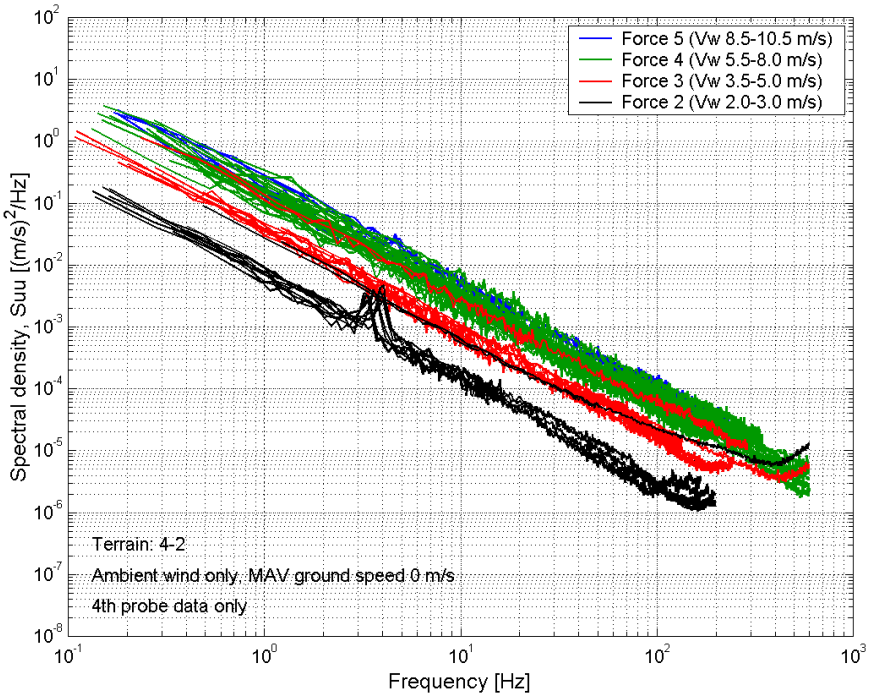

Figure 4: Atmospheric u-component spectral levels for different wind conditions, terrain 4-2, three different locations (ambient wind only, i.e. MAV effective ground speed 0 m/s).

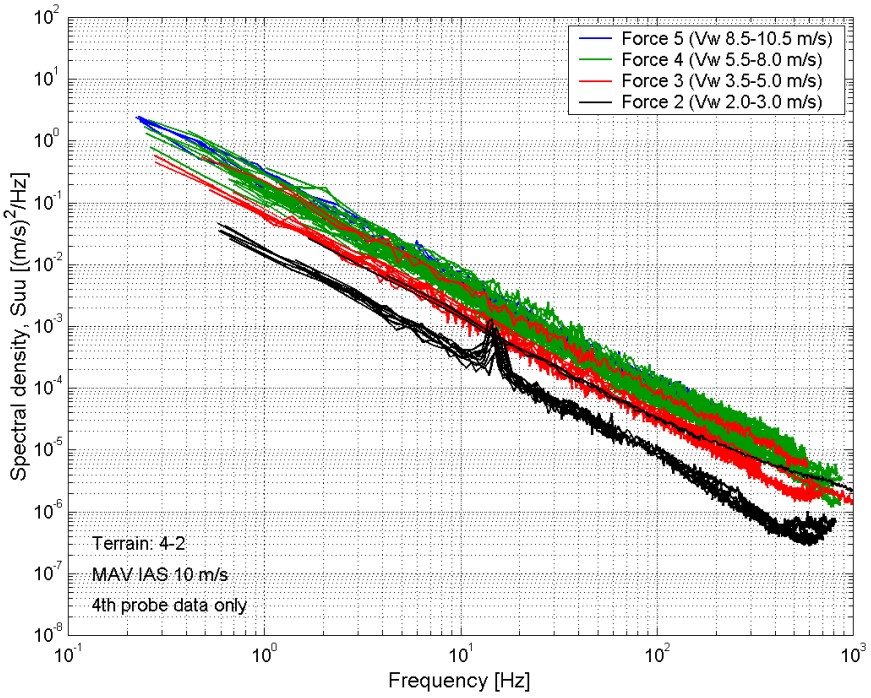

Figure 5: Perceived u-component spectral levels for different wind conditions, terrain 4-2, three different locations (MAV IAS 10 m/s).

As can be seen in Figure 4, the spectra fall roughly into groupings based on the wind strength during the measurements, although there is some scatter and especially the higher wind force groupings tend to overlap. This is not entirely unexpected, as the characteristics of atmospheric turbulence are so complex that it would be naïve to believe that the simple terrain and wind classifications used here could definitively categorise them. There are also variations in terrain within the 4-2 category, and the ambient wind can also originate from any direction within a particular location, thus also potentially changing the upstream conditions. All of these factors mean that the relative groupings indicated in Figure 4 and Figure 5, with their attendant scatter, are quite reasonable in the circumstances. This is further indicated by Figure 6, where the ambient wind spectra have been plotted for only one location and there is still significant scatter and overlap evident between the wind force groupings.

Despite the overlap and scatter between wind groupings, Figure 4 and Figure 5 indicate approximate ranges of spectral fluctuations that can be expected in terrain 4-2, and are therefore valuable tools both for modelling simulations and evaluating wind tunnel flows for the purposes of MAV testing. These plots, combined with the overall turbulence intensities and length scales given in Appendix C, describe the turbulence characteristics found in terrain 4-2 for the given wind conditions.

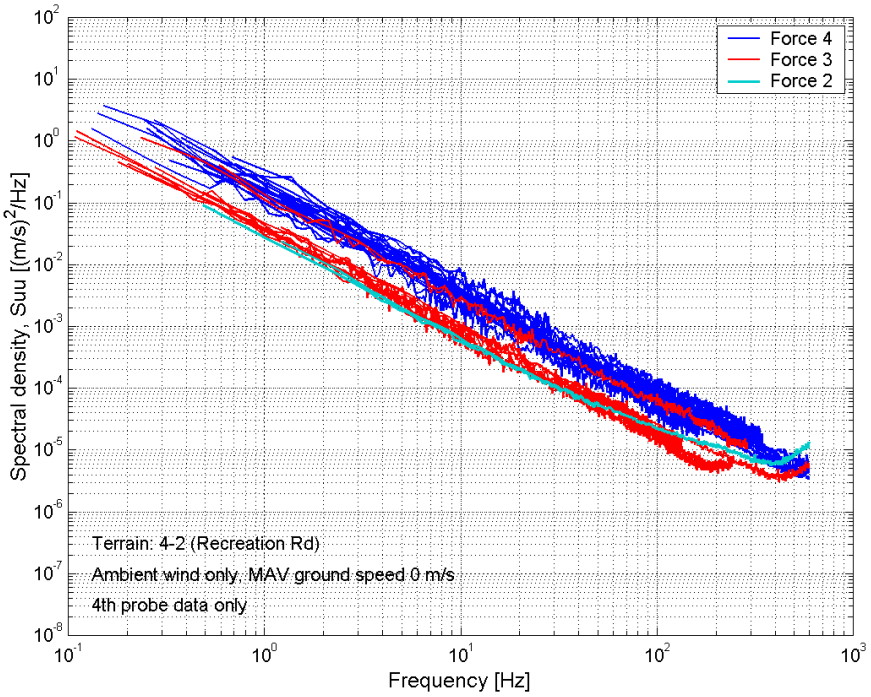

Figure 6: Atmospheric u-component spectral levels for different wind conditions, terrain 4-2, Recreation Rd (ambient wind only, i.e. MAV effective ground speed 0 m/s).

The main difference between the ambient conditions spectra (Figure 4) and those that have been corrected to an MAV IAS of 10 m/s (Figure 5) is that the latter have been compressed together slightly, and shifted to the right and slightly downwards within the plot axes (both plots are on the same axes, in order to facilitate direct comparison). This illustrates how moving at any speed through atmospheric turbulence tends to compress the turbulence and reduces the perceived overall turbulence levels, length scales[16], and flow angles. These aspects will be discussed in more detail in Section 7.2, along with the specific meaning of the power spectra used here to display the data. For the moment it is enough to realise that there are relative levels of energy within the flow, based on the wind strength and the terrain type.

[16] There is a direct relationship between frequency and length scales within turbulence: high frequencies are small length scales, while low frequencies are large length scales. Therefore a shift in the spectra to higher frequencies also implies that the perceived length scales will be smaller.

Finally, for the purposes of testing MAVs, it is not only the u-component velocity that is of importance. As pitch angle variations have been identified as important factors in roll and pitch inputs to MAV platforms, and other factors may later also be found to be relevant, both v- and w-component velocities are also important (pitch angle is formed from a combination of the u- and w-component velocities). Appendix C, Section 13, therefore contains results from the other velocity components in the form of both spectral plots and overall turbulence intensities and length scales.

7 Monash Wind Tunnel Flow Conditions

The atmospheric turbulence measurements taken in Section 6 have characterised the turbulence environment experienced by MAVs in a range of terrains and light to moderate wind conditions. For the purposes of developing and refining early MAV design to cope with these conditions, it is more efficient and provides greater control over testing variables if prototype MAVs can be tested in a wind tunnel environment; this negates the need to deal with the vagaries of weather conditions and testing in different terrains. However, in order to achieve this it is necessary to first ascertain whether the turbulence environment within a wind tunnel can replicate that found outside in atmospheric turbulence.

Accordingly, testing was undertaken in the Monash 1.5 MW wind tunnel (Monash University, Melbourne, Australia), in order to characterise the flow environment within the tunnel and determine whether it could replicate the conditions found in atmospheric turbulence in Section 6. Monash wind tunnel was considered an appropriate facility for such testing for several reasons:

- It has a large enough test section for testing of a range of MAVs (150 – 1000 mm wingspan)
- It has automotive and wind engineering[17] test sections, both of which are designed for moderate turbulence levels (as opposed to smooth flow or aeronautical wind tunnels) and therefore better replicate the conditions found in the atmospheric boundary layer.
- Because of the two different test sections, it was specifically designed to easily enable some large or significant configuration changes to be made to the tunnel, thus facilitating large scale changes to the flow environment in order to vary turbulence levels.

The following sub-sections detail the methodology used to take the measurements and summarise the results. Section 8 then examines these results in more detail and compares them to the atmospheric turbulence measurements taken in Section 6.

7.1 Methodology

In order to measure the turbulence levels in the Monash wind tunnel, a similar test configuration to that used in the prior on-road testing was again utilised. This configuration consisted of four Cobra Probes mounted on an aerodynamically faired bracket, equally spaced in the lateral direction. The bracket with probes was then mounted at the approximate centre of the wind-engineering test section in the Monash wind tunnel (Figure 7), and measurements were taken for different tunnel configurations in order to investigate the turbulence levels and scale obtainable within the tunnel. Appendix A, Section 11, shows the layout used and defines the relevant terminology and variables.

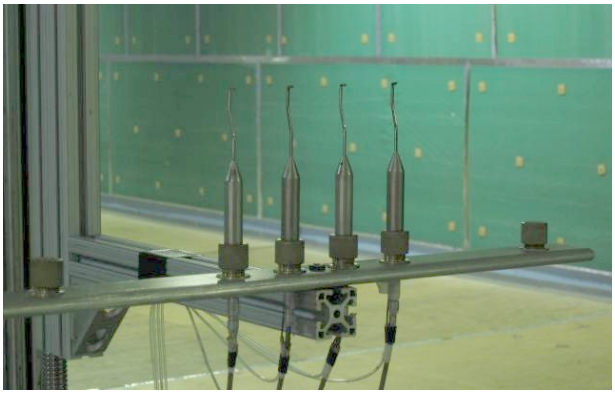

Figure 7: Cobra Probes mounted on the traverse in the centre of the wind engineering test section.

[17] Wind engineering is a branch of aerodynamics that deals with the wind loading and forces on large structures such as buildings, bridges etc. as a result of atmospheric winds.

The Monash wind tunnel is a closed-circuit wind tunnel and was designed as a multiple use facility with three working sections: an automotive, open-jet test section on the lower level; a low speed wind-engineering, closed test section on the upper level; and a high Reynolds number section, also on the lower level. The tunnel is driven by two 5-metre diameter, fixed pitch, variable speed, axial fans situated at the start of the lower circuit. The wind engineering test section that was used to take the measurements for this research has a 4-metre high by 12-metre wide test section and is typically used for simulations of the atmospheric boundary layer over scale models of large structures, urban and cityscapes. See Appendix D, Section 14, for a schematic of the Monash tunnel layout and photos of the various test configurations used for this testing.

Table 6 shows the various combination of tunnel configurations used during testing. By changing the configuration of both the jet and collector around the automotive or lower test section, it is possible to significantly change the flow quality in the wind engineering test section in the upper level of the tunnel circuit. In addition to this, a fine wire mesh screen at the entrance to the wind engineering test section, and extra flat panels used upstream of the automotive test section, can be used to affect the general flow quality. Various combinations of these measures (as shown in Table 6) were used in an effort to reproduce turbulence conditions within the wind tunnel that replicated those found during on-road testing.

Measurement samples were 5 minutes in length and data were acquired at 5 kHz and then filtered and down sampled to 1.25 kHz to avoid aliasing effects. Processing consisted of calculating the relevant statistics (mean values, standard deviations and turbulence intensity), followed by the power spectral density versus normalised frequency (wave number, $k = f/V_t$), pitch variation fluctuation and pitch angle coherence between probes.

The following sections detail the results of the measurements within the Monash wind tunnel, and possible techniques that could be further used to change turbulence levels within the tunnel, in particular by increasing the flow length scale. These latter methods were not tried during the current testing because the results using the configurations in Table 6 were deemed adequate for most small MAV planforms (i.e. for a 150 mm or 6” wingspan).

Table 6: Configurations used during testing in the Monash wind tunnel

Tunnel configurations[a]	Jet position	Collector position	Screen presence	Panel presence
1. Baseline 2. Baseline (with screen)	down	forward	no yes	-
3. Effect of jet position 4. Effect of jet position (with screen)	up	forward	no yes	-
5. Effect of collector position 6. Effect of collector position (with screen)	up	back	no yes	-
7. Effect of panel presence, 300 mm 8. Effect of panel presence, 600 mm 9. Effect of panel presence, 600 mm (with screen)	up	back	no no yes	300 mm panels 600 mm panels 600 mm panels

[a] See Appendix D for photos of the various configurations

7.2 Results

The results from the testing of the various configurations detailed in Table 6 are summarised in Figure 8, for configurations without use of the screen, and Figure 9, for configurations with the screen. The results are plotted as energy spectra or power spectral density of the u-component velocity versus wave number. Results for the v- and w- components and more detailed results for the various

configurations are shown in Appendix E. The plots below are also annotated with the longitudinal turbulence intensity for each configuration. A full listing of turbulence intensities for all 3 velocity components and length scales is also given in Appendix E.

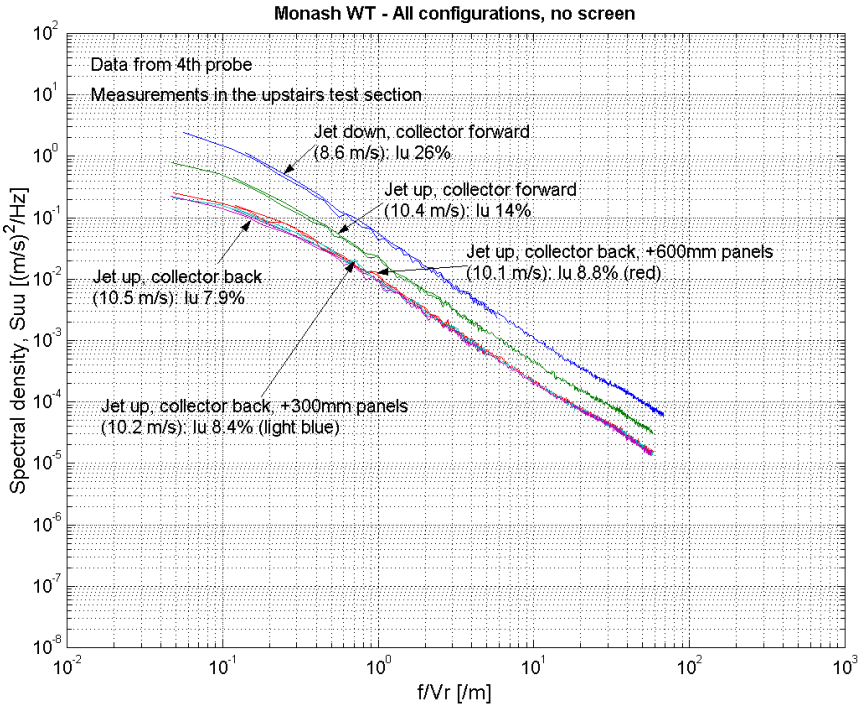

Figure 8: Absolute spectral levels, all configurations, no screen.

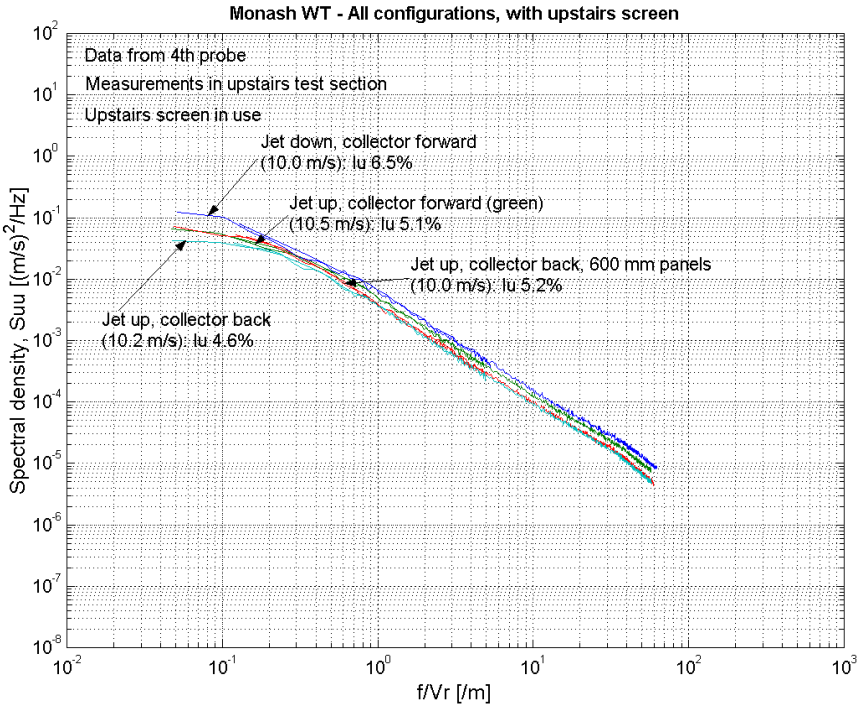

Figure 9: Absolute spectral levels, all configurations, with screen.

Figure 8 shows that without the use of the screen at the entrance of the wind engineering test section, changes in the tunnel configuration have a significant effect on the turbulence levels in the upper test section. Moving the jet up from the baseline configuration reduces turbulence levels by almost half, and moving the collector back then further reduces the turbulence levels by another third. The addition of the 300 mm wide and 600 mm wide panels upstream of the automotive test section is shown to have minimal effect on the turbulence levels in the wind engineering test section, most likely because the turbulence they generate has decayed by the time it travels from the lower to the upper test section.

Figure 9 shows overall lower turbulence levels during all configurations due to the smoothing effect of the screen at the entrance to the wind engineering test section. However, this also has the effect of reducing the differences between the various test configurations. Moving the jet up reduces the turbulence levels by 1/5, and moving the collector back further reduces levels by only another 1/10. Again, use of the panels has only a minimal effect on the turbulence levels in the upper test section.

The results in both Figure 8 and Figure 9 show a reasonable range of turbulence levels, which will be examined in further detail in Section 8 to ascertain whether or not they adequately simulate atmospheric turbulence conditions found during earlier on-road testing.

8 Replication of Atmospheric Turbulence in a Wind Tunnel

The main objective of measuring the turbulence characteristics in the Monash wind tunnel was to ascertain whether the tunnel flow conditions could be used to replicate those found in atmospheric turbulence in different terrains. Therefore, the Monash results were also compared to typical atmospheric turbulence found during earlier on-road testing. This was accomplished for two main conditions: a typical MAV flight speed, or indicated air speed (IAS), of 10 m/s; and for an effective IAS of 0 m/s, i.e. for an MAV effectively holding it's position with respect to the ground.

8.1 Comparison for an MAV speed of 10 m/s

In order to compare the on-road and Monash wind tunnel measurements, it is necessary to make some corrections to the raw data. If an MAV were flying through the atmosphere in a particular terrain, it would move with a particular indicated air speed (IAS) that is a combination of the atmospheric wind conditions within which it is flying and it's own propulsion. A typical IAS for the MAVs considered in this research is 10 m/s and this has accordingly been chosen as an appropriate point of reference for all measurements.

If an MAV were being tested in a wind tunnel, the most common testing configuration would be to mount or suspend the model on a sting, at a stationary position within the test section. Under these conditions, the correct tunnel speed to simulate an IAS of 10 m/s would be a tunnel flow speed of 10 m/s.

However, in taking measurements of atmospheric turbulence in the real world, wind conditions, instrumentation limitations and the effects of road conditions on vehicle speed mean that the overall relative velocity (equivalent to an IAS) will not be 10 m/s. Therefore the atmospheric data requires some correction to bring it to an IAS of 10 m/s. Firstly, this entails mathematically removing the mean vehicle speed (if there was one), thus bringing the data back to an equivalent stationary measurement consisting only of the ambient wind characteristics. Secondly, the data has a mean velocity component mathematically added back to it to simulate an IAS of 10 m/s, i.e. whatever the mean atmospheric wind speed, a mean u-component speed is added to the data to bring the mean relative velocity up to 10 m/s, thus simulating an MAV flying through the atmospheric wind at an IAS of 10 m/s[18]. By correcting the atmospheric data to an IAS of 10 m/s, it is thus possible to make a direct comparison between the two sets of data, atmospheric and wind tunnel data.

The first part of this correction procedure is justified because the on-road measurements were taken at an effectively constant vehicle speed, with only very low frequency fluctuations that are outside the frequency range of interest to this research and can therefore be neglected. Early testing with a Global Positioning System in the test vehicle verified this as well as providing a convenient way of calibrating the vehicle speedometer, thus ensuring a high level of confidence in the observed vehicle speed.

The second part of the correction procedure is necessary to properly simulate the statistical and spectral turbulence characteristics that an MAV flying through turbulence at an IAS of 10 m/s would actually experience. Moving through turbulent air structures changes the perceived turbulence levels, pitch and yaw angles from that perceived if an observer were stationary. This is because the overall u-component velocity, u, is integral to the calculation of all these parameters: turbulence intensities for the three velocity components, I_u, I_v and I_w; flow pitch angle, α; and the flow yaw angle, Ψ.

$$I_u = \frac{\sqrt{\overline{(u')^2}}}{\overline{Vr}} \quad I_v = \frac{\sqrt{\overline{(v')^2}}}{\overline{Vr}} \quad I_w = \frac{\sqrt{\overline{(w')^2}}}{\overline{Vr}}, \text{ where } \overline{V_r} = \overline{\sqrt{u^2 + v^2 + w^2}}$$

[18] As the measurements were taken into the ambient wind (i.e. a head wind situation), the indicated airspeed will always be greater than the perceived ground speed.

$$\alpha = \tan^{-1}\left(\frac{w}{u}\right), \quad \psi = \tan^{-1}\left(\frac{v}{u}\right)$$

When MAV propulsion adds an extra mean component of speed to that of the ambient wind, the above equations become:

$$J_u = \frac{\sqrt{\overline{(u')^2}}}{\overline{Vr}} \quad J_v = \frac{\sqrt{\overline{(v')^2}}}{\overline{Vr}} \quad J_w = \frac{\sqrt{\overline{(w')^2}}}{\overline{Vr}}, \text{ where } \overline{V_r} = \overline{\sqrt{(u+V_{MAV})^2 + v^2 + w^2}}$$

$$\alpha = \tan^{-1}\left(\frac{w}{(u+V_{MAV})}\right), \quad \psi = \tan^{-1}\left(\frac{v}{(u+V_{MAV})}\right)$$

where V_{MAV} is the speed of the MAV relative to a stationary observer, i.e. ground speed. (Note that with the addition of the vehicle speed, the turbulence intensity is given by J_i, rather than I_i, the latter being used only for ambient atmospheric turbulence and the former for the turbulence perceived by a moving object.)

In all cases the denominator will increase due to an added speed component in the x-direction, but the numerator remains unchanged[19], thus the turbulence intensities, pitch and yaw angles are all decreased when flying into an ambient wind at a given speed than if a vehicle or person were stationary in the same wind conditions[20].

The above observations have important implications for MAV response and control and it is therefore essential to correctly simulate these characteristics when comparing atmospheric to wind tunnel data. Whatever nominal speed is chosen as the relevant IAS of interest for MAV control, measurements taken in atmospheric turbulence must be corrected to achieve this IAS in order to simulate the conditions experienced by an MAV, at that speed, in real atmospheric turbulence.

The following sections compare the data taken in the Monash wind tunnel with data taken in various wind conditions and terrains during on-road measurements (for an MAV IAS of 10 m/s). Comparisons are made by examining the spectral content of the velocity components and the fluctuation levels in pitch angle variation with lateral spacing.

8.1.1 Spectral Levels

Spectral levels of flow velocity components give an indication of the amount of velocity fluctuation in a given component versus frequency. Spectral levels, as they are plotted here, are in units of $\overline{(m/s)^2}/Hz$ (or mean square velocity per Hertz) and each point in a spectral plot is essentially the variance (or fluctuation level) of the velocity component at that frequency (see Appendix B, Section 12.1, for the calculation procedure for energy spectra). In contrast turbulence intensities (I_u, I_v, I_w, J_u, J_v, J_w) are overall normalised measures of the velocity-component fluctuations. Spectral levels and turbulence intensities are thus closely related, with the latter being a single figure estimate of the velocity fluctuations without any frequency information. However, in simulating flow conditions for dynamic and response applications it is very important to simulate the flow fluctuations at frequencies of interest, rather than the overall turbulence levels. Thus spectral levels provide important information that turbulence intensities do not. For this reason, Monash wind tunnel and atmospheric turbulence data are compared by plotting their energy spectra versus wave number, $k = f/V_r$ (essentially, frequency scaled with mean flow speed, or inverse wave length of the turbulence structures).

The results presented in this section are annotated with the longitudinal turbulence intensity for each configuration, where I_u indicates the natural longitudinal turbulence level in the atmospheric wind, and

[19] Note that *u'* is the instantaneous fluctuating part of the overall flow u-component, i.e. it is that part of *u* minus any mean component, and it is therefore unchanged by the addition of a mean velocity component.

[20] This is true whether flying into the wind or downwind, as long as the mean ambient wind speed is < 10 m/s and the added mean component V_{MAV} brings the mean relative velocity or IAS up to 10 m/s.

J_u is the resulting longitudinal turbulence level if an MAV was moving through that atmospheric wind with an indicated air speed (IAS) of 10 m/s. The atmospheric spectra in each plot have been corrected to an IAS of 10 m/s, while the Monash spectra in each plot were measured with a tunnel speed of ~10 m/s, thus simulating an IAS of 10 m/s if an MAV model were mounted stationary in the tunnel for testing. Plots of u-component spectra for selected cases are presented here, while the spectra for the v- and w-components are in Appendix F, Section 16. Comparisons between the spectral turbulence levels in the Monash wind tunnel and atmospheric turbulence for gentle (Figure 10), moderate (Figure 11) and fresh (Figure 12) breezes in various terrains are shown below.

Above a wave number (k) of ~0.5, the wind tunnel and atmospheric data coincide very well (within the plotted confidence levels of ±25%), and show that a wind tunnel configuration can be found to simulate the turbulent velocity fluctuations, for a moderate range of wind and terrain conditions and an MAV speed of 10 m/s, above this wave number.

In contrast, the overall turbulence intensities for an equivalent MAV speed of 10 m/s (J_u) are significantly different between the Monash wind tunnel data and that of the atmospheric turbulence, with the latter usually being at least three times larger than the former. This is because the atmospheric turbulence includes large length scale (i.e. low frequency) turbulence that is not found in the Monash wind tunnel. This is reflected in the spectral plots by the difference between the wind tunnel and atmospheric data below a wave number of ~0.5. The larger spectral levels in the atmospheric data below k = 0.5 cause corresponding larger levels in J_u, and illustrate why comparing the overall turbulence intensities is not appropriate in this situation.

It has previously been determined that the frequency range of most relevance to an MAV with a 150 mm wingspan is between wave numbers of 0.7 to 65, and so the agreement in spectral levels between the wind tunnel and atmospheric data within this range is good. The conclusion that can be drawn from this is that various configurations in the Monash wind tunnel simulate light to moderate wind conditions in built-up to more open terrains quite well for the purposes of testing MAV control.

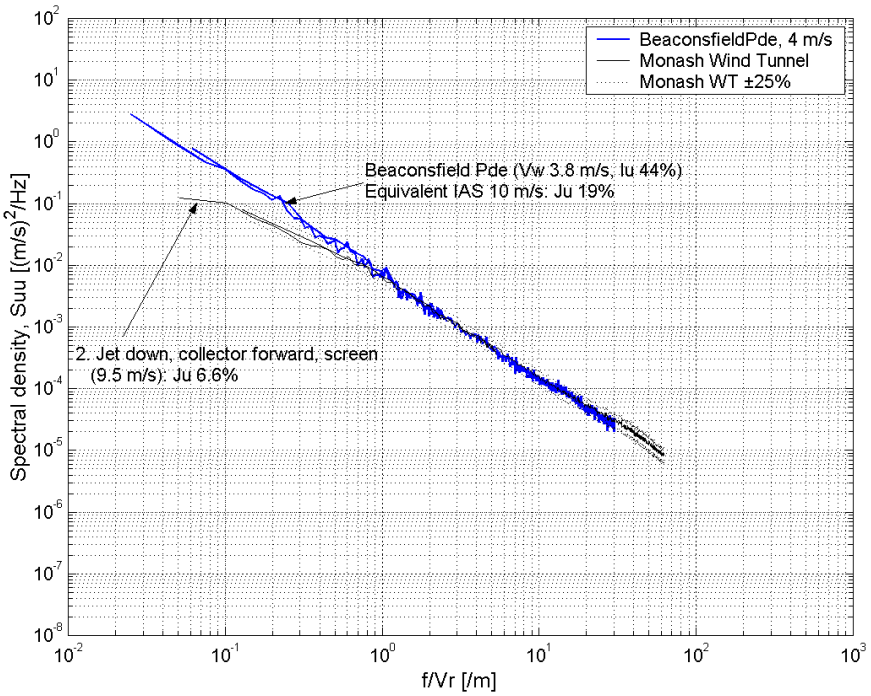

Figure 10: Comparison of u-component spectral levels in a gentle breeze: metropolitan area, terrain 7-2 (built-up urban area, 2-3 story buildings, with prevailing wind from across the city).

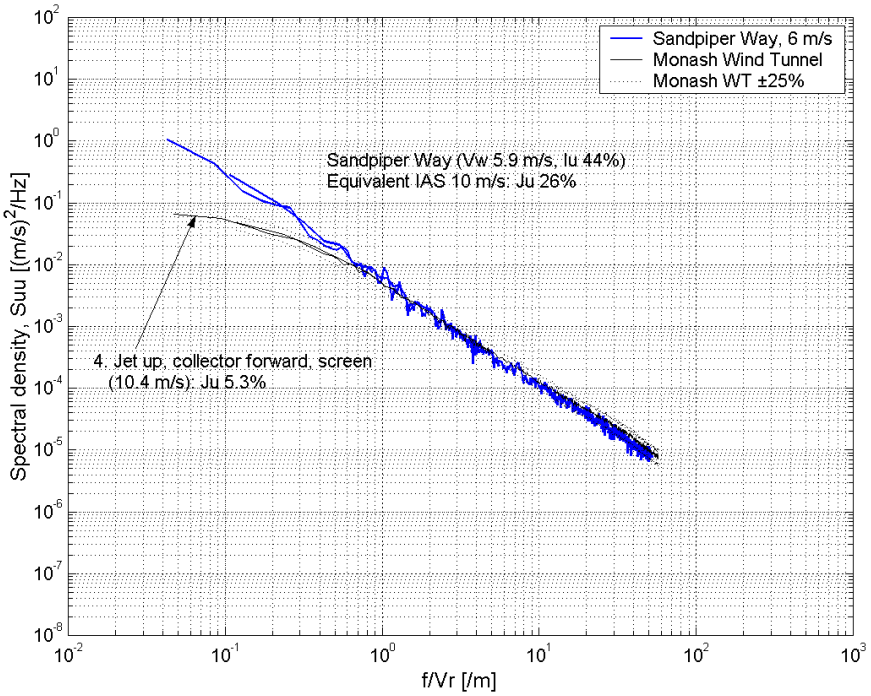

Figure 11: Comparison of u-component spectral levels in a moderate breeze: low suburbs, terrain 6-2 (low, well-spaced buildings and no high trees).

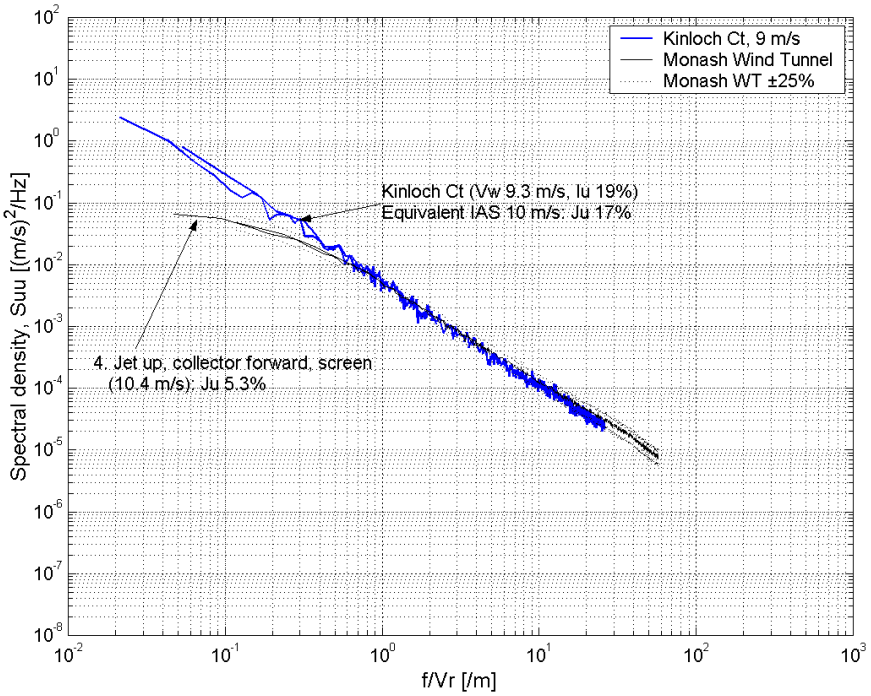

Figure 12: Comparison of u-component spectral levels in a fresh breeze: open farmland, terrain 4-2 (low crops and plant cover, occasional obstacles separated by > 20H).

However, for an MAV wingspan of 1 metre, for which the relevant frequency range extends over wave numbers of 0.1 to 10, the wind tunnel cannot simulate the large length scales necessary to adequately replicate the spectral levels. For the testing of larger MAVs, other methods of generating turbulence within the wind tunnel (other than passive configuration changes) are required, and this is discussed further in Section 8.4.

Figure 13 shows the spectral turbulence levels in the Monash wind tunnel versus atmospheric turbulence in a light breeze in very open terrain. It can be seen that over the relevant frequency range (k = 0.7 to 65), the atmospheric turbulence levels are ~90% lower than those found in the wind tunnel. So even with the tunnel in its smoothest configuration, it cannot simulate the turbulence found in the atmospheric boundary layer under these conditions. This could be improved with the addition of extra screens immediately upstream of the test section, and/or other major alterations to the tunnel structure. However, the use of a specifically aeronautical tunnel (as opposed to a wind-engineering and automotive tunnel), with very smooth flow, would make more sense.

The inability to simulate smoother conditions in the wind tunnel used for this testing is not considered a problem, as it is necessary to test MAV control under the more challenging wind conditions in order to develop control systems that can cope with the range of wind conditions found in the atmospheric boundary layer. It does illustrate, however, that the ability to achieve the complete range of wind conditions found in the atmospheric boundary layer in one facility will be a significant challenge. Whether using a wind-engineering tunnel, such as the Monash wind tunnel, where it may be difficult to simulate smoother wind conditions, or an aeronautical tunnel, where simulating more turbulent conditions and large length scales can be problematic, either option will require significant, expensive and large alterations to the tunnel structure in order to achieve the complete range of atmospheric turbulent fluctuations.

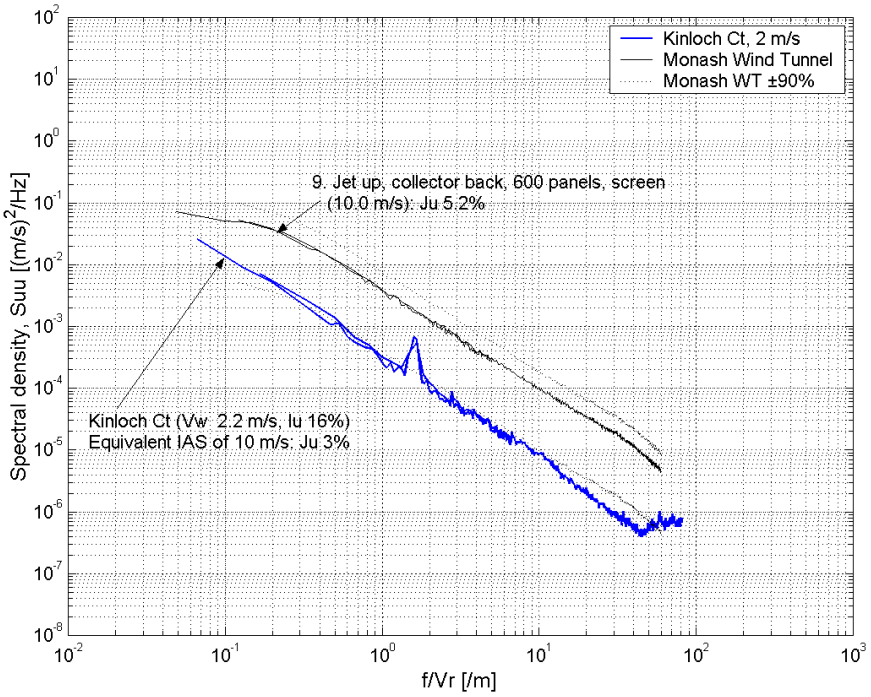

Figure 13: Comparison of u-component spectral levels in a light breeze: open farmland, terrain 4-2 (low crops and plant cover, occasional obstacles separated by > 20H).

8.1.2 Fluctuations in pitch variation with lateral spacing

Pitch variation is defined here as the difference in pitch angle between two laterally spaced points on the MAV wingspan (or two laterally spaced flow measurements using the Cobra Probes),

$$\Delta\alpha_{ij} = \alpha_j - \alpha_i$$

Therefore a measure of the fluctuation in the pitch variation between two such points is given by the standard deviation of the pitch variation, $\sigma_{\Delta\alpha}$.

$$\sigma_{\Delta\alpha} = \lim_{T\to\infty}\sqrt{\frac{1}{T}\int_{t=0}^{T}\left(\Delta\alpha(t) - \overline{\Delta\alpha}\right)^2 dt}$$

The magnitude of pitch variation fluctuation has units of degrees (°). This quantity has a direct impact on the difference in lift generated at the two points on the wingspan, and therefore on the amount of roll input to an MAV wing. It is, however, an overall measure of the roll input for a given lateral spacing, and does not take account of the frequency information contained within the turbulent structures (i.e. turbulent length scales). This is analogous to the way that turbulence intensities are overall measures of velocity fluctuations but contain no information about the magnitude of those velocity fluctuations with frequency.

However, the lateral spacing in itself ensures that the pitch variation fluctuation only contains information from the smaller length scales (in effect acting as a high pass filter), as length scales of the order of or larger than the measurement point spacing should have a similar pitch angle at the two points and therefore not contribute significantly to observed variations in pitch angle. In this respect, some frequency information is contained within the pitch variation fluctuation parameter.

Although pitch variation fluctuation does not completely reflect the frequency information inherent in turbulent flow fluctuations, it is still a measure of the overall roll inputs to an MAV wing in atmospheric turbulence. Therefore, as a first step, the Monash wind tunnel and atmospheric turbulence data are compared using pitch variation fluctuation. The atmospheric turbulence data in each plot have been corrected to an IAS of 10 m/s before calculation of the pitch variation fluctuation, while the Monash wind tunnel data were measured with a tunnel speed of ~10 m/s, thus simulating an IAS of 10 m/s if an MAV model were mounted stationary in the tunnel for testing. Comparisons between the pitch variation fluctuations in the Monash wind tunnel and atmospheric turbulence for gentle (Figure 14), moderate (Figure 15) and fresh (Figure 16) breezes, in various terrains, are shown below. These plots use the same data as that presented earlier in Section 8.1.1.

The pitch angle coherence, a more complete measure of the pitch angle correlation between two points in space with frequency was also calculated for all data collected. However, as the pitch variation fluctuation was found to provide the information required in order to evaluate the atmospheric and wind tunnel environments for the purposes of answering the research objectives, analysis of this more complex parameter is not included in this report, but is left for future work.

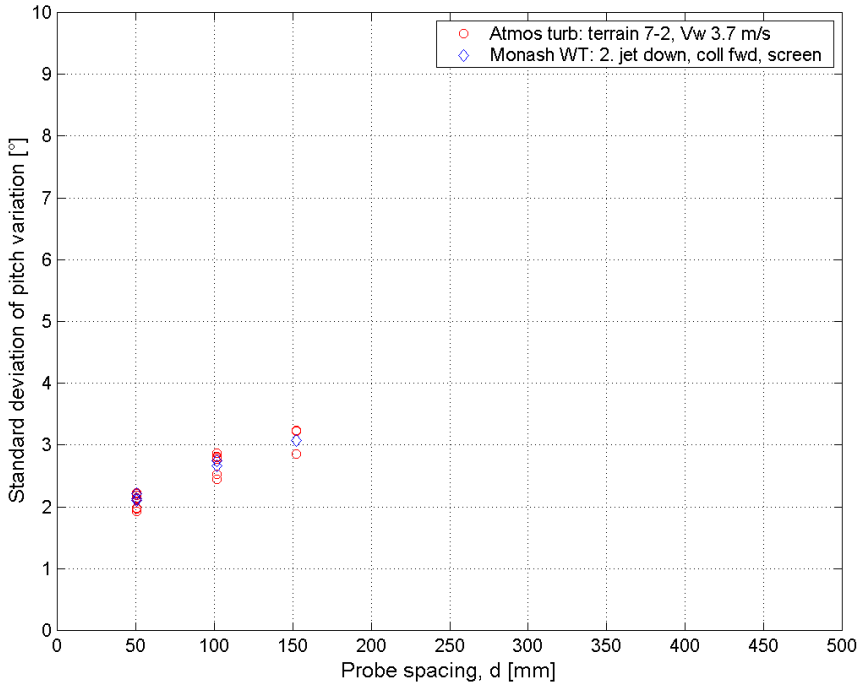

Figure 14: Comparison of fluctuation levels in pitch variation with lateral spacing in a gentle breeze: metropolitan area, terrain 7-2 (built-up urban area, 2-3 story buildings, with prevailing wind from across the city).

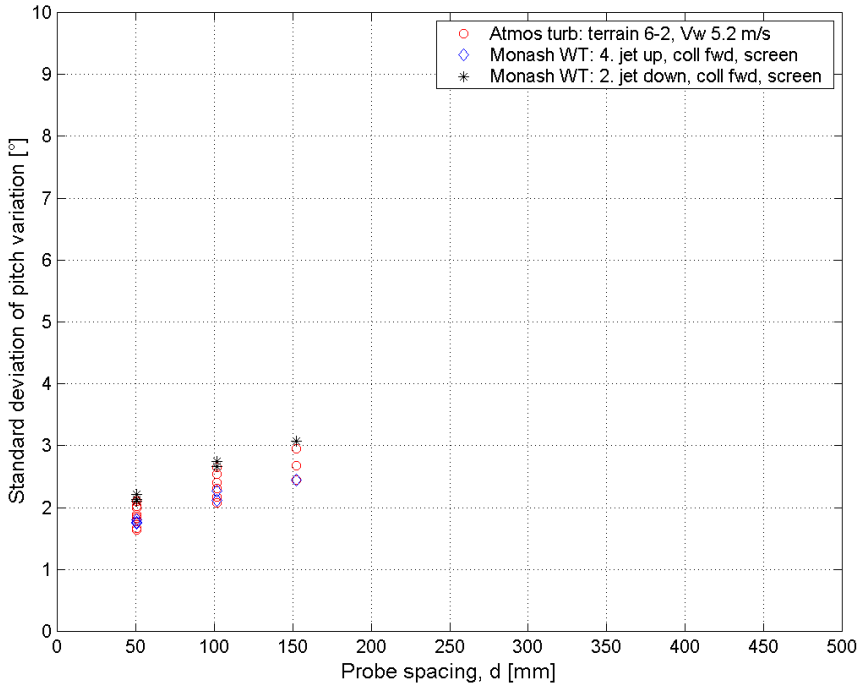

Figure 15: Comparison of fluctuation levels in pitch variation with lateral spacing in a moderate breeze: low suburbs, terrain 6-2 (low, well-spaced buildings and no high trees).

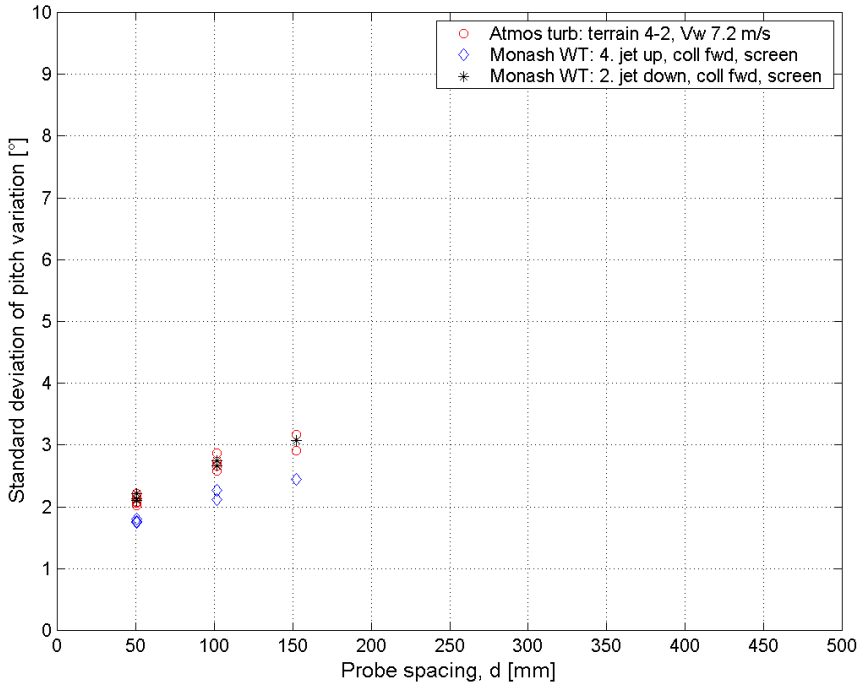

Figure 16: Comparison of fluctuation levels in pitch variation with lateral spacing in a fresh breeze: open farmland, terrain 4-2 (low crops and plant cover, occasional obstacles separated by > 20H).

All three plots compare the atmospheric turbulence data to the Monash wind tunnel configurations that were found to best match the atmospheric energy spectra previously shown in Section 8.1.1 (Figure 10 to Figure 13). Figure 14 shows that the same wind tunnel configuration as that used in Figure 10 for the spectral results also produces a very good match with pitch variation fluctuations. However, Figure 15 and Figure 16 show that the data for best tunnel configuration in Section 8.1.1 (blue diamonds) does not necessarily produce the best match in pitch variation fluctuations. These latter two figures also plot the atmospheric data against another Monash wind tunnel configuration (black stars) that could be interpreted to provide a better or more appropriate match.

The difference in the most appropriate wind tunnel configuration to match particular atmospheric turbulence conditions can be understood by further examining the flow pitch angle spectra. In Section 8.1.1, the velocity spectra were examined and used to determine the best tunnel configuration. However, the velocity spectra are produced from data of only one velocity component, that of *u*, *v* or *w*. Pitch angle is determined by a combination of two velocity components, *u* and *w*, and the best tunnel configuration may be better indicated by energy spectra of the flow pitch angle.

Figure 19 shows the pitch angle spectra for the case presented in Figure 14, where a good match with the same wind tunnel data was found in the u-component spectra and the pitch variation fluctuation. While Figure 18 shows the pitch angle spectra for the case presented in Figure 16, where the pitch variation fluctuation did not indicate such a good match. Both figures indicate that the original Monash case determined as a good match for the atmospheric data (black line) is a reasonable match to the atmospheric data down to a wave number *k* of 0.6 in Figure 19 and 1.5 in Figure 18. It is the critical region between a *k* of 0.6 and ~1.5 that appears to be the cause of the mismatch in pitch variation fluctuation. The second wind tunnel case, determined in Figure 16 to be a better match for the pitch variation fluctuation, is also plotted in Figure 18 (green line) and can be seen to be a better fit to the atmospheric data between wave numbers of 0.6 – 1.5. The somewhat higher spectral levels at wave numbers above 1.5 is probably not critical, as the pitch variation fluctuations at the lower wave numbers would tend to swamp the contributions from these higher frequency regions.

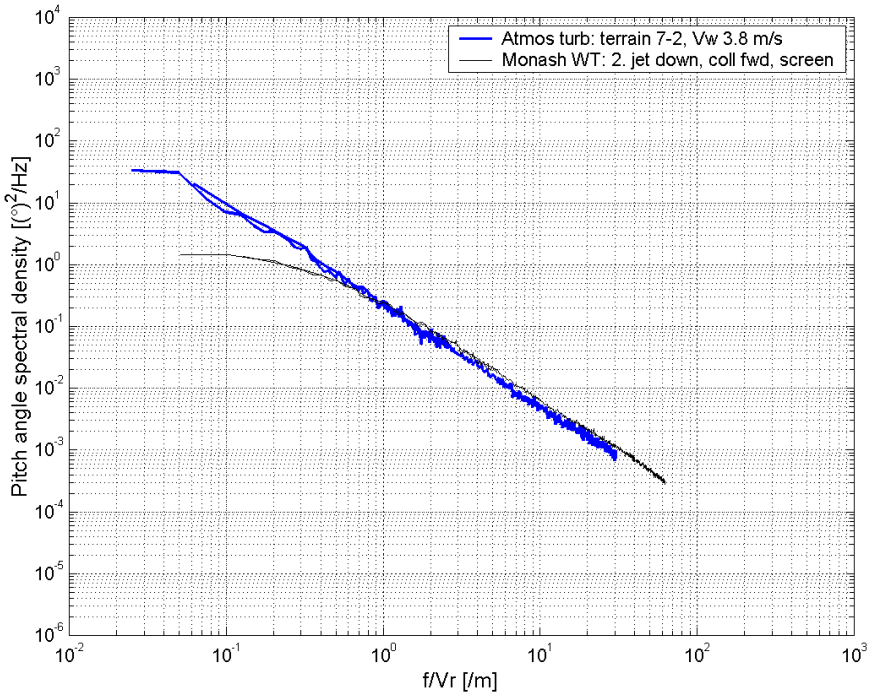

Figure 17: Comparison of pitch angle spectral levels in a gentle breeze: metropolitan area, terrain 7-2 (built-up urban area, 2-3 story buildings, with prevailing wind from across the city).

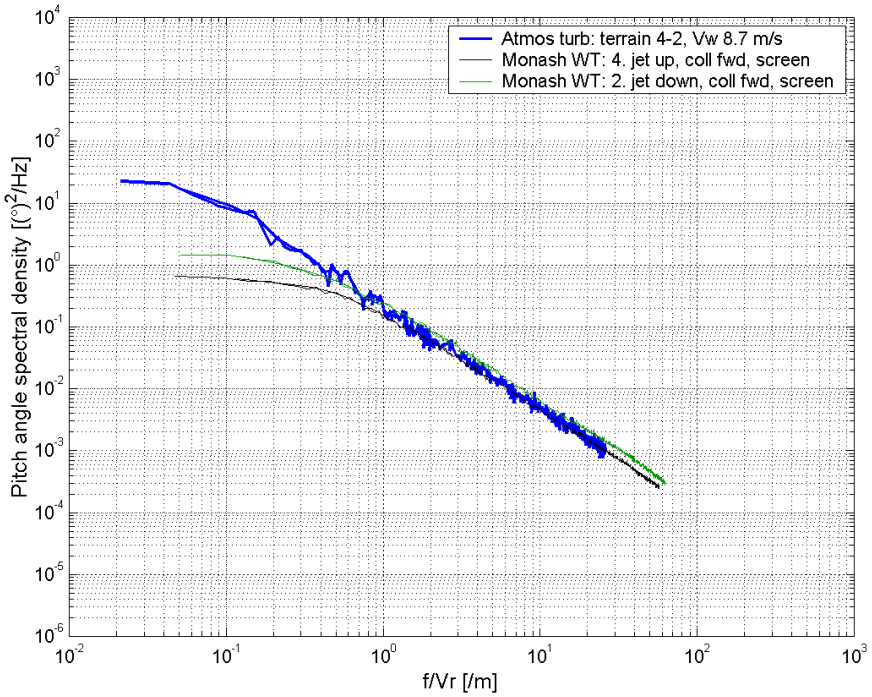

Figure 18: Comparison of pitch angle spectral levels in a fresh breeze: open farmland, terrain 4-2 (low crops and plant cover, occasional obstacles separated by > 20H).

So it appears that, in terms of matching a suitable tunnel configuration to given atmospheric conditions in a particular terrain, pitch angle energy spectra and pitch variation fluctuations are the more suitable means of comparing the two environments for the purposes of significant roll inputs to an MAV wing. It also appears that higher frequency spectral levels, above a wave number of 2 are probably not as important as wave numbers between 0.6 and 2 for 50 mm spaced measurement points. Below a wave number of ~0.6, the turbulent length scales in this region do not appear to significantly affect the pitch variation fluctuation for the given atmospheric data *and* 50 mm spaced measurement points.

Finally, Figure 19 shows the pitch variation fluctuations for the spectral levels presented earlier in Figure 13, and again show the large disparity between the atmospheric and wind tunnel data in open terrain and very light wind conditions. This reinforces the conclusion in Section 8.1.1 that even with the tunnel in its smoothest configuration, it cannot simulate the turbulence found in the atmospheric boundary layer under these conditions. As stated earlier, simulating such smooth conditions for the testing of MAV control is not considered of high importance, as it is the more challenging turbulence conditions that are required to develop control systems able to cope with a range of wind conditions.

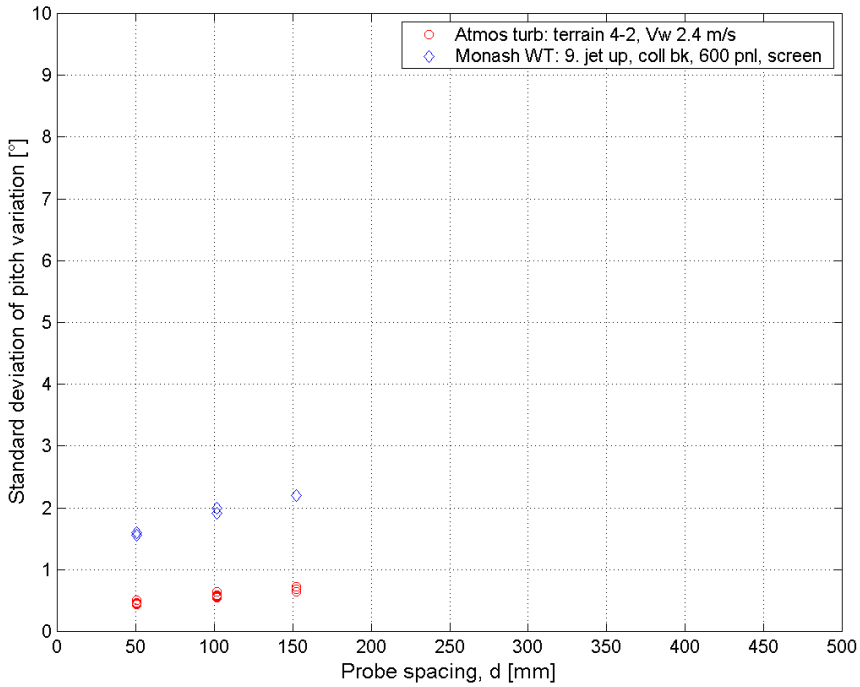

Figure 19: Comparison of fluctuation levels in pitch variation with lateral spacing in a light breeze: open farmland, terrain 4-2 (low crops and plant cover, occasional obstacles separated by > 20H).

8.2 Comparison for a stationary MAV (effective ground speed 0 m/s)

As moving more quickly through turbulence reduces the effective turbulence levels (J_u) experienced by a moving object, comparing the data at an IAS of 10 m/s gives lower turbulence levels than if the data were compared at a IAS equivalent to the prevailing wind speed, i.e. an effective ground speed of 0 m/s or hovering. Trying to hold a stable position or hover in turbulence is a worst-case scenario and requires larger length scales in order to be properly simulated within a wind tunnel. This is illustrated in Figure 20, Figure 21 and Figure 22 below, where atmospheric data consisting only of the ambient wind characteristics (i.e. the data has not been corrected to an IAS of 10 m/s) is directly compared to data from the Monash wind tunnel at approximately the same speed. As the wind tunnel speed must be matched to the atmospheric ambient wind speed in order to make this comparison,

and only two tunnel speeds were used during testing, there are limited on-road cases available for comparison.

The figures below indicate that for the cases chosen, the Monash wind tunnel is able to produce pitch angle turbulence levels of the right order of magnitude, as there is generally a tunnel configuration that produces both higher and lower spectral levels than that found in the atmospheric data. In each case, the Monash configuration that produces lower spectral levels than that found in the atmospheric data could better simulate the atmospheric conditions by the addition of extra turbulence generation panels immediately upstream of the test model. It is likely, however, that the spectral levels could only be matched down to a wave number of ~1 to 1.5, and thus the use of active turbulence generation would most likely be required in order to sufficiently simulate the atmospheric conditions for a stationary MAV (see Section 8.4 for further discussion on active turbulence generation). But it can be concluded that for the range of cases shown, that it is possible to simulate the atmospheric conditions for light to moderate winds in a wind tunnel, in order to simulate an MAV with an effective ground speed of 0 m/s.

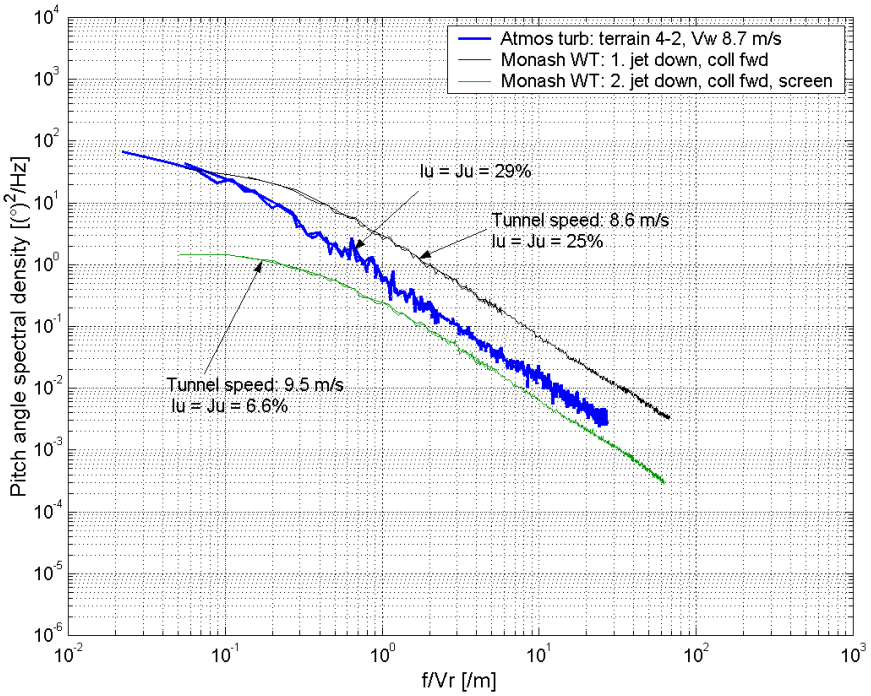

Figure 20: Comparison of pitch angle spectral levels in a fresh breeze (IAS 8.7 m/s, ground speed 0 m/s): open farmland, terrain 4-2 (low crops and plant cover, occasional obstacles separated by > 20H).

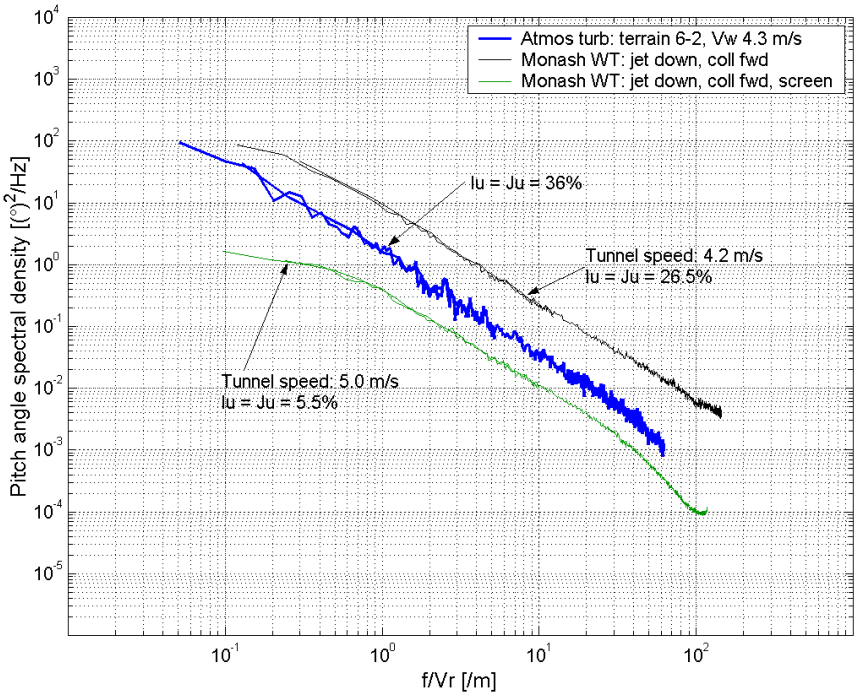

Figure 21: Comparison of pitch angle spectral levels in a gentle breeze (IAS 4.3 m/s, ground speed 0 m/s): low suburbs, terrain 6-2 (low, well-spaced buildings and no high trees).

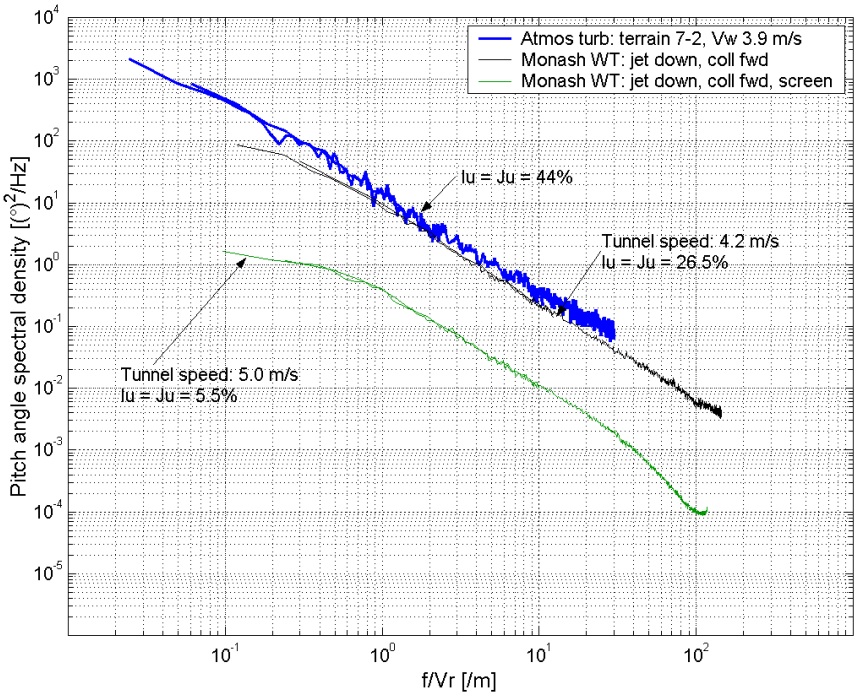

Figure 22: Comparison of pitch angle spectral levels in a gentle breeze (IAS 3.9 m/s, ground speed 0 m/s): metropolitan area, terrain 7-2 (built-up urban area, 2-3 story buildings, with prevailing wind from across the city).

8.3 Normalisation of Pitch Variation Fluctuation

As pitch variation appears to be a useful single figure measure of possible roll inputs at a given point on a wing, it is instructive to examine it further and determine whether it has certain universal properties within the turbulence environments examined in this research. This entails investigating whether or not appropriate normalisation can cause the pitch variation fluctuation data from all measurements to collapse, thus illustrating a common or underlying relation.

In terms of an underlying functional relationship between pitch variation fluctuation and measurement spacing there is evidence for a logarithmic trend. When pitch variation fluctuations from a single measurement with the four probes (in a particular terrain and wind conditions) are plotted, and a logarithmic trend is fitted, the regression coefficient for the fit is typically 0.98-0.99 for the majority of atmospheric data taken. An example of this is shown in Figure 23 below. Note that there are actually six data points on this plot, as a single measurement with the four probes produces 6 total combinations of measurement spacings: three 50 mm spacings between probes 1 to 2, 2 to 3, and 3 to 4; two 100 mm spacings between probes 1 to 3, and 2 to 4; and finally one 150 mm spacing between probes 1 to 4.

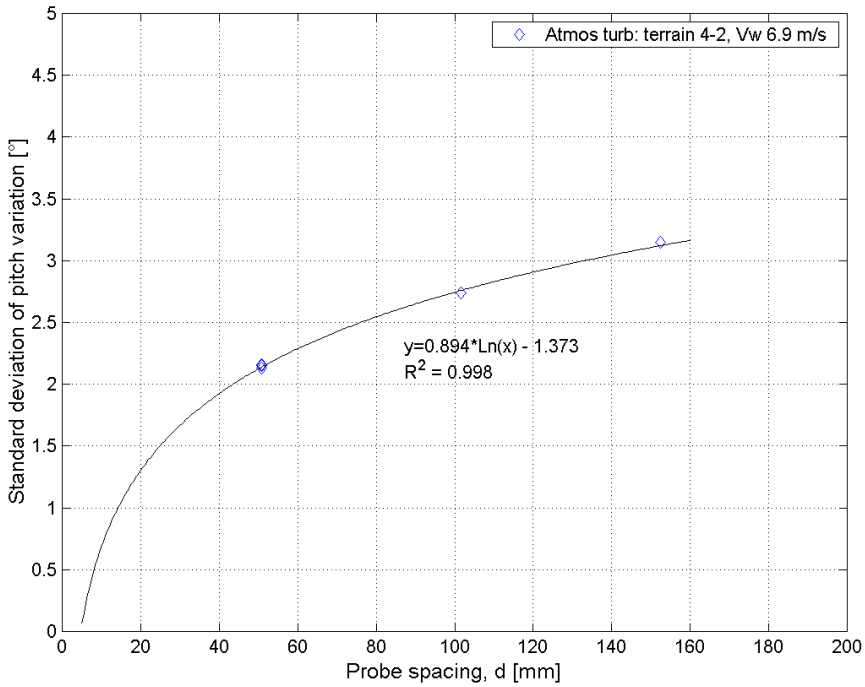

Figure 23: Pitch variation fluctuation levels with lateral spacing in a light breeze: open farmland, terrain 4-2 (low crops and plant cover, occasional obstacles separated by > 20H).

If all the data from the wind tunnel measurements and a selection of data from the atmospheric measurements are plotted on the same plot without any normalisation, Figure 24 results. (The reason for only plotting a selection of the atmospheric data will become apparent after the normalisation is discussed below.) As can be seen in Figure 24, there is no apparent trend to the data as a whole, despite the already observed logarithmic trend noted in each individual set of measurements (Figure 23).

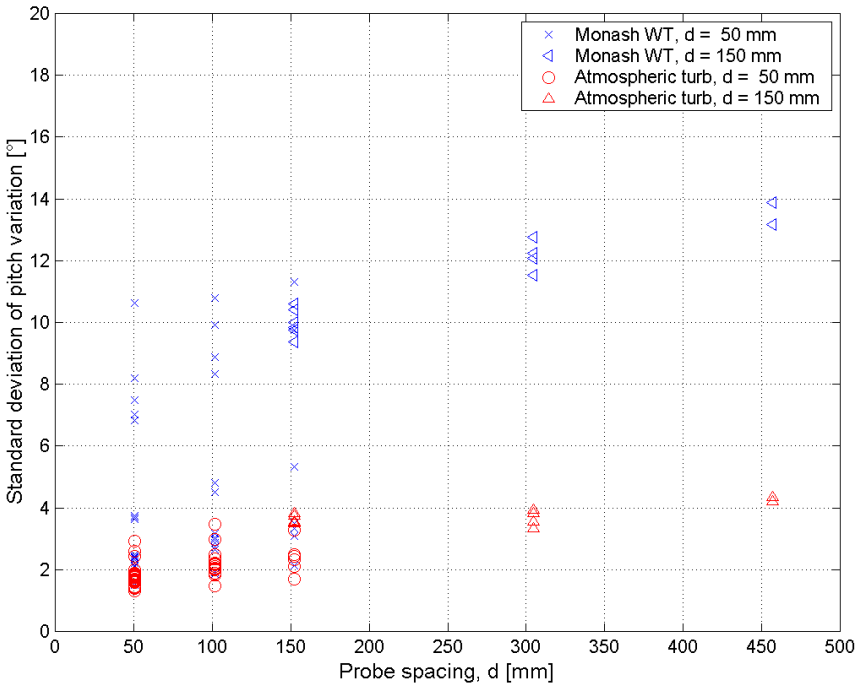

Figure 24: Pitch variation fluctuation levels for both wind tunnel and atmospheric data with no normalisation. All atmospheric data has been corrected to an equivalent IAS of 10 m/s, and wind tunnel data was taken at a tunnel speed of 10 m/s.

In order to normalise pitch variation fluctuation, it is necessary to do so in both the independent variable (probe spacing) and the dependant variable (pitch variation fluctuation). For the latter, as it is the standard deviation of the difference in pitch angle between two points, the standard deviation of the pitch angles at the individual points would seem appropriate measures for normalisation.

$$\frac{\sigma_{\Delta\alpha}}{\sqrt{\sigma_{\alpha_i}\sigma_{\alpha_j}}}$$

For normalisation of the independent variable, the spacing between measurement points has dimensions of length, and it is expected that the difference in pitch angle between two laterally spaced points would depend on the length scale of the turbulent flow structures that are convecting past those points. That is, if a turbulent structure was of the order of, or much larger than, the spacing between the measurement points, it is expected that the pitch angle measured at those two points would be very similar, thus giving a small or negligible pitch variation. While for length scales much smaller than the measurement point spacing, there should be no correlation between the pitch angles at the points and therefore large pitch variation. So it seems reasonable that the characteristic length scale of the turbulent flow would be appropriate to normalise the measurement point spacing.

$$d / L_x \text{ or } d / L_y$$

If the same data from Figure 24 is taken and normalised as discussed above, Figure 25 shows the resulting data trend. Note that in order to get reasonable estimates of the length scale L_x, it was necessary to only use data that had particularly long time samples, e.g. 5 minutes or greater. This was the reason for only using a selection of the atmospheric measurements, as many of them only consisted of ~60 second samples. The atmospheric data used is therefore limited to terrains where long measurements were taken; typically more open farmland, rather than built-up areas, as there was more chance of getting samples uninterrupted by traffic and in positions not in the immediate wake of any particular object.

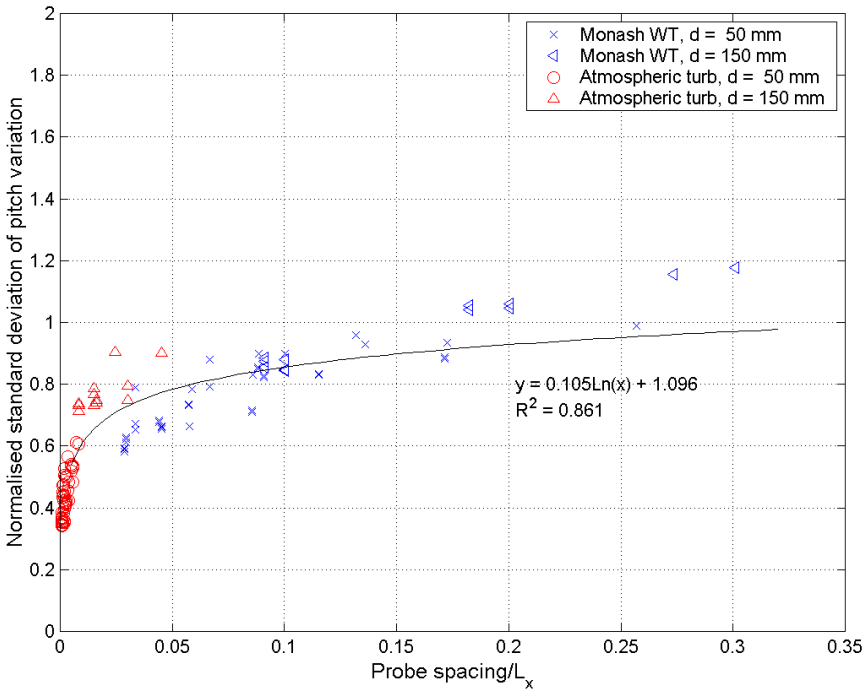

Figure 25: Pitch variation fluctuation levels for both wind tunnel and atmospheric data; y-axis normalised with the individual pitch fluctuation levels, x-axis normalised with the longitudinal length scale, L_x. All atmospheric data has been corrected to an equivalent IAS of 10 m/s, and wind tunnel data was taken at a tunnel speed of 10 m/s.

The only data used with significantly shorter time samples was the atmospheric data with 150 mm spacing. This data was from early investigatory measurements taken 3 years ago, where the time samples were limited to 100 seconds. Because of this, the length scale estimates for this data are felt to be more inaccurate, and may explain why this particular data does not appear to fall in with the observed trend quite as well.

There is also a fair amount of scatter in the overall data collapse, most likely due to the uncertainties in the length scale values, which were very hard to consistently determine even with 5-10 minute samples. Despite this, the regression coefficient for a logarithmic fit to the data in Figure 25 is still 0.861. Given the two different data sets (wind tunnel and atmospheric data), and the variety of wind conditions and open-country terrain, this is a reasonable collapse of the data.

Normalising the probe spacing using L_y produces a similar collapse of the data, with a logarithmic trend with a slightly lower regression coefficient. Without better length scales estimates it is not possible to evaluate the relative merits of normalisation using L_x or L_y, although as the measurements are laterally spaced, L_y may be a more rigorous choice of normalisation parameter. However, the results show that normalising by a longitudinal length scale appears to be an appropriate measure. That the underlying functional relationship is logarithmic is also clearly shown by the results. There is undoubtedly a theoretical explanation for such a logarithmic trend based on the fundamental equations describing turbulent flow. However, an exploration of this aspect is beyond the scope of this research project.

Finally, it is pleasing to see that the wind tunnel and atmospheric data appear to collapse onto the same trend, as this indicates that the two sets of data are just from different parts of the turbulence spectrum; both sets of data exhibit similar properties, but with different length scales and therefore frequency content. This had already been inferred from the fact that the Kolmogorov slope of –5/3 had already been shown to fit the wind tunnel spectra very well, thus illustrating that the turbulent cascade observed in many atmospheric flows was also present within the wind tunnel flow. This gives

confidence that the wind tunnel flow has the correct turbulence properties to simulate the observed atmospheric winds, as long as the pitch angle spectral levels and pitch variation fluctuations are also suitable within the required frequency range. Not all wind tunnel flows will necessarily have these properties and so it is important to check them before deeming a particular tunnel suitable for the dynamic testing of MAVs.

8.4 Additional Turbulence Generation Methods

In addition to the basic tunnel configuration changes used in Section 7.1 to affect the tunnel turbulence levels, other methods are also applicable. Large bluff objects or plates at the entrance to the wind engineering test section would significantly increase the turbulence levels, but the scale of turbulence generated would be limited to the size of the object (which is itself limited due to blockage considerations in the test section in order not to overload the fans).

Another method of increasing the turbulence levels, and more importantly the scale of turbulence within the test section, is to actively generate turbulence using an oscillatory motion (Figure 26). This technique was used by Cheung et al (2003) using a 600 mm high active paddle or flap mounted on the floor of the automotive (lower) test section at the jet exit. The flap was as wide as the jet, hinged at the attachment point on the floor, and was activated by a pneumatic cylinder to oscillate with adjustable stroke and frequency.

In Cheung el al (2003), the final settings that gave the most satisfactory results with regard to increased length scale involved oscillations of the flap from approximately –5° to 35° from vertical at a frequency of 0.08 Hz. This increased the longitudinal length scale (L_x) within the upper test section by approximately a factor of 6, from 0.14 m to 0.80 m, and moved the velocity spectrum to the left (see Figure 26). Such an increase would be required in order to better simulate atmospheric turbulence characteristics for MAVs with wingspans of the order of 1 m.

Unfortunately, the active paddle equipment was unavailable at the time of the current test sessions in the Monash wind tunnel. However, the results shown in Figure 26 give confidence that such a turbulence generator could simulate the correct turbulence characteristics for larger MAVs, not only in the Monash wind tunnel but also in other facilities. Variables that would affect the amount and size of turbulence generated include the position of the turbulence generator within the tunnel circuit, the amount and frequency of oscillation, and the size of the flap used. Using such a device allows the generation of larger length scales that would not otherwise be possible by passive methods within a wind tunnel, and is therefore a valuable tool for better simulating the turbulence levels and scale found in atmospheric turbulence.

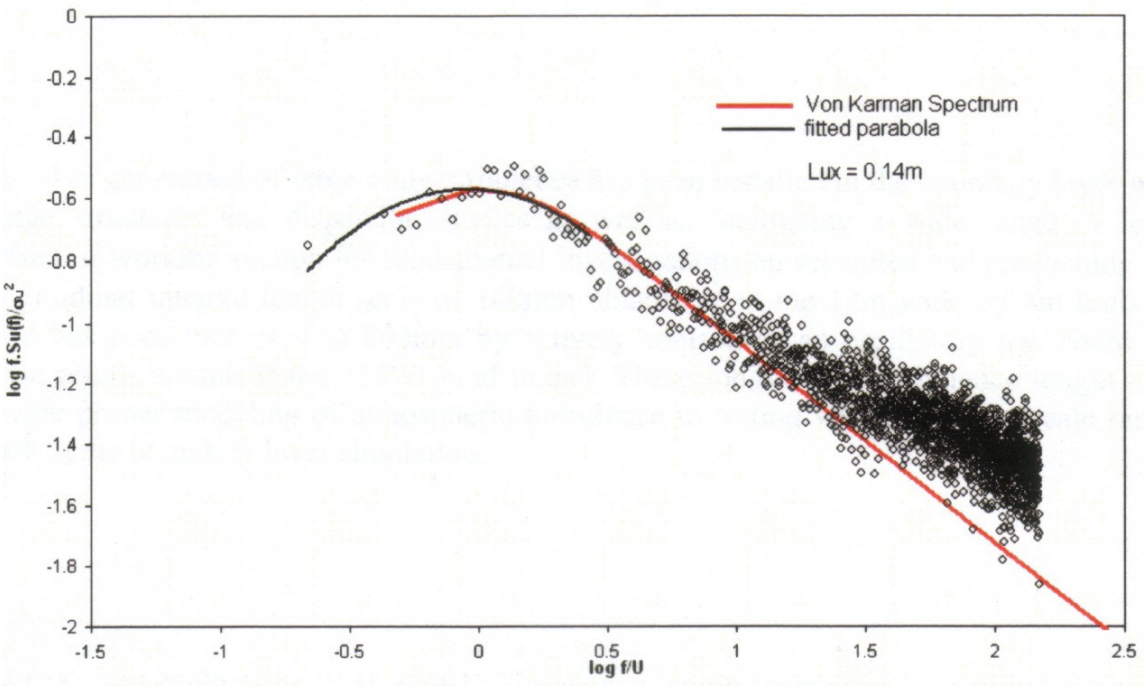

(a)

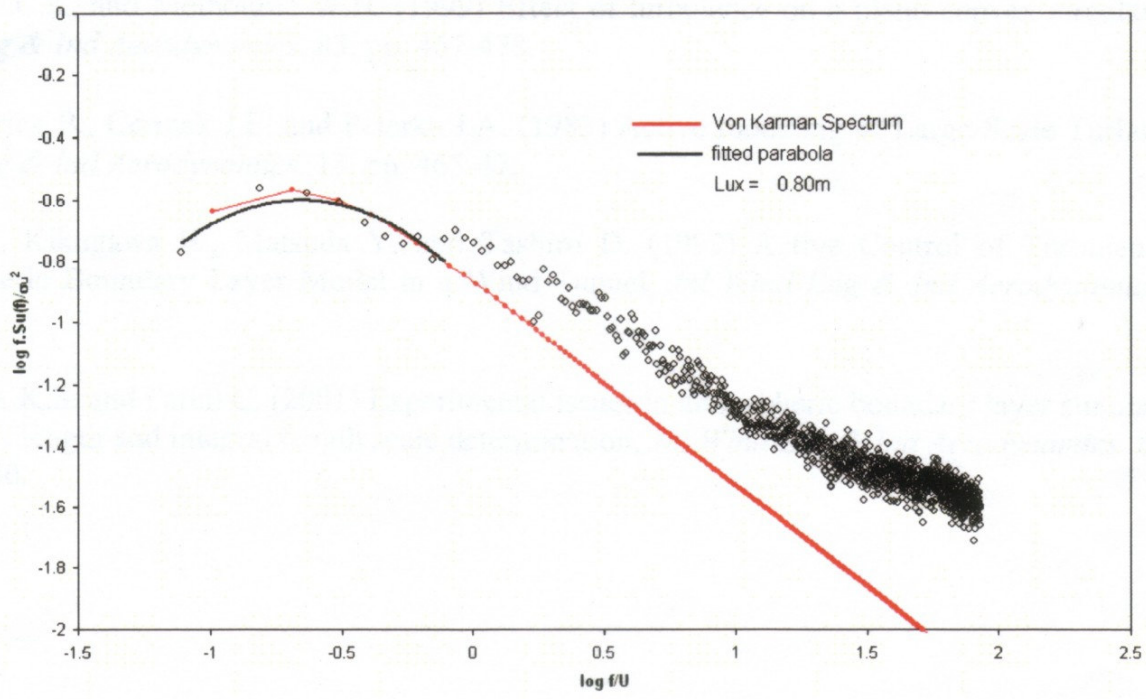

(b)

Figure 26: Normalised velocity spectrum in the wind engineering test section of the Monash wind tunnel at 8 m/s (jet up, collector back, no screen), after Cheung et al (2003): (a) without active generation of turbulence; (b) with active generation of turbulence.

9 Conclusions & Recommendations

9.1 Conclusions

The experimental and analytical research detailed in this report has tried to achieve 3 main objectives as outlined in Section 4.3, and restated below:

1. Provide detailed descriptions of the outdoor flight environment, including the spatial and temporal variations, experienced by MAVs (either natural or man-made) encompassing flight speeds from hovering to 10 m/s, under typical atmospheric winds
2. Determine the levels and characteristics of turbulence most relevant to MAV flight for flow simulations (which could be either CFD or EFD)
3. Reproduce typical outdoor turbulent flow environments in a wind tunnel, utilising the same probe systems and statistical parameters as used to gather the outdoor data.

Measurements of atmospheric turbulence were taken using a program of on-road testing. The results of this testing produced a range of parameters for open to moderately built-up terrains, in light to moderate wind conditions (with wind speeds < 10 m/s), at a height of ~4 m above the ground. The parameters gathered include spectral levels, turbulence intensities, length scales and pitch variation fluctuation and are detailed in the plots in Section 6.3 and further results in Appendix C, Section 13. These parameters describe both the spatial and temporal variations in the atmospheric turbulence for the given conditions. The data were analysed for both an MAV condition where its effective ground speed was 0 m/s (i.e. hovering) and the condition where its IAS was 10 m/s. These data characterise the MAV atmospheric turbulence environment for the given terrain and wind conditions, directly addressing research objectives 1 and 2, and will be valuable for future experimental and computational modelling of MAVs.

A second program of experimental testing was conducted within a large wind-engineering wind tunnel in order to simulate the turbulence characteristics found during the on-road testing phase. The results showed that atmospheric turbulence characteristics for the important roll inputs can be simulated within the existing wind tunnel for the entire relevant frequency range for 150 mm (6 inch) span MAVs, but that 1 m (40 inch) span MAVs might require additional active turbulence generation techniques. The latter would be required in order to adequately replicate the larger length scales that affect the roll inputs of the larger span MAVs. It was noted that such techniques exist and should prove effective to achieve this goal. The successful replication of MAV-relevant turbulence characteristics within the wind tunnel directly addresses research objective 3.

The discussion in Section 4 identified both the range of spatial and temporal turbulence characteristics required, and further identified the most important parameters to a stable MAV-mounted viewing platform and MAV control, that of roll and pitch inputs, but most importantly roll inputs. This in turn identified the key flow parameters within atmospheric turbulence to examine: pitch and velocity variation in time and space.

In the process of achieving research objective 3, the critical wave number (normalised frequency) range for the accurate replication of pitch variation fluctuation within the wind tunnel, for a 150 mm (6 inch) span MAV, was found to be between $k = 0.6$ to ~2. Below a wave number of ~0.6, the turbulent length scales did not appear to significantly affect the pitch variation fluctuation for the given atmospheric data and 50 mm spaced measurement points, while accurate replication of spectral levels above a wave number of 2 also did not appear as important (Section 8.1.2).

As pitch variation fluctuation had been identified as an important measure of the roll inputs to a wing, this critical wave number range defines the critical turbulence scales of relevance to small MAV wingspans (150 mm or 6 inches). The critical range for a corresponding larger wingspan, say 1 metre, would be between $k = 0.1$ to 0.3. These results define the critical turbulence characteristics relevant to MAV flight, while the critical levels within this wave number range are given by the results of the on-road testing used in achieving research objective 1. The identification of the MAV-relevant turbulence

characteristics and levels thus achieves research objective 2. These results are again valuable for future experimental and computational modelling of MAVs.

With the above results, all the research objectives have been achieved. However, there is still further work with the existing data that could be undertaken. Although the effective roll inputs to an MAV wing have been identified as the most crucial parameter for the evaluation of MAV flight capability in atmospheric turbulence, the effective pitch inputs are also important and would benefit from further analysis. This could be done as a first step using the data already collected for this research program, but may require some additional measurements at a later stage. Evaluation of the pitch angle coherence from the existing data could also be included in such work, thus completing a full analysis of all the data collected during this research.

9.2 Recommendations and future work

The work to date has enabled the replication of typical unsteady flight environments in a wind tunnel for the first time. This controlled replication permits understanding and development of MAVs that offer enhanced utility in real world conditions and can be used in two main ways:

- Flight experiments of existing MAVs, in order to measure the sensitivity and controllability of man-made craft. The facility also permits study of bird and insect flight which will enable us to gain greater insight into how nature has evolved systems to permit flying in turbulent winds and;
- Measurements of flight loads and inputs from atmospheric turbulence that can be used to develop aircraft platforms to mitigate the effects of turbulence, and control systems to enable stable viewing platforms. We are currently developing a new MAV force balance to permit the direct measurements of dynamic loads on small craft.

The data obtained from 'flying' the probes through appropriate wind conditions can be used as the inputs to MAV simulations. We have started a simulation model for MAVs using a quasi-static approach (i.e. we use our measured unsteady velocity inputs as a function of time and space with aerofoil data that have been gained from smooth flow experiments or CFD simulations). However the considerable limitation of this is that there appear to be no data regarding the characteristics of aerofoils in turbulent flow.

Thus we propose:

1. Offering the Wind Tunnel Facility to developers and users of existing MAVs for the evaluation and development of their own platforms
2. A series of controlled, yet unrestrained, flight experiments on different scales and geometries of MAVs
3. Commissioning of the MAV force balance, including dynamic calibration and evaluation
4. Dynamic force and moment measurements on relevant aerofoils and planforms under correctly scaled turbulence simulations. This information would then be utilised in the MAV simulation thus alleviating the restricting quasi-static approach.

These recommendations will form the basis of two 'white papers' for future research.

10 References

Anon (1997) 'UAVs Applications are Driving Technology – Micro Air Vehicles', *UAV Annual Report*, Defence Airborne Reconnaissance Office, Pentagon, Washington, 6 November, p.32.

Anon (2001) 'Small Unit Operations', *Int. Defence Review*, Janes, UK, 34 (November), p.36.

Aylor D., Wang Y. and Miller D. (1993) 'Intermittent wind close to the ground within a grass canopy', *Boundary-Layer Meteorology*, **66** (March).

Balzer, L.A. (1977) 'Atmospheric turbulence encountered by high-speed ground vehicles', *J Mech Eng Sci*, **19**.

Burger, K. (2002) 'Budget Boost for UAVs and Counter-terrorism', *Janes Defence Weekly*, Janes Publications, UK, (2 January), **37**(1), p.6.

Chen J., Haynes B.S., and Fletcher D.F. (2000) 'Cobra Probe measurements of mean velocities, Reynolds stresses and higher-order velocity correlations in pipe flow', *Exp Thermal and Fluid Sci*, **21**: 206-217.

Cheung, J.C.K., Eaddy, M. and Melbourne, W.H. (2003) 'Active generation of large scale turbulence in a boundary layer wind tunnel', *Proceedings of the 10th Australasian Wind Engineering Society Workshop, Sydney, Australia*.

Cooper, R.K. (sic) (1984) 'Atmospheric Turbulence With Respect to Ground Vehicles', *Journal of Wind Engineering and Industrial Aerodynamics*, **17**.

Davenport, A.G. (1960) 'Rationale for determining design wind velocities', *J Struct Div Am Soc Civ Eng*, **86**: 39-68.

ESDU, 'Characteristics of atmospheric turbulence near the ground. Part I: Definitions and general information', Item No. 74030, ESDU International, London, 1974.

ESDU, 'Characteristics of atmospheric turbulence near the ground. Part II: Single point data for strong winds (neutral atmosphere)', Item No. 85020, ESDU International, London, 1985.

ESDU, 'Characteristics of atmospheric turbulence near the ground. Part III: Variations in space and time for strong winds (neutral atmosphere)', Item No. 86010, ESDU International, London, 1986.

Flay, R.G.J. (1978) 'Structure of a rural atmospheric boundary layer near the ground', PhD Thesis, Department of Mechanical Engineering, University of Canterbury, New Zealand, November 1978.

Gade, S. and Herlufsen, H. (1987a) 'Windows to FFT analysis (Part I)', *Technical Review*, Brüel & Kjær, Nærum, Denmark, **1987**(3).

Gade, S. and Herlufsen, H. (1987b) 'Windows to FFT analysis (Part II)', *Technical Review*, Brüel & Kjær, Nærum, Denmark, **1987**(4).

Grasmeyer, J.M. and Keennon, M.T. (2001) 'Development of the Black Widow Micro Air vehicle', *AIAA Paper*, American Institute of Aeronautics and Astronautics, AIAA-2001-0127.

Hinze, J.O. (1975) *Turbulence*, 2nd edn, McGraw Hill, New York.

Holmes J. D. (2001) *Wind Loading of Structures*, Spon Press, London (ISBN 0-419-24610-X).

Hooper, J.D. and Musgrove, A.R. (1997) 'Reynolds Stress, Mean Velocity, and Dynamic Static Pressure Measurement by a 4-Hole Pressure Probe', *Exp Thermal and Fluid Sci*, **15**(4): 375.

Hoover A. (1999) 'The size of Bluejays: Tiny planes to show their stuff in competition', viewed March 2005, http://www.napa.ufl.edu/99news/MAV99.htm

Howell J. (2000) 'Real environment for vehicles on the road', *Progress in Vehicle Aerodynamics*, Eds. J. Wiedemann and W.-H. Hucho, Expert-Verlag (ISBN 3-8169-1843-3).

Jenkins, D.A., Ifju, P.G., Abdulrahim, M. and Olipra, S. (2001) 'Assessment of controllability of Micro Air Vehicles', *Proceedings of the 16th International Conference on UAVs, 2-4 April*, Bristol, UK.

Lawson T. V. (1980) *Wind Effects on Buildings*, Applied Science Publishers Ltd, London (ISBN 0853348936).

Melbourne W.H. (1994) *Bluff Body Aerodynamics for Wind Engineering; A State of the Art in Wind Engineering*, Wiley Eastern Ltd.

Nelson R. C. (1998) *Flight Stability and Automatic Control*, 2nd ed, McGraw-Hill, New York.

Pope, S.B. (2000) *Turbulent Flows*, Cambridge University Press, Cambridge, UK.

Raupach, M.R., Finnigan, J.J. and Brunet, Y. (1996) 'Coherent eddies and turbulence in vegetation canopies: the mixing layer analogy', *Boundary-Layer Meteorology*, **78**: 351-382.

Ricketts, P. (2001) 'UAV Market Survey Indicates Operational Trial', *The Defence Reporter – Australia & Asia Pacific*, Aust. Public Affairs Info. Service, Canberra, (October), **27**(6): 34-36.

Saunders, J.W., Watkins S., Hoffmann, P.H. and Buckley, F.T. (1985) 'Tractor-trailer aerodynamic devices; Fuel saving predictions and comparison of on-road and wind-tunnel tests', *Proceedings of the International Congress of the Society of Automotive Engineers America, Detroit, February 1985*, also in the transactions of the SAE America, SAE 850286.

Sinha, A.K., Kusumo, R., Scott, M.L., Bil, C. and Mahondas, P. (2001) 'A System Approach to Issues and Challenges of UAV Systems', *16th Bristol International UAV Systems Conference, 3-5 April*, Bristol, UK.

Spedding, G.R. & Lissaman, P.B.S. (1998) 'Technical aspects of microscale flight systems', *Proceedings of the International Symposium on Optimal Migration*, eds. A. Hedenstrom & T. Alerstam, Kluwer.

Sutton, O.G. (1953) *Micrometeorology*, McGraw-Hill Books, New York.

Tennekes H. (1996) *The Simple Science of Flight*, MIT Press, Cambridge, Mass. (ISBN 0-262-70065-4)

Van Der Hoven, I. (1957) 'Power spectrum of horizontal wind speed in the frequency range from 0.0007 to 900 cycles per hour', *J. Meteorology*, **14**:160-164.

Watkins, S. (1990) 'Wind tunnel modelling of vehicle aerodynamics: With emphasis on turbulent wind effects on commercial vehicle drag', PhD Thesis, Department of Mechanical Engineering, RMIT University, Melbourne, Australia.

Watkins, S. (2002) 'Development of a Micro Air Vehicle', *Proceedings of the 17th Bristol International Conference on Unmanned Air Vehicle Systems, April 8-10*, Bristol University, UK.

Watkins, S. and Saunders, J.W. (1998) 'A review of the wind conditions experienced by a moving vehicle", *Proceedings of the International Congress of the Society of Automotive Engineers America, Detroit, February 1998*, SAE 981182, also in Special Publication 1318 (ISBN 0-7680-0138-2).

Watkins, S., Saunders, J.W., Hoffmann, P.H. and Holmes, J.D. (1995) 'Measurements of Turbulence Experienced by Moving Vehicles, Part I, Turbulence Intensity', *Journal of Wind Engineering and Industrial Aerodynamics*, **57**:1-17.

Wilson and Schnepf (2001) 'Micro Air Vehicles – New Military Capability', *Proceedings of the 16th International Conference on UAVs, 2-4 April*, Bristol, UK.

11 Appendix A: Instrumentation & mounting configurations

11.1 Cobra Probes

Four TFI (Turbulent Flow Instrumentation) Series 100 Cobra Probes (Figure 27), were used to take all flow measurements for both the on-road and wind tunnel measurements during this research. The Cobra Probe is a robust pressure measuring device that has several advantages over hot-wire anemometers: it withstands rough treatment and contaminated flows; is fully pre-calibrated; measures fluctuating static pressure as well as all three fluctuating velocity components; and is very quick and easy to use.

The Cobra Probe does not replace hot-wire anemometers, but is a useful adjunct where the flow is greater than 2-3 m/s and 1% turbulence intensity, very fine spatial resolution is *not* required, and a frequency response up to ~2 kHz *is* required. In terms of measurements in atmospheric turbulence, it is the most practical choice of instrumentation, as it will not suffer from broken sensing elements due to dust, debris, knocks or sudden wind gusts, it has the required frequency response and is extremely stable with regard to changes in temperature.

Figure 27: TFI Series 100 Cobra Probe.

11.1.1 Principles of operation

The principle of operation of the probe is to relate the pressure field detected by four pressure tap locations, on the faceted head, to the magnitude of the instantaneous local velocity vector, the flow yaw and pitch angles and the instantaneous static pressure. Pressure signals measured by the transducers in the probe body are linearised to correct for amplitude and phase distortions that are generated in the tubes connecting the probe head to the transducers. The four pressure values are then converted to non-dimensional ratios. These are used as the independent variables that are related to the four dependent variables of total pressure, dynamic pressure, yaw angle and pitch angle through pre-calculated calibration surfaces (generated by the manufacturer before a probe is supplied). Converting data via the calibration surfaces is performed for all samples, in real time.

Cobra Probes are thus able to resolve all three components of velocity within a cone of ±45° around the probe x-axis (Figure 28), as well as local static pressure. This enables resolution of the constantly fluctuating velocity vector in turbulent flow, as long as the probe is approximately aligned with the freestream flow direction, and the turbulence intensities are not excessively large (below 30% turbulence intensity in the y and z directions is preferred). Data that fall outside the ±45° acceptance cone are indicated by the software.

During use, the local temperature and barometric pressure at a test location need to be entered into the probe control software before starting a series of measurements. Zeroing the probe must also be performed regularly to circumvent drift in the transducer outputs, and for the testing conducted during this research was performed at the start of a measurement session in a particular test location and at regular intervals (~½ to 1 hour). This was done by either: disconnecting the reference pressure ports and then shielding the probe heads using an enclosed box over the mounting bracket, while the vehicle was stationary, or; turning off the wind tunnel flow. The Cobra Probe control software then measured and removed the offsets from the transducer voltage signals.

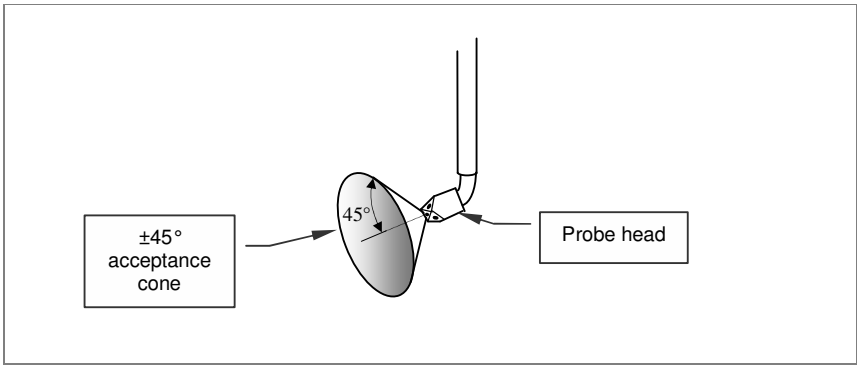

Figure 28: Cobra Probe acceptance cone: the area within which flow data must occur in order to be measured by the probe.

Static calibration of the probe transducers is required to be occasionally performed by applying known pressures to the probe reference pressure port, and entering the pressure values into the control software. The Cobra Probe software then calculates the volts-to-pressure ratios for each transducer and subsequently applies them to any measured data.

11.1.2 Accuracy

Accuracy of measurements is somewhat dependent on turbulence levels but is generally within ±0.5 m/s and ±1° pitch and yaw up to about 30% turbulence intensity. The Cobra Probe remains relatively accurate in flows with greater than 30% turbulence intensity and the probe can measure the above flow parameters within a ±45° acceptance cone of the probe head orientation (Figure 28). The particular probe used for measurements in this thesis had 2.5 kPa (0.3 psi) pressure transducers, and was dynamically calibrated by TFI to allow accurate flow measurements up to ~50 m/s. Spatial resolution of the measurements was determined by the size of the probe head (2.6 mm) giving an accurate spatial resolution of flow structures down to ~20 mm.

For validation of the Cobra Probe's frequency response and ability to accurately determine second-order and higher flow velocity correlations the reader is referred to Chen, Haynes and Fletcher (2000) and Hooper and Musgrove (1997).

11.2 Axes system and flow variable definitions

The axes system and flow variable definitions used while taking measurements for this research are shown in Figure 29 below. The definition of pitch and yaw angle used here are actually different from that used by the Cobra Probe control system, which uses elevation and azimuth definitions (as defined in a spherical coordinate system) for its version of pitch and yaw. However, for the purposes of this research, the raw *u*, *v* and *w* data were post-processed to produce the pitch and yaw angles as defined in Figure 29.

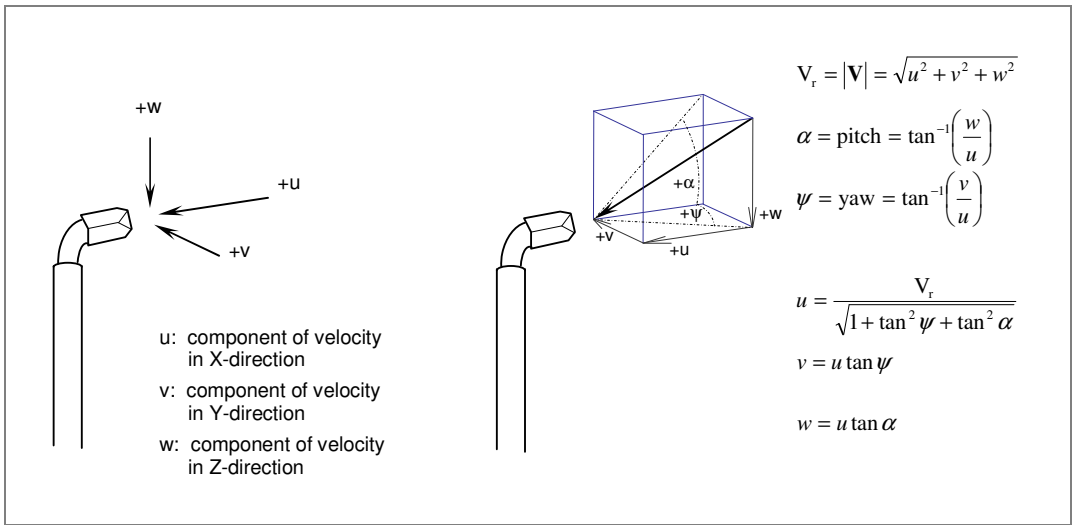

Figure 29: Cobra Probe axes system and flow variable definitions.

11.3 Vehicle mounting configuration

For the on-road measurements, the cobra probes were mounted on a car roof rack and set at an appropriate height and spacing to collect the necessary data. The system designed for the task is illustrated in Figure 30, with relevant mounting dimensions shown in Figure 31. Detailed drawings of the mast and probe bracket are provided at the end of this appendix in Section 11.5.

There were two driving factors in this design. The first was to hold the probes as rigidly as possible at a known orientation to the airflow and known spacing, and the second was to get the probes as high from the ground as possible to reduce the interference effects from the car and the ground. It has been shown in previous work (Watkins, 1990) that the influence from the car is minimal at zero yaw angles; however, the influence increases as the yaw angle increases. Getting the probes as far from the car as possible ensures these effects are at a minimum. The mast height was therefore set just under the maximum road legal height of 4 metres.

Figure 30: Mast and probes mounted to the RMIT station wagon.

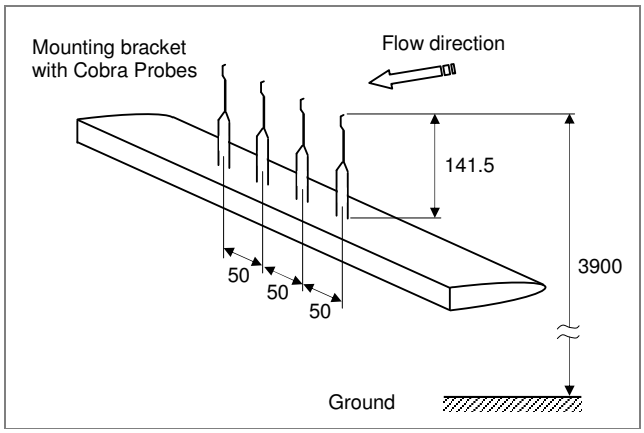

Figure 31: Instrumentation configuration for vehicle mounting, all dimensions in millimetres. Probe spacing could be set at 50 or 150 mm.

The basic mast design consists of a steel tube that is held by stays at multiple points in order to provide the stiffness required. Some problems were encountered early on in the testing program when the mast was only supported by a single set of stays and experienced resonance at ~7-10 Hz during vehicle motion. For calm wind conditions (V_w of ~1-2 m/s) the resonance vibration could be up to 50% of the flow velocity measured by the Cobra Probes, as the motion of the mast caused an induced velocity at the probe head. The addition of a second set of stays significantly reduced the resonance problem, by approximately an order of magnitude, to a level that was considered acceptable and was not noticeable in the majority of all on-road measurements.

The probe bracket that was fitted to the top of the mast (Figure 32) was required to correctly align the probes and hold them securely. In addition, the bracket was easily removable in order to reduce risk to the instrumentation when driving between test sites. The bracket has the ability to mount the probes in both 50 mm and 150 mm spacings (for a detailed drawing see Section 11.5). This means that the probe spacing can be easily changed while consistently reproducing the same probe separations. It was also able to accommodate a three-axis accelerometer that was initially used to evaluate the stiffness of the mast during the test program. The same probe-mounting bracket was used in the wind tunnel tests as described below in Section 11.4.

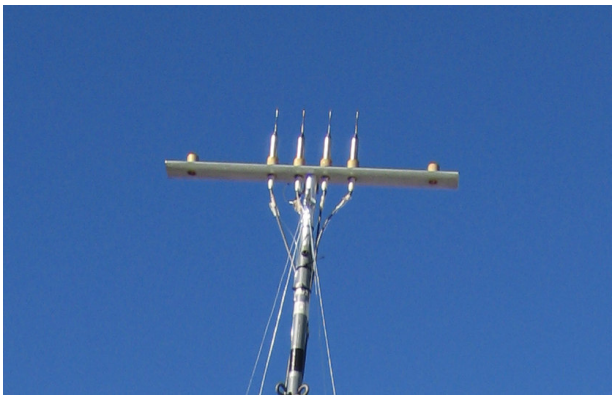

Figure 32: Probe bracket fitted to mast with probes in situ.

11.4 Wind tunnel mounting configuration

For the wind tunnel measurements, the four Cobra Probes were mounted on the aerodynamically faired bracket, Figure 33, equally spaced in the lateral direction, at spacings of either 50 or 150 mm (see Section 11.5 for a detailed drawing of the bracket). The bracket with probes was then mounted at

the approximate centre of the wind-engineering test section in the Monash wind tunnel using the facility traverse (Figure 34), with the probe heads approximately 1.5 metres above the tunnel floor.

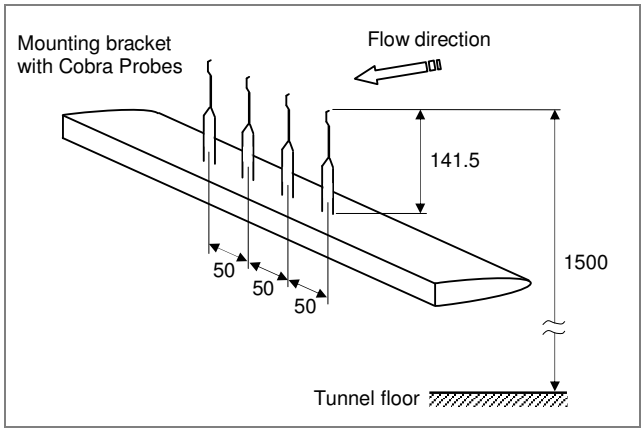

Figure 33: Instrumentation configuration for wind tunnel mounting, all dimensions in millimetres. Probe spacing could be set at 50 or 150 mm.

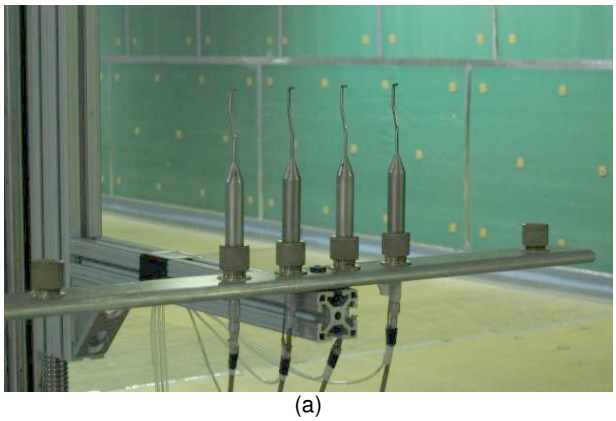

(a)

(b)

Figure 34: Cobra Probes mounted on the traverse in the centre of the wind engineering test section: (a) close-up of the probe mounting; (b) full view showing the extent of the vertical traverse.

11.5 Mast & bracket details

On the following two pages are detailed drawings of the mounting bracket used for the four Cobra Probes, and the mast used to hold the mounting bracket on a vehicle during on-road testing.

12 Appendix B: Equations & Data Processing

12.1 General equations

12.1.1 Statistical quantities

Mean value: $\bar{x} = \lim_{T\to\infty} \frac{1}{T} \int_{t=0}^{T} x.dt$

Standard deviation: $\sigma_x = \lim_{T\to\infty} \sqrt{\frac{1}{T} \int_{t=0}^{T} \left(x - \bar{x}\right)^2 dt}$

Turbulence intensity: $I_x = \frac{\sqrt{\overline{(x')^2}}}{\overline{Vr}}$, where *x* can be the *u*, *v* or *w* component of relative velocity.

Where turbulence intensity is calculated for ambient atmospheric wind, it is designated by I_x, as shown above. However, when turbulence intensity is calculated for a moving object, such as a vehicle or moving MAV, it is designated by J_x.

Note: that the velocity components are made up of both a fluctuating and a mean component: $u = \bar{u} + u'$, where the mean component is determined by the equation as given above, and the fluctuating component *u'* is the remaining portion of *u* after the mean is subtracted.

12.1.2 Determining ambient wind characteristics (subtraction of vehicle speed)

During vehicle measurements, it was necessary to mathematically determine the ambient wind conditions that occurred while the vehicle was moving at essentially constant speed in a straight line. If there is no local atmospheric wind and no roadside obstacles, a vehicle experiences a relative mean flow from the direction in which the vehicle is proceeding. This mean flow is said to have a zero yaw angle, $\psi = 0°$. This yaw angle is determined by those components of the flow in the plane parallel to the ground on which the vehicle is travelling. Any local atmospheric wind or other disturbances will cause the vehicle to experience a relative flow from a direction different to that in which the vehicle is heading, i.e. a non-zero yaw angle, Figure 35.

Since the vehicle can proceed in any direction relative to the local atmospheric wind, the wind direction relative to the vehicle direction subscribes a circle, as shown in Figure 35. The base of V_r is thus also always situated on this circle, and incidentally this means that there will occur a maximum possible vehicle yaw angle for given mean vehicle speed and local mean wind conditions. This is advantageous when taking measurements with the Cobra Probes, as by travelling at a given speed it is possible to ensure that the likely range of flow yaw angles always remains within the probes acceptance cone of ±45° to the probe x-axis[21].

In terms of the research presented here, as the vehicle speed was known and the probes measured the relative velocity and yaw angle, it was then possible to work backwards and find the ambient wind conditions, as given by the equations below.

$$V_w = \sqrt{{V_v}^2 + {V_{\mathrm{Re}l}}^2 - 2V_v V_{\mathrm{Re}l} \cos\psi}$$

[21] In particularly turbulent environments, it is sometimes impossible to take stationary measurements for this reason, and so measurements taken while moving are preferred, as well as having the advantage of compressing a given 'length' of atmospheric turbulent structures into a shorter time sample.

$$\phi = \cos^{-1}\left(\frac{V_r^{\,2} - V_w^{\,2} - V_v^{\,2}}{2V_w V_v}\right)$$

where V_v is the vehicle speed, V_w is the ambient wind speed and ϕ is the direction of the ambient wind to the vehicle direction of travel.

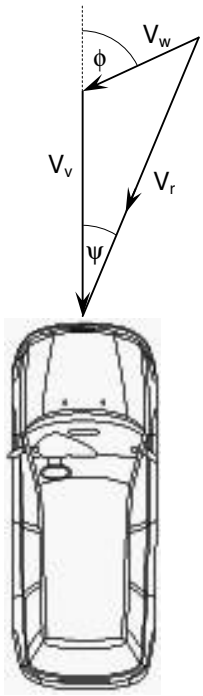

V_v	flow due to vehicle direction of travel
V_w	flow due to ambient wind
V_r	relative flow over vehicle
ϕ	angle of wind to vehicle direction of travel
ψ	flow yaw angle

$$V_r = \sqrt{V_w^{\,2} + V_v^{\,2} + 2V_w V_v \cos\phi}$$

$$\psi = \tan^{-1}\left(\frac{\frac{V_w}{V_v}\sin\phi}{1 + \frac{V_w}{V_v}\cos\phi}\right)$$

Figure 35: Yaw angle of the relative flow due to ambient wind conditions, with respect to the vehicles direction of travel.

Alternatively, the ambient wind speed and direction can also be derived by converting the data from V_r, α and Ψ to u, v and w (Figure 29), subtracting the vehicle speed from u, and then recalculating V_r, α and Ψ. Once the vehicle speed is removed from the data, V_r is then equivalent to the ambient wind speed V_w, and Ψ is equivalent to the wind direction with respect to the vehicle's direction of travel, ϕ.

12.1.3 Correction to an IAS of 10 m/s

Correction to an indicated airspeed of 10 m/s involved adding a mean u-component velocity onto the stage 2 data that brought the total mean relative velocity up to 10 m/s.

$$u = u + (10 - \bar{u})$$

Once this was done, the relative velocity, pitch and yaw angles were then recalculated using the equations given in Figure 29, followed by the statistical parameters, spectra, pitch variation fluctuation and pitch angle coherence.

12.2 Calculation of length scale

Auto-correlation of a velocity measurement at a single point in space was performed in order to estimate the longitudinal length scale of the flow. This used Taylor's frozen turbulence approximation which assumes that if the flow is statistically stationary, and the constant mean velocity is large with respect to the turbulence fluctuations, the eddies or vortex lines do not change appreciably in shape as they pass a given point. In this situation the auto-correlation with time delay, τ, can approximate

the space correlation (cross-correlation) with separation $-V_r\tau$, Hinze (1975, pp.46-47), Pope (2000, p.224). The length scale is then calculated by,

$$L_x = V_r \int_0^c \rho_{uu}(s).ds$$

where *c* is the first zero crossing of the auto-correlation coefficient function ρ_{UU} of the u-component velocity and *s* is the time delay or lag. The auto-correlation coefficient function is given by,

$$\rho_{uu}(\tau) = \frac{\lim_{T\to\infty} \frac{1}{T} \int_o^T \left\{u(t) - \bar{u}\right\}\left\{u(t+\tau) - \bar{u}\right\}.dt}{(\sigma_u)^2}$$

The corresponding longitudinal length scales for the y- and z-axes, L_y and L_z, can be calculated by respectively substituting *v* or *w* for *u* in the above equations.

The assumption that the constant mean velocity is large with respect to the turbulence fluctuations is not always satisfied in light to moderate atmospheric winds, with 'large' referring to a factor of at least 5 or more. This was certainly the case with some of the measurements taken during this research, however, as the mean velocity was still at least several times larger than the velocity fluctuations, the above method still provides an estimate of the likely length scales, albeit with larger error bands.

Ideally, in order to accurately determine length scales of the order of 20 – 100 metres found in the atmospheric boundary layer just above the ground, time samples of the order of 30 minutes or greater would also be required. This was not possible for this testing due to the difficulties in getting good measurements without traffic or other disturbances, and within the Cobra Probes cone of acceptance. Using shorter time samples still provides estimates, albeit also with larger error bounds.

Despite the above two limitations, it was still thought important to obtain 'rough' estimates of the length scales as they are an important flow descriptor and were required to investigate normalisation options for the pitch variation fluctuation. Although it is difficult to estimate a definitive error band for these length scales, a rough idea can be obtained by examining the variation in estimated length scales between the 4 probes for a simultaneous measurement.

For the atmospheric measurements with 50 mm spacing (10 minute samples): length scale variations between the 4 probes were typically < 5% for L_x and L_y, and 3-25% for L_z, so it is thought that ±15% is a reasonable guide to the accuracy of L_x and L_y, and ±60% for L_z. For the atmospheric measurements with 150 mm spacing (1-2 minute samples): length scale variations between the 4 probes were typically < 13% for L_x and L_y, and 35-40% for L_z, therefore L_x and L_y would reasonably be ±30%, and ±100% for L_z.

Finally, for the wind tunnel measurements (5 minute samples): variations in estimated length scale between the 4 probes were typically < 3% for L_x and L_y, and 3-13% for L_z, therefore L_x and L_y would reasonably be ±10%, and ±35% for L_z. These estimations are, however, based only on the variation between length scales from the 4 probes, assuming a Gaussian distribution in error to estimate the 95% confidence bounds, and with a safety margin added. Given that Taylor's frozen turbulence approximation does not necessarily apply to all the data, and due to the short time samples, these error bands should not be considered definitive.

12.3 Calculation of power spectral density

The average power spectral density of a data sequence, *x(t)*, divided into multiple segments is given by:

$$S_{xx}(w) = \frac{1}{F_s K} \sum_{r=0}^{K-1} \frac{1}{N} \left| X_r(e^{jw}) \right|^2$$

where $X_r(e^{jw})$ is the Fourier transform of the r^{th} segment of the time series *x(t)*, *K* is the total number of averages or segments in the entire sample, *N* is the number of points used to calculate the Fourier transform of each segment, and F_s is the data sampling frequency. *S* is a function of continuous frequency *w* (rad/s), where $w = 2\pi f$, with *f* being frequency in Hz. This is sometimes also known as the autospectrum or power spectrum. The equivalent discrete expression is:

$$S_{xx}[m] = S(w_m) = \frac{1}{F_s K}\sum_{r=0}^{K-1}\frac{1}{N}\left|X_r[m]\right|^2$$

where $w_m = 2\pi f\, m/N, \quad m = 0,1,...(N-1)$, $X_r[m]$ is the discrete Fourier transform of the r^{th} segment of the digital sequence *x[n]*, and other variables are as before. If two different data sequences are used rather than the same one, replacing $|X_r[m]|^2$, with $|X_r[m]Y_r[m]|$ gives the cross-spectrum of *x(t)* and *y(t)*, designated by S_{xy}.

As the data being examined was broadband in nature, without significant tonal peaks, the data segments were not specifically windowed (effectively equivalent to a rectangular or 'boxcar' window), and therefore no bias correction was required to correct the spectral levels.

In order to decrease the variance of the spectral estimate (an unavoidable consequence of only taking finite data sequences for analysis), the data segments within a given sequence (measurement) were overlapped by 50%. Overlapping segments by up to 50% increases the total number of averages used to calculate a spectral estimate without overly compromising the statistical independence of the segment Fourier transforms, and is therefore an effective way to reduce the variance (overlapping by more than 50% does not continue to reduce the variance as the segments become progressively less independent with increasing overlap).

The implementation of this procedure within Matlab® (version 5.3 R11) required the following lines of code, where *data* is the array containing the 5 minute data sequence to be processed:

```
N = 1024;                                   % number of points in the FFT
Fs = 1250;                                  % data sampling frequency
window = boxcar(N);                         % data window function
overlap = N/2;                              % amount of overlap (= 50%)
data = detrend(data,'constant');            % remove the mean/DC component
(Pxx, f) = pwelch(data, N, Fs, window, overlap);   % calculate the spectrum density
```

The resulting spectrum had the units of $\overline{(m/s)^2}/Hz$ (for a velocity component) or $\overline{(°)^2}/Hz$ (for a flow angle) and was usually plotted against wave number, $k = f/V_r$, where V_r is the mean relative velocity for that measurement and *f* is the frequency array returned with the calculated spectrum.

12.3.1 Spectral errors

As the spectra were broadband spectra the bias error of the spectral estimate was mainly a function of signal resolution or quantisation. With a 16-bit A/D card on a 10 V input range this was negligible compared to other sources of error: $1/2^{16} * 10V = 0.15$ mV (0.0015%) or equivalent to 0.2 m/s or 2% in velocity. The normalised random error (ε_r) for spectral estimates is a function of the number of averages (*K*) used to calculate a spectrum. For spectral density calculated using a rectangular window and 50% overlap, this is given by Gade & Herlufsen (1987a, p.8; 1987b, Appendix D) as:

$$\varepsilon_r = \frac{\sigma}{m} = \frac{1}{2\sqrt{BT_t}}, \quad BT_t = K(BT_{eff})$$

where $BT_{eff} = 0.660$ for processing using a rectangular window with 50% overlap, and K = 730 for 1024 point Fourier transforms with 50% overlap for a 5 minute data sequence at 1250 Hz sampling frequency. Therefore $\varepsilon_r = 0.023$. Assuming a Gaussian distribution in the random error, the 95% confidence limits for the normalised precision error (*P*) in the spectral estimate are:

$$\frac{P_{Ampl}}{Ampl} = \pm 1.96\varepsilon_r = \pm 0.045 \text{ or } \pm 4.5\% \text{ (5 minute sample, K = 730)}$$

or alternatively for the other sample lengths used during testing:

$$\frac{P_{Ampl}}{Ampl} = \pm 1.96\varepsilon_r = \pm 0.10 \text{ or } \pm 10\% \text{ (1 minute sample, K = 145)}$$

$$\frac{P_{Ampl}}{Ampl} = \pm 1.96\varepsilon_r = \pm 0.08 \text{ or } \pm 8\% \text{ (1.5 minute sample, K = 218)}$$

$$\frac{P_{Ampl}}{Ampl} = \pm 1.96\varepsilon_r = \pm 0.03 \text{ or } \pm 3\% \text{ (10 minute sample, K = 1463)}$$

12.4 Coherence

Coherence is defined as the Fourier transform of the cross-correlation coefficient of two measurements, *x(t)* and *y(t)*. The cross-correlation coefficient is given by,

$$\rho_{xy}(\tau) = \frac{\lim_{T\to\infty} \frac{1}{T} \int_0^T \left\{x(t) - \bar{x}\right\}\left\{y(t+\tau) - \bar{y}\right\} dt}{\sigma_x \sigma_y}$$

and is calculated for a range of τ, known as the time lag, from 0 to a maximum equivalent to the length of the data sequence.

Or equivalently coherence can be defined using power spectra, as given by Section 12.2, and the equation below.

$$C_{xy} = \frac{\left|S_{xy}\right|^2}{S_{xx} S_{yy}}$$

where C_{xy} is the coherence of the data sequences *x(t)* and *y(t)*., and S_{xy} and S_{xx} are as defined in Section 12.2. Both the cross correlation definition and the power spectra definition are equivalent and produce the same outcome. Coherence as calculated above is dimensionless, as it is a normalised quantity.

As the pitch variation fluctuation was found to provide the information required in order to evaluate the atmospheric and wind tunnel environments for the purposes of answering the research objectives, coherence results are not included in this report, but their analysis is left for future work.

12.5 Pitch variation fluctuation

Pitch variation is defined as the difference in pitch angle between two laterally spaced points in space, where lateral spacing refers to the horizontal direction perpendicular to the probe or vehicle orientation,

$$\Delta\alpha_{ij} = \alpha_j - \alpha_i$$

Therefore a measure of the fluctuation in the pitch variation between two such points is given by the standard deviation of the pitch variation, $\sigma_{\Delta\alpha}$.

$$\sigma_{\Delta\alpha} = \lim_{T\to\infty} \sqrt{\frac{1}{T} \int_{t=0}^{T} \left(\Delta\alpha(t) - \overline{\Delta\alpha}\right)^2 dt}$$

The magnitude of pitch variation fluctuation has units of degrees (°). This quantity has a direct impact on the difference in lift generated at two points on a wingspan, and therefore on the amount of roll input to an MAV wing.

12.6 Data processing

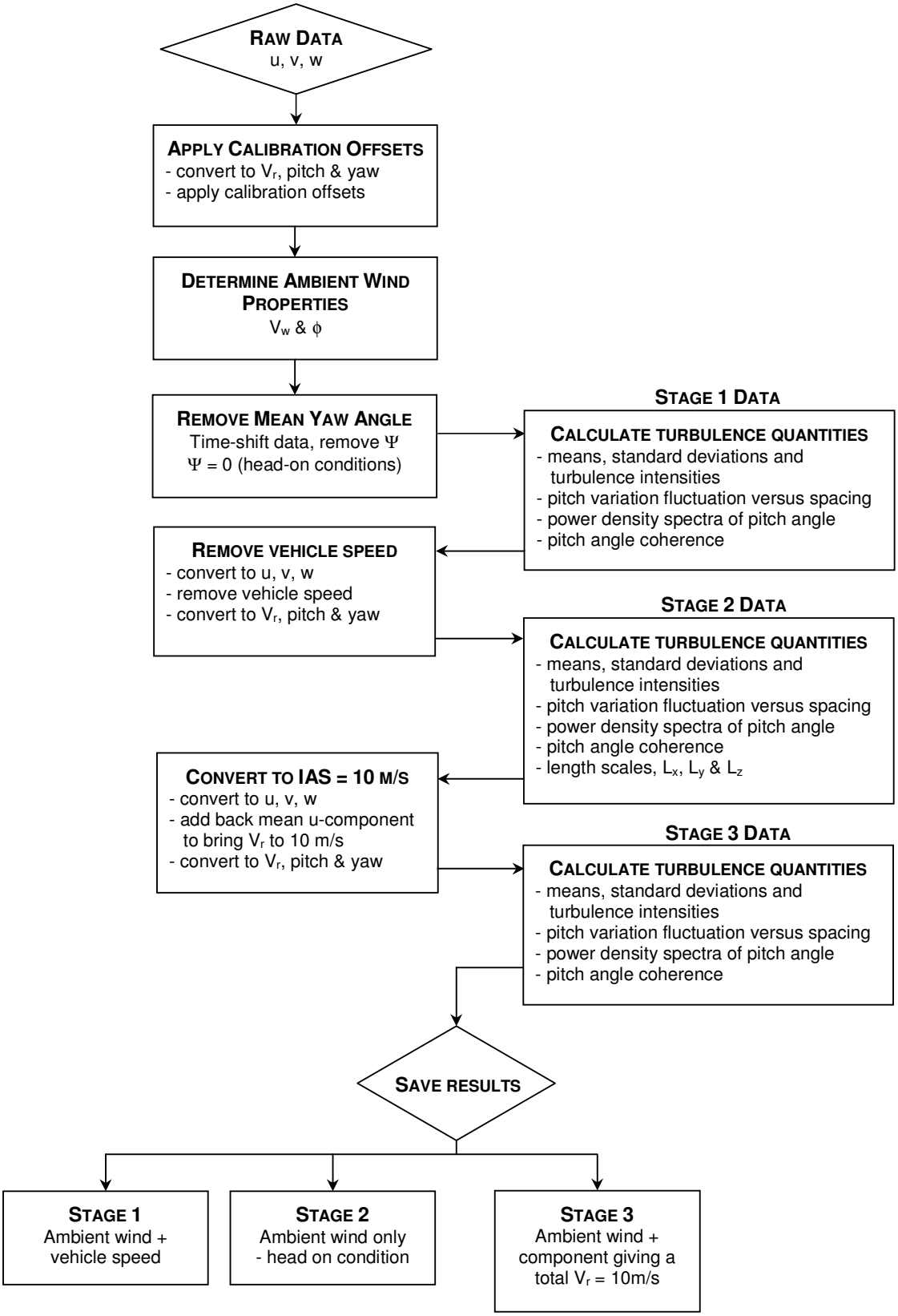

13 Appendix C: On-Road Results

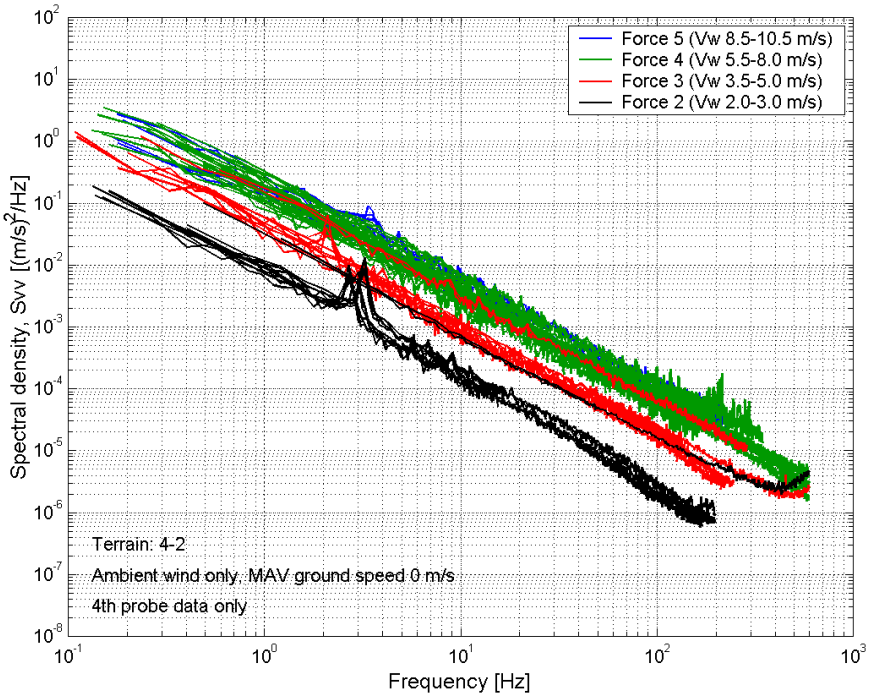

Figure 36: Atmospheric v-component spectral levels, different wind conditions, terrain 4-2 (ambient wind only, i.e. MAV effective ground speed 0 m/s).

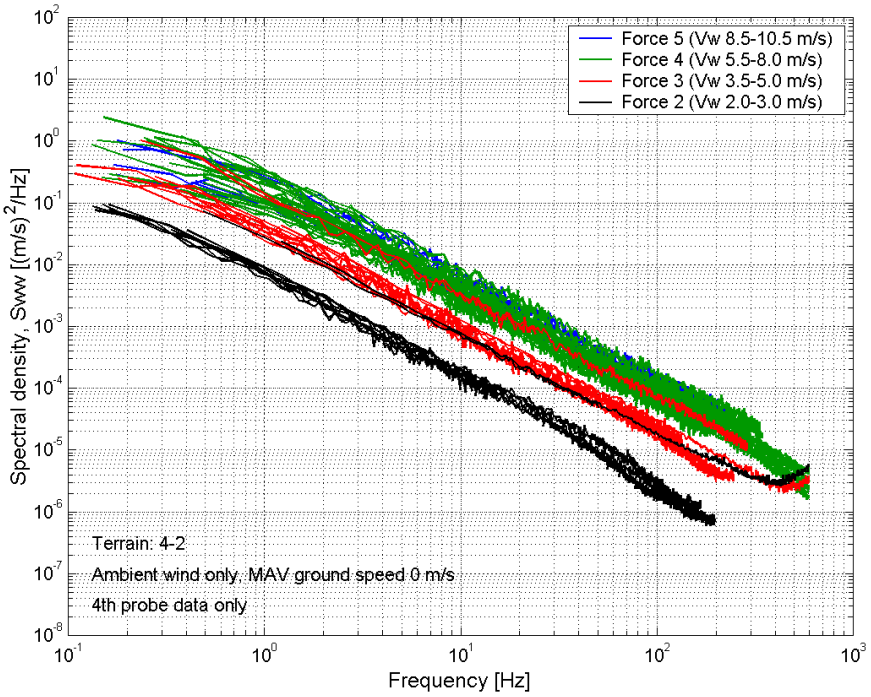

Figure 37: Atmospheric w-component spectral levels, different wind conditions, terrain 4-2 (ambient wind only, i.e. MAV effective ground speed 0 m/s).

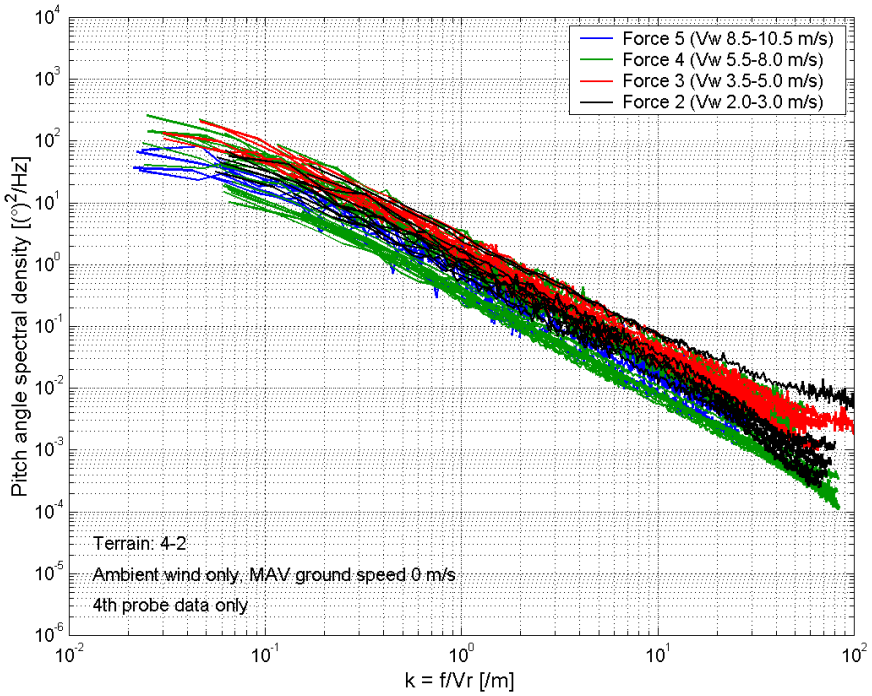

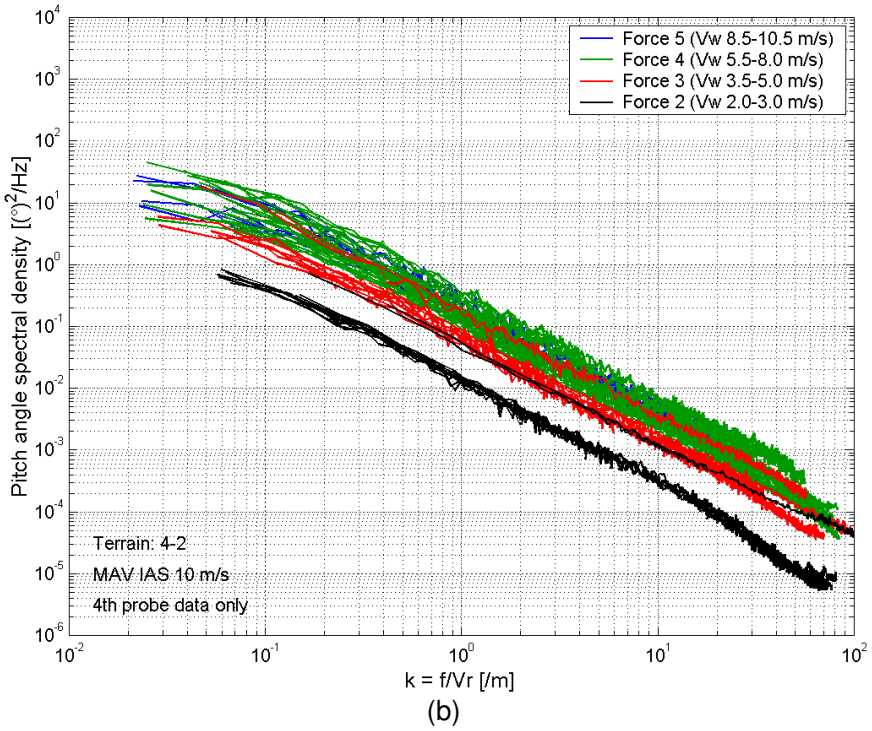

Figure 38: Atmospheric pitch angle spectral levels, different wind conditions, terrain 4-2: (a) ambient wind only; (b) MAV IAS of 10 m/s.

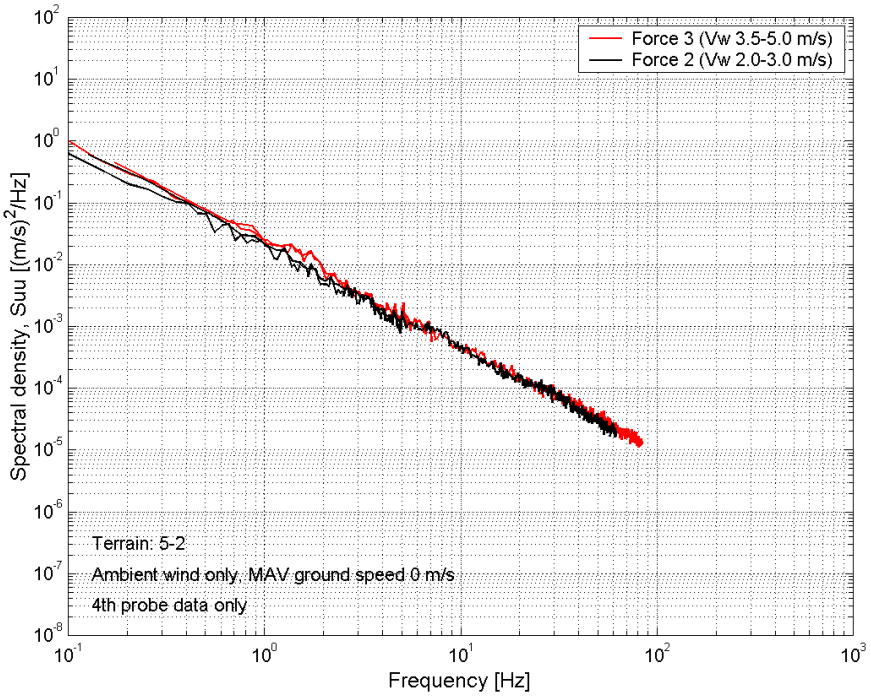

(a)

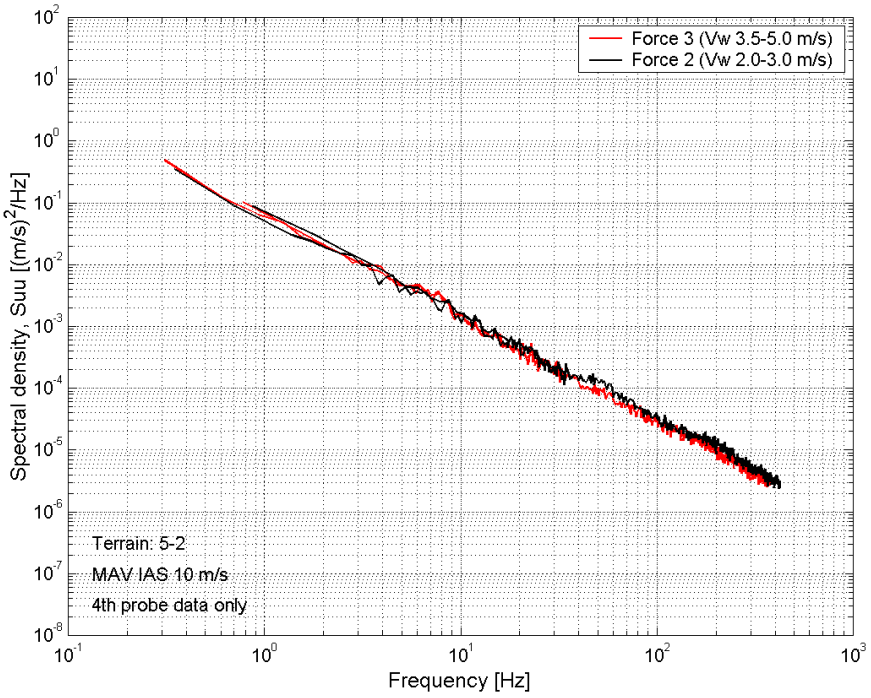

(b)

Figure 39: Atmospheric u-component spectral levels, different wind conditions, terrain 5-2: (a) ambient wind only; (b) MAV IAS of 10 m/s.

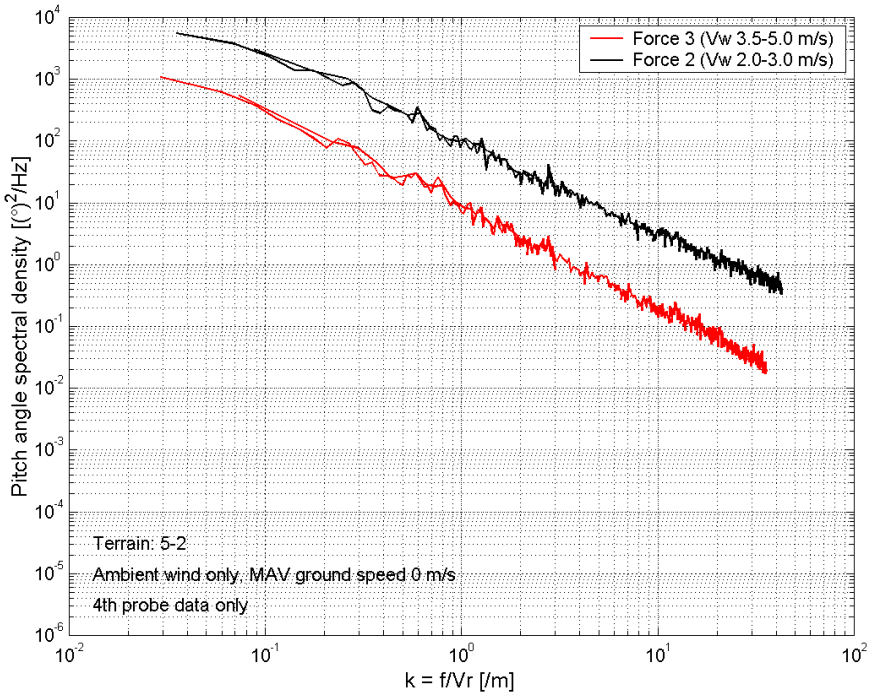

Figure 40: Atmospheric pitch angle spectral levels, different wind conditions, terrain 5-2: (a) ambient wind only; (b) MAV IAS of 10 m/s.

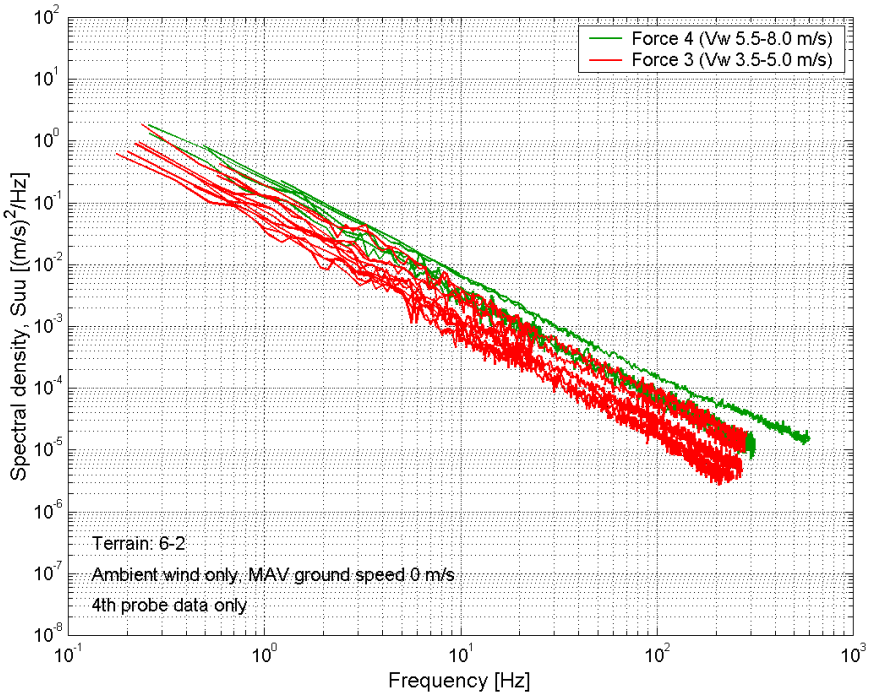

(a)

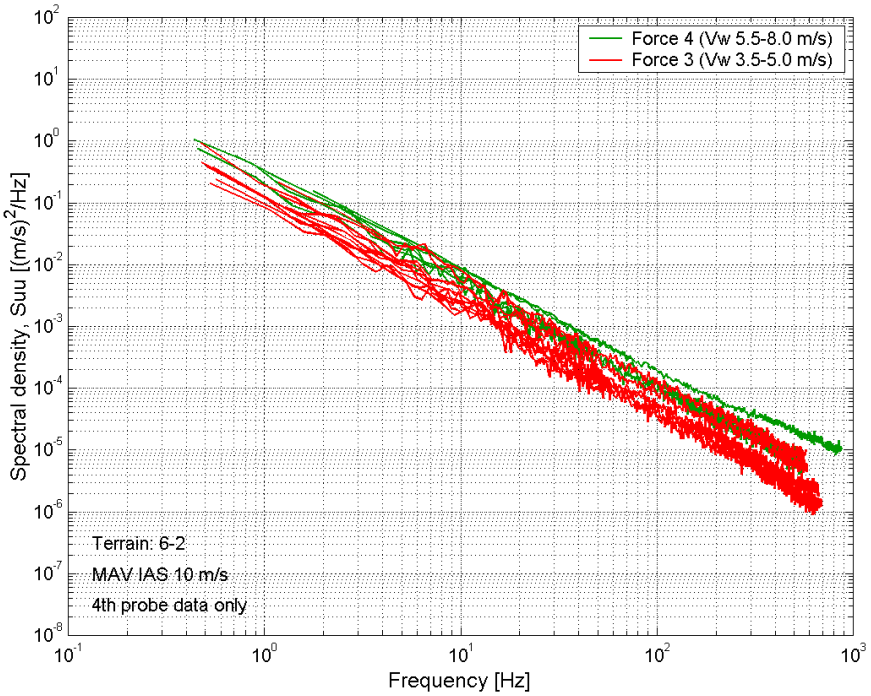

(b)

Figure 41: Atmospheric u-component spectral levels, different wind conditions, terrain 6-2: (a) ambient wind only; (b) MAV IAS of 10 m/s.

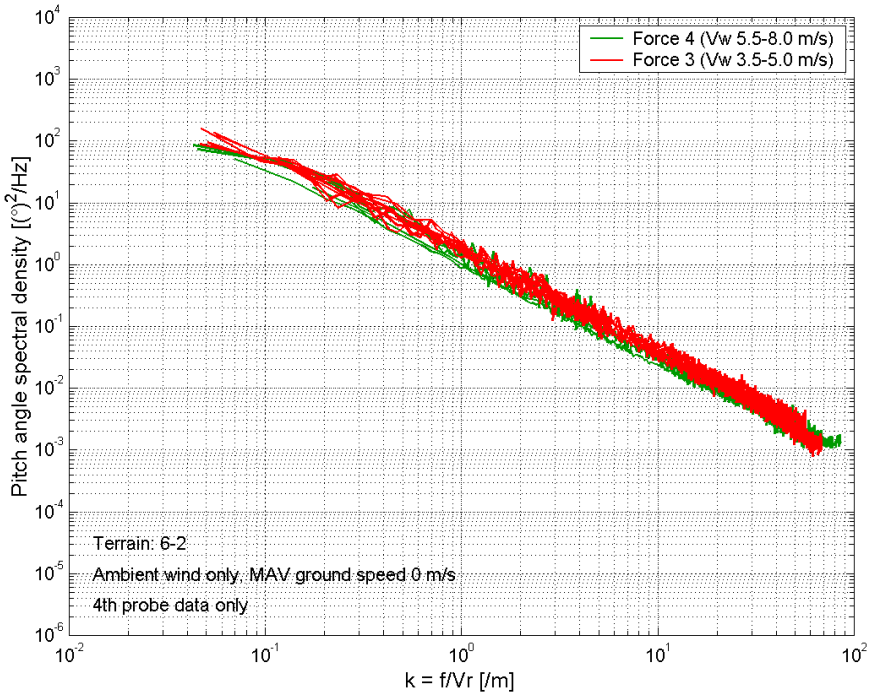

(a)

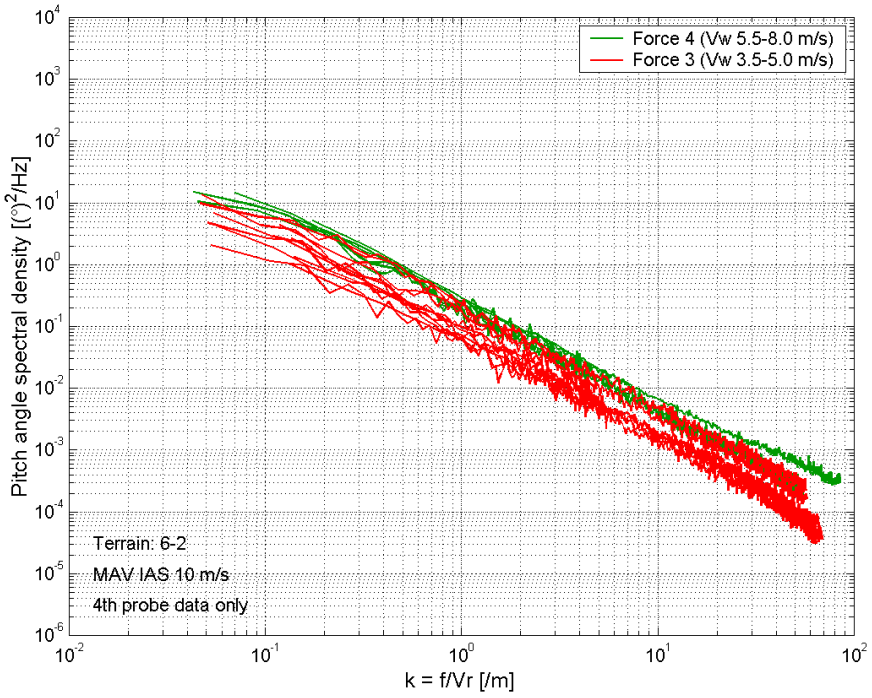

(b)

Figure 42: Atmospheric pitch angle spectral levels, different wind conditions, terrain 6-2: (a) ambient wind only; (b) MAV IAS of 10 m/s.

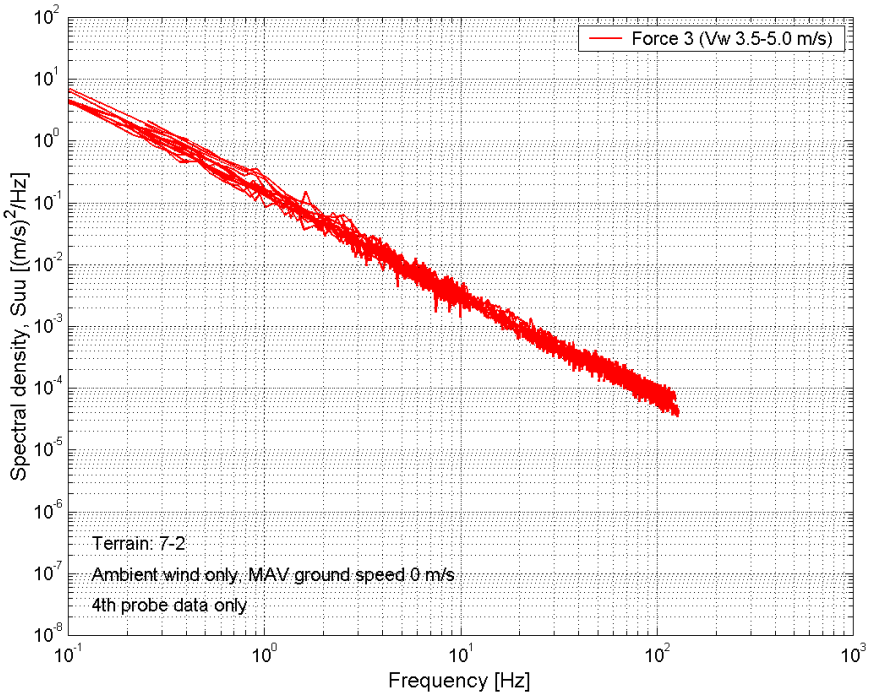

(a)

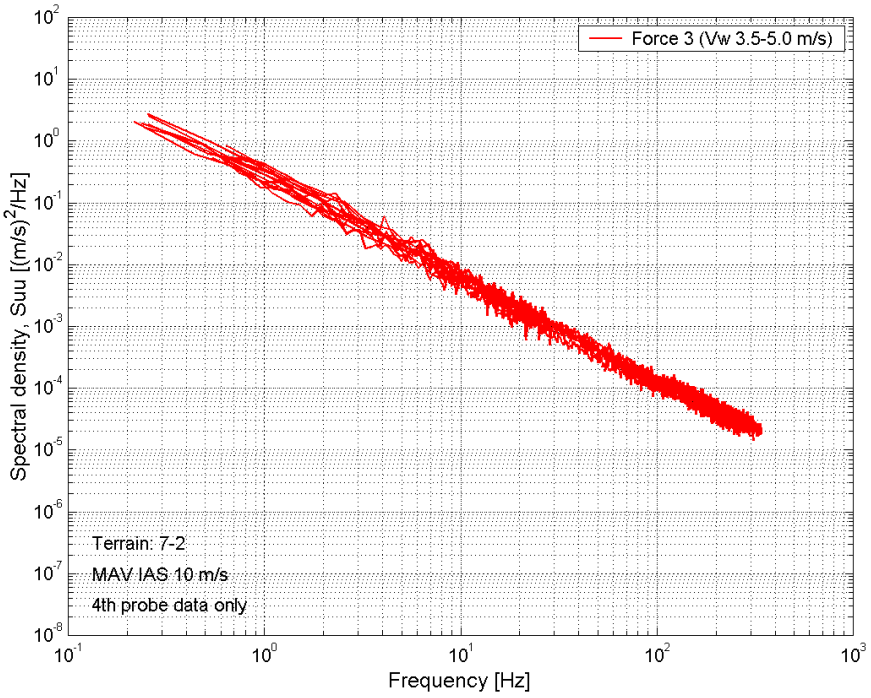

(b)

Figure 43: Atmospheric u-component spectral levels, different wind conditions, terrain 7-2: (a) ambient wind only; (b) MAV IAS of 10 m/s.

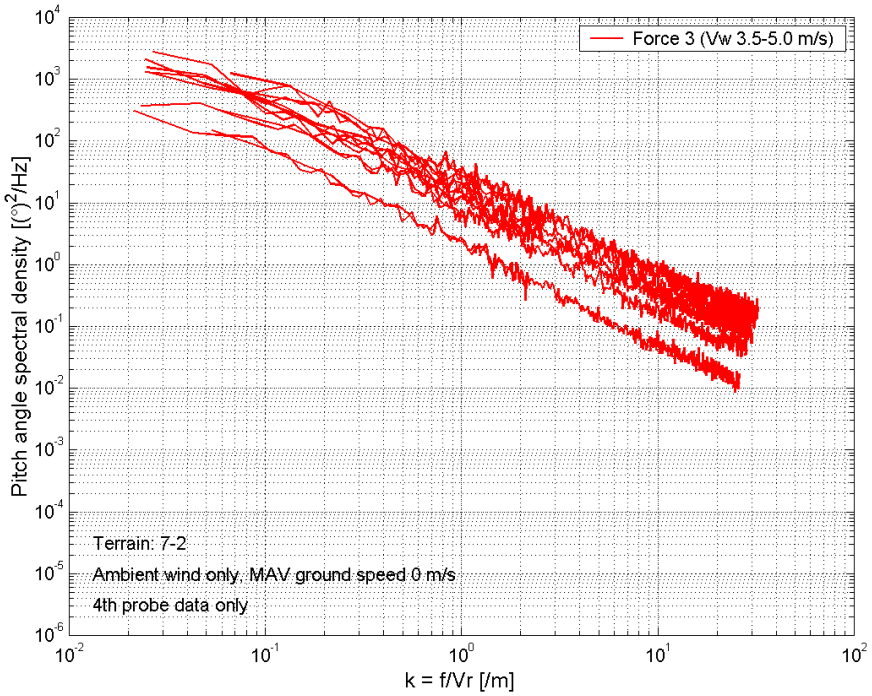

(a)

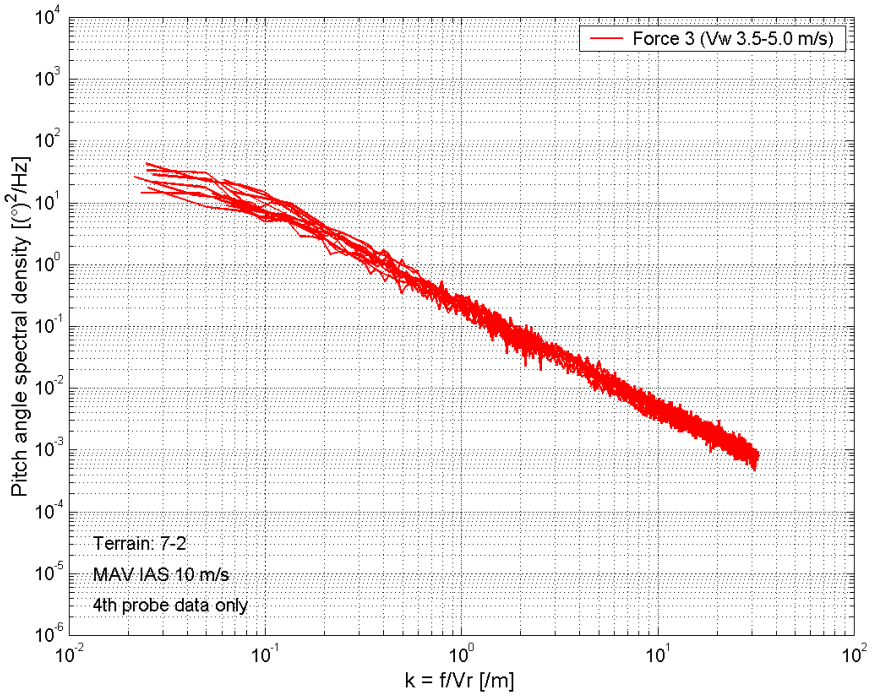

(b)

Figure 44: Atmospheric pitch angle spectral levels, different wind conditions, terrain 6-2: (a) ambient wind only; (b) MAV IAS of 10 m/s.

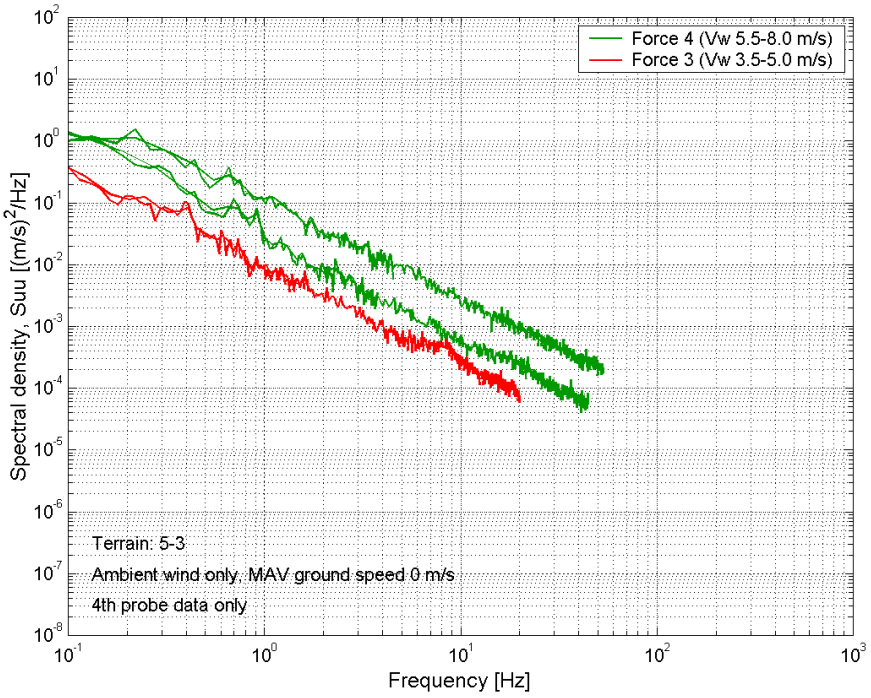

(a)

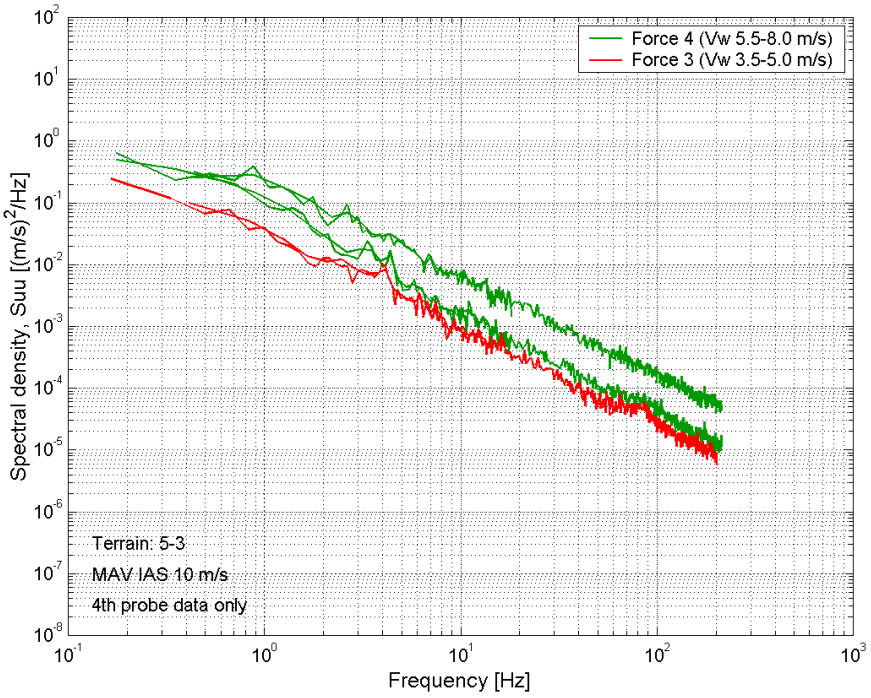

(b)

Figure 45: Atmospheric u-component spectral levels, different wind conditions, terrain 5-3: (a) ambient wind only; (b) MAV IAS of 10 m/s.

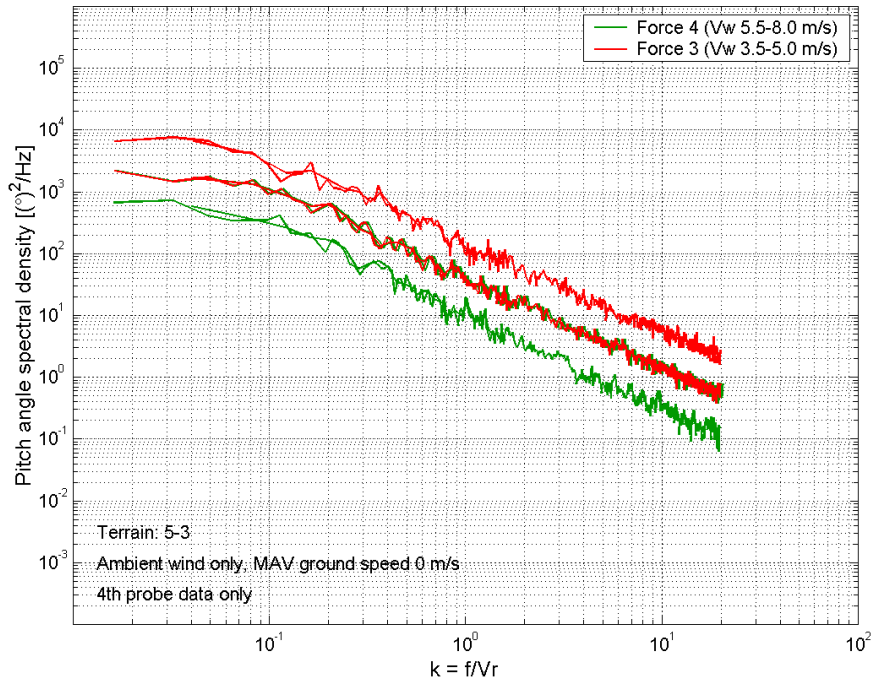

(a)

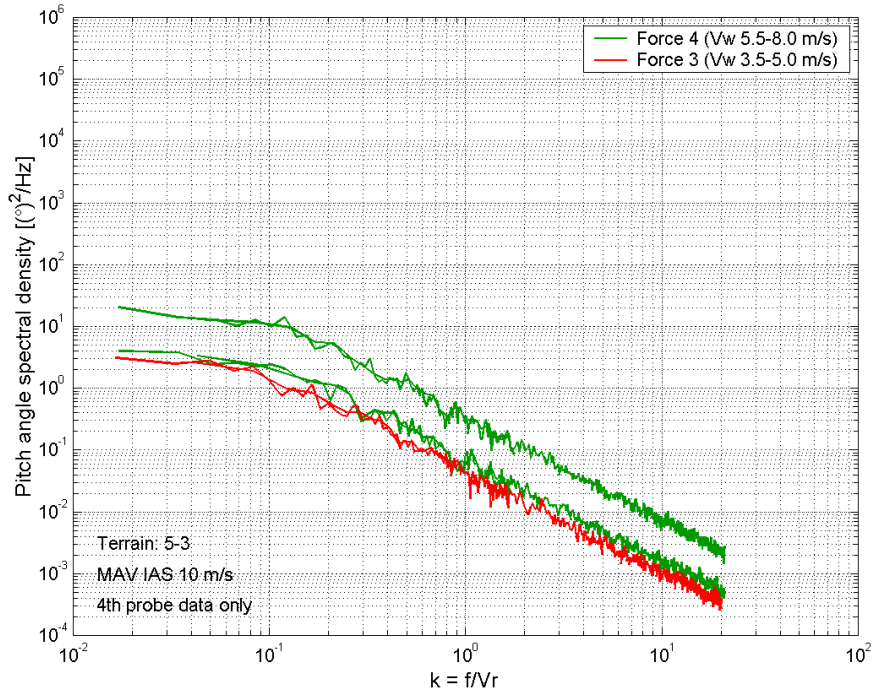

(b)

Figure 46: Atmospheric pitch angle spectral levels, different wind conditions, terrain 5-3: (a) ambient wind only; (b) MAV IAS of 10 m/s.

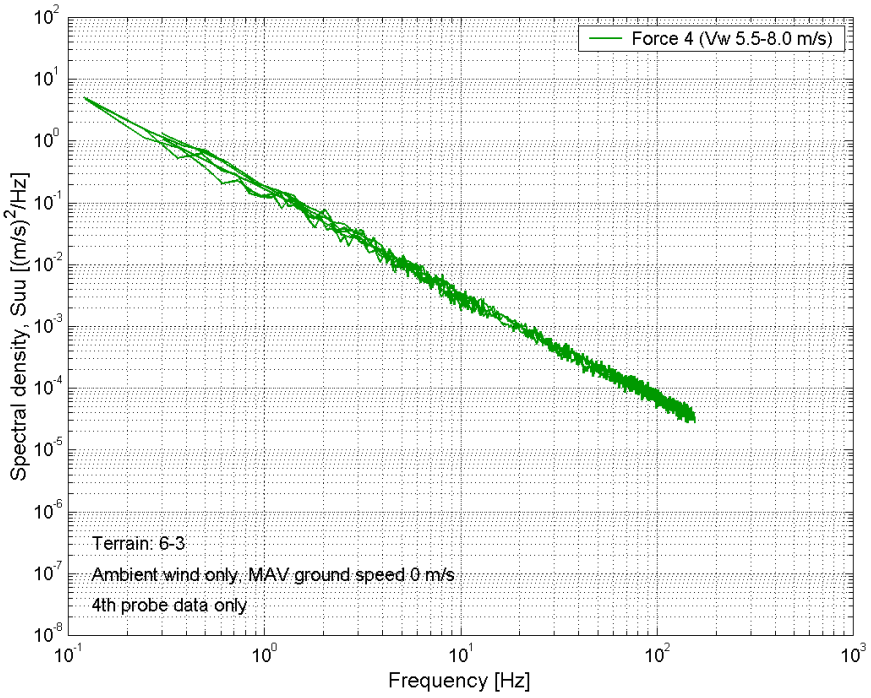

(a)

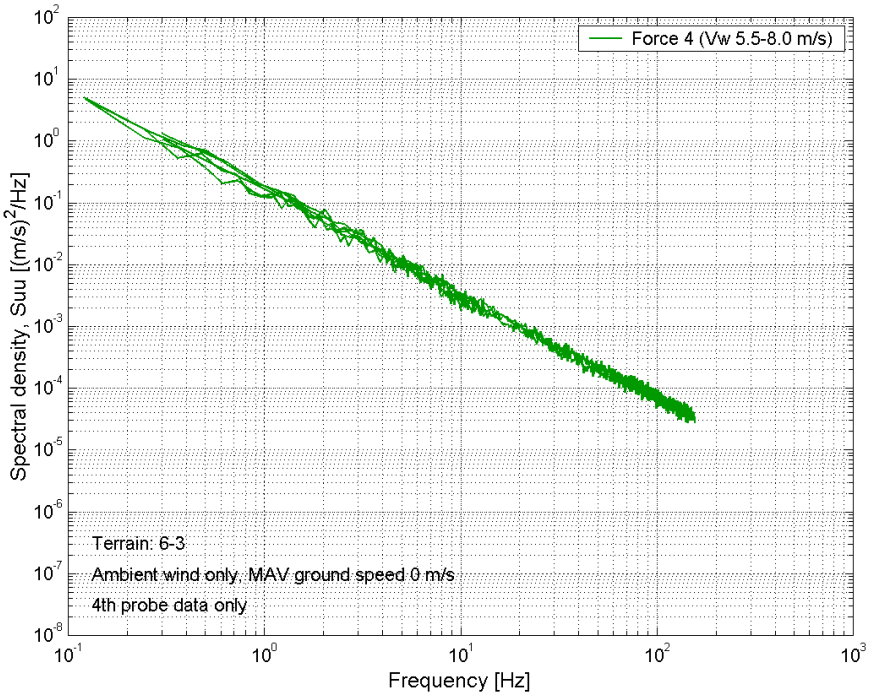

(b)

Figure 47: Atmospheric u-component spectral levels, different wind conditions, terrain 6-3: (a) ambient wind only; (b) MAV IAS of 10 m/s.

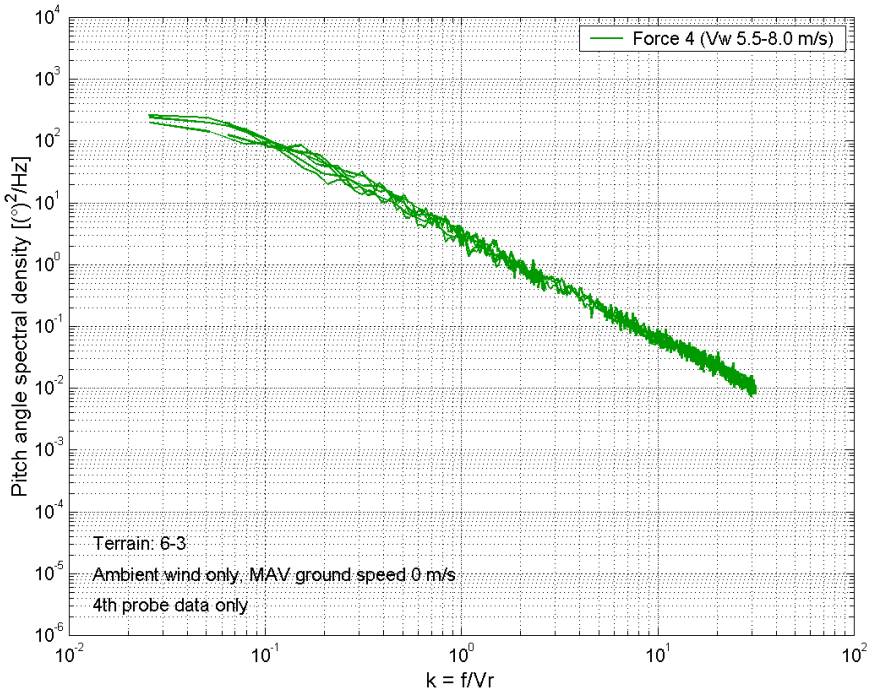

(a)

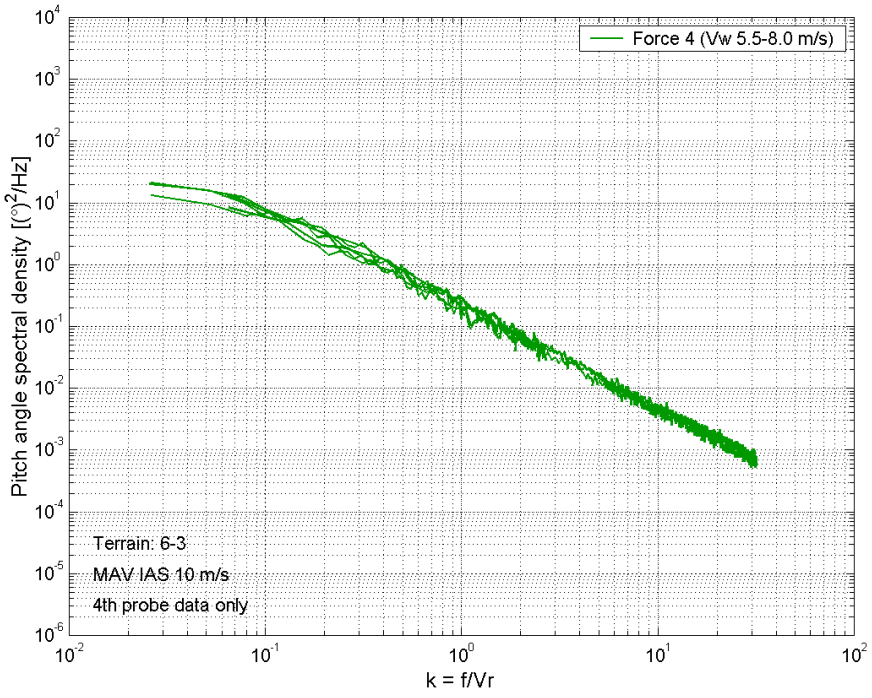

(b)

Figure 48: Atmospheric pitch angle spectral levels, different wind conditions, terrain 6-3: (a) ambient wind only; (b) MAV IAS of 10 m/s.

14 Appendix D: Tunnel Configurations

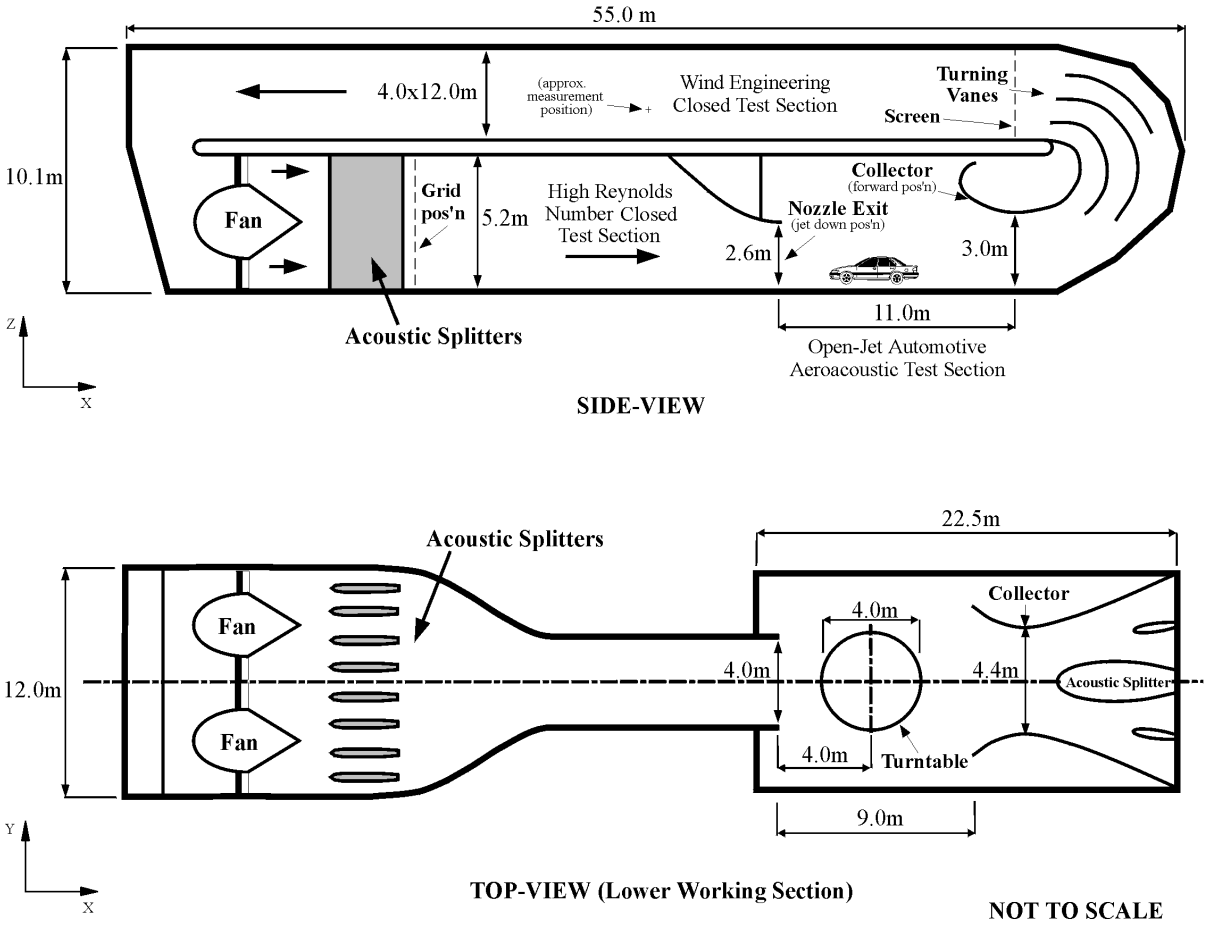

Figure 49: Schematic of the Monash wind tunnel, showing the standard automotive configuration: jet down and collector forward.

(a) (b)

Figure 50: Photos showing changes in jet configuration, downstream of the fans, before the automotive test section: (a) jet down, standard automotive configuration; (b) jet up, wind engineering configuration.

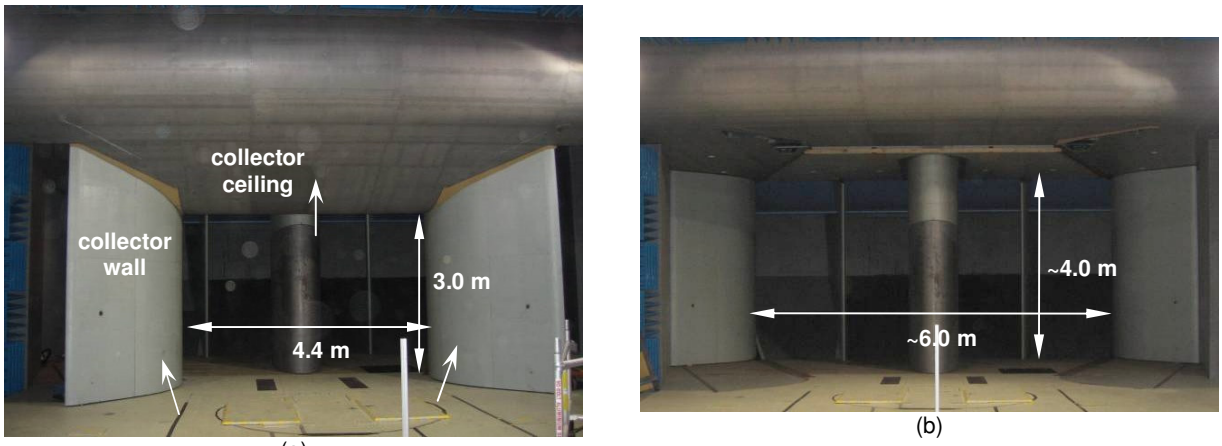

(a) (b)

Figure 51: Photos showing changes in collector configuration in the automotive test section: (a) collector forward, standard automotive configuration; (b) collector back, wind engineering configuration.

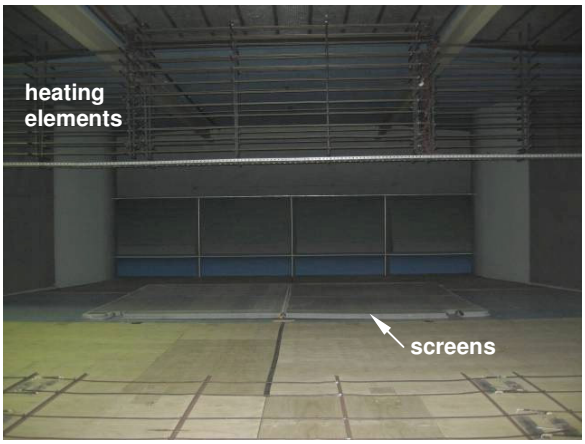

Figure 52: Entrance to the wind engineering test section (12m x 4m) showing the screens down (lying on the floor), and the in-situ heating elements (not used for this testing).

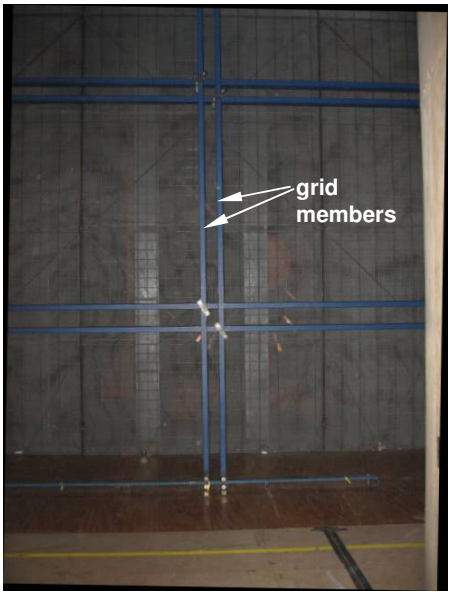

Figure 53: Grid installed just downstream of the fans (12m x 5m tunnel section) for the mounting of turbulence panels (the acoustic splitters can just be seen behind the safety screen).

(a) (b)

Figure 54: Grid installed with turbulence panels in the 12m x 5m tunnel section, just downstream of the fans: (a) 300 mm panels; (b) 600 mm panels.

15 Appendix E: Wind Tunnel Results

Table 7: Turbulence intensities and length scales in the wind engineering test section, for various tunnel configurations and a tunnel flow speed of ~10 m/s (4th probe data only).

Tunnel configurations	I_u (%)	I_v (%)	I_w (%)	L_x (m)	L_y (m)	L_z (m)
1. Baseline (8.5 m/s)	25.9	22.1	20.3	1.73	0.64	0.62
2. Baseline, with screen (9.5 m/s)	6.6	6.2	5.7	0.87	0.48	0.40
3. Effect of jet position (jet up) (10.3 m/s)	13.8	12.0	10.3	1.69	0.62	0.41
4. Effect of jet position, with screen (jet up) (10.4 m/s)	5.3	4.9	4.4	0.78	0.39	0.27
5. Effect of collector position (10.5 m/s) (jet up, collector back)	7.9	6.8	6.0	1.13	0.59	0.28
6. Effect of collector position, with screen (10.2 m/s) (jet up, collector back)	4.6	4.0	3.7	0.58	0.32	0.26
7. Effect of panel presence, 300 mm (10.2 m/s) (jet up, collector back)	8.4	7.3	6.3	1.46	0.65	0.31
8. Effect of panel presence, 600 mm (10.1 m/s) (jet up, collector back)	8.8	7.4	6.5	1.11	0.65	0.30
9. Effect of panel presence, 600 mm, with screen (10.0 m/s) (jet up, collector back)	5.2	4.3	3.9	0.72	0.37	0.26

Figure 55 shows an example of the relative levels of u, v and w components for a particular tunnel configuration. As these relative levels were similar for all cases, for reasons of clarity the remaining plots only show the u-component spectra.

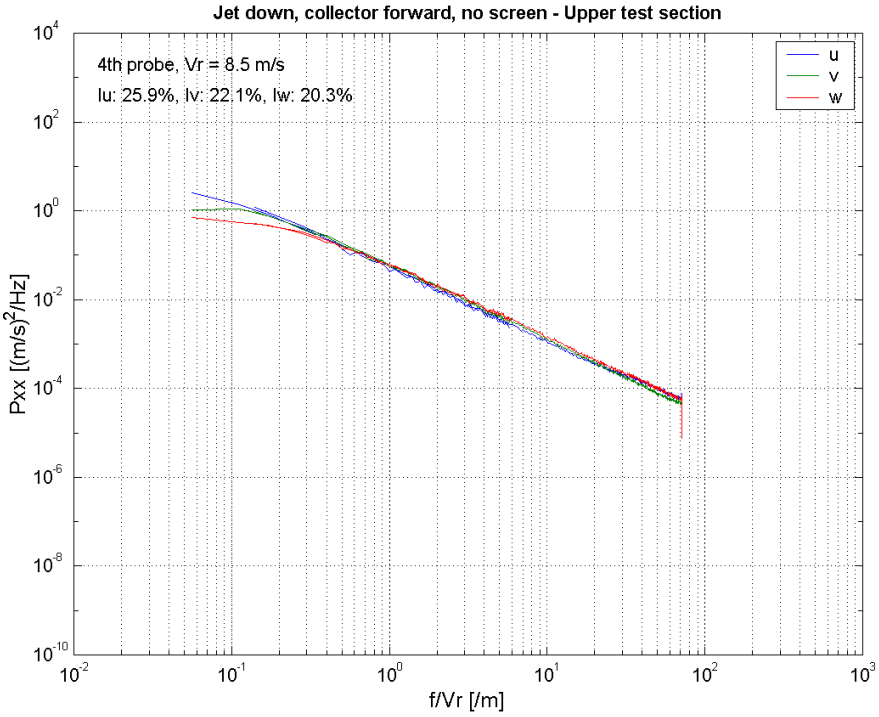

Figure 55: Absolute spectral levels in the upstairs test section for the baseline configuration (1), jet down, collector forward, no screen (5 minute sample).

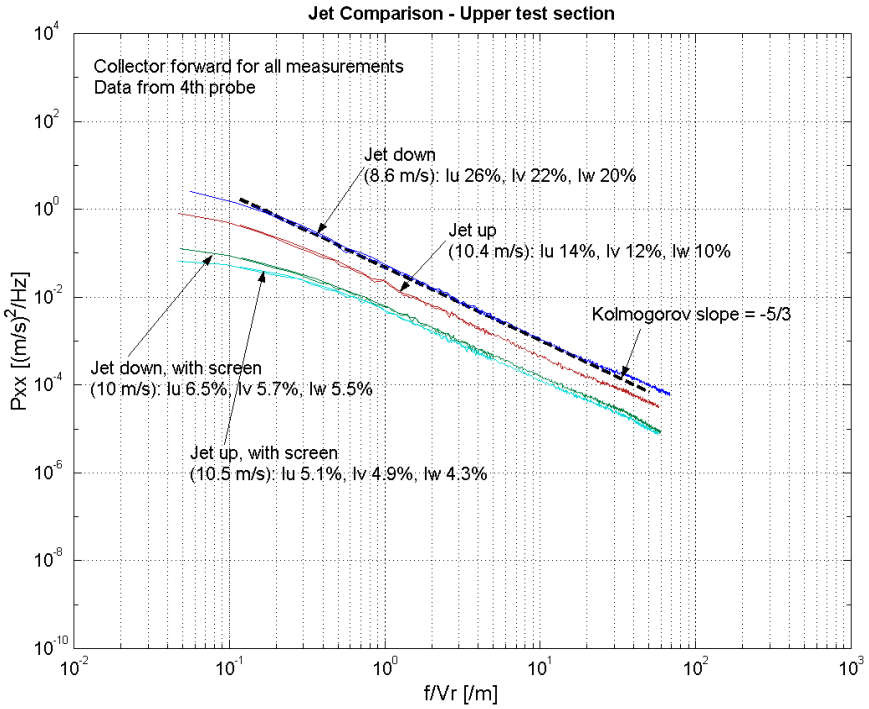

Figure 56: Absolute spectral levels in the wind engineering test section showing the effect of jet position, with and without a screen in the test section, configurations 1, 2, 3 & 4, (5 minute samples).

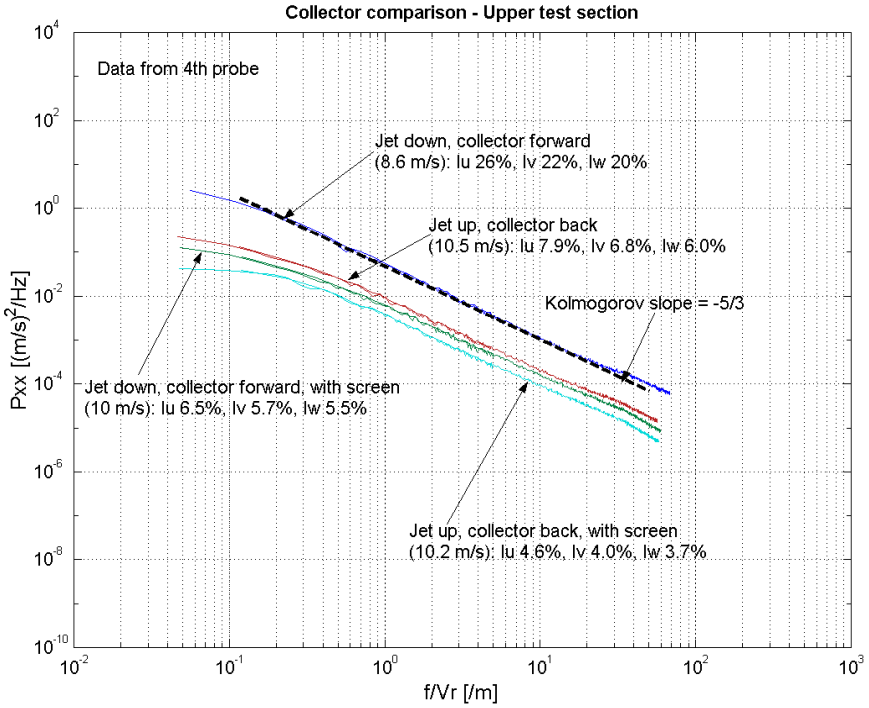

Figure 57: Absolute spectral levels in the wind engineering test section showing the effect of collector position, with and without a screen in the test section, configurations 1, 2, 5 & 6, (5 minute samples).

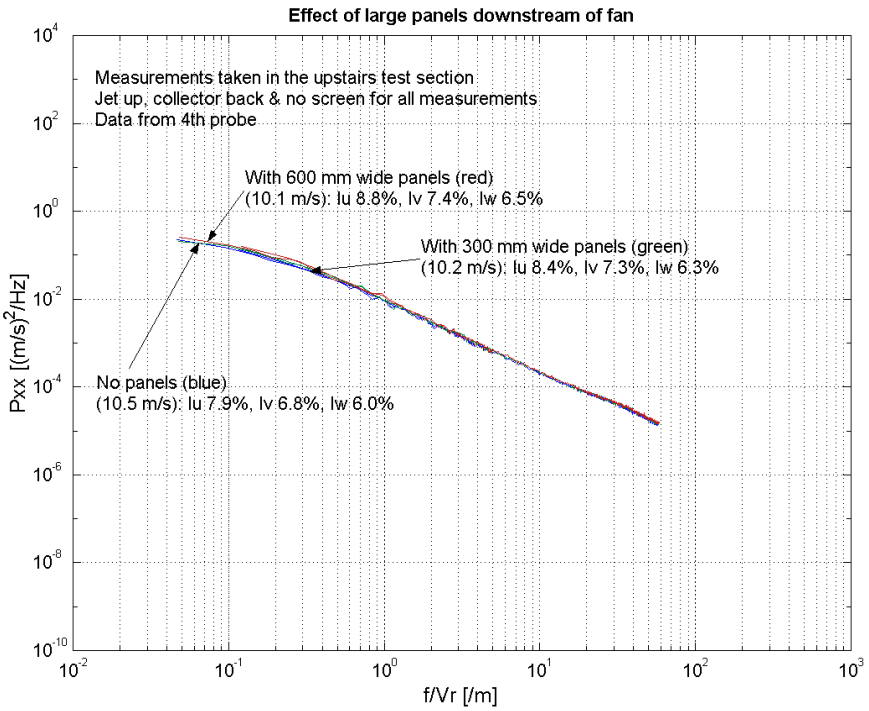

Figure 58: Absolute spectral levels for the wind engineering test section with large panels added downstream of the fans, configurations 5, 7 & 8, (5 minute samples).

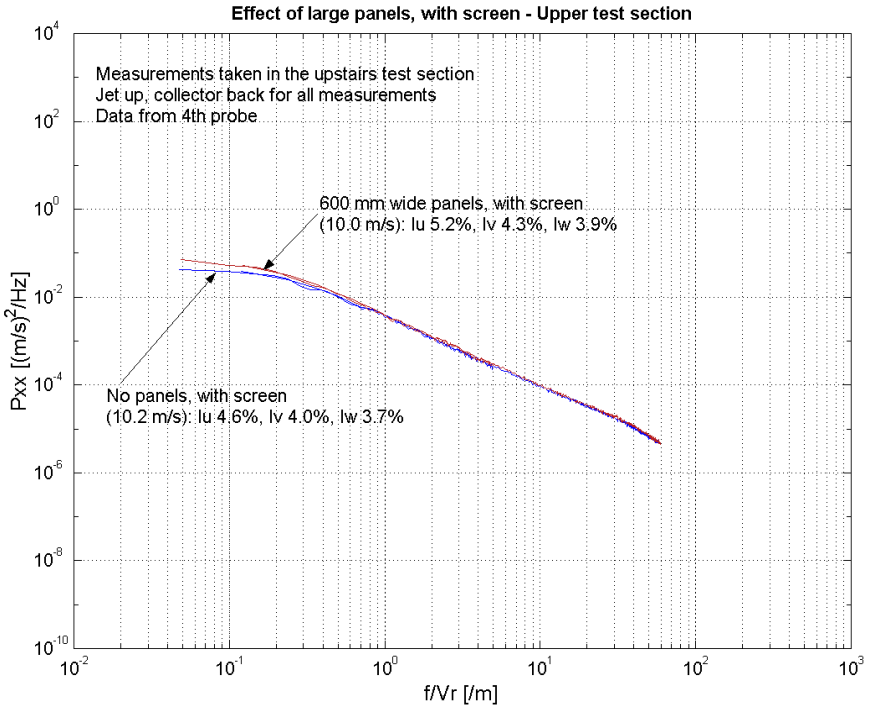

Figure 59: Absolute spectral levels for the wind engineering test section with screen, and large panels downstream of the fans, configurations 6 & 9 (5 minute samples).

16 Appendix F: Comparison Between Atmospheric & Wind Tunnel Results

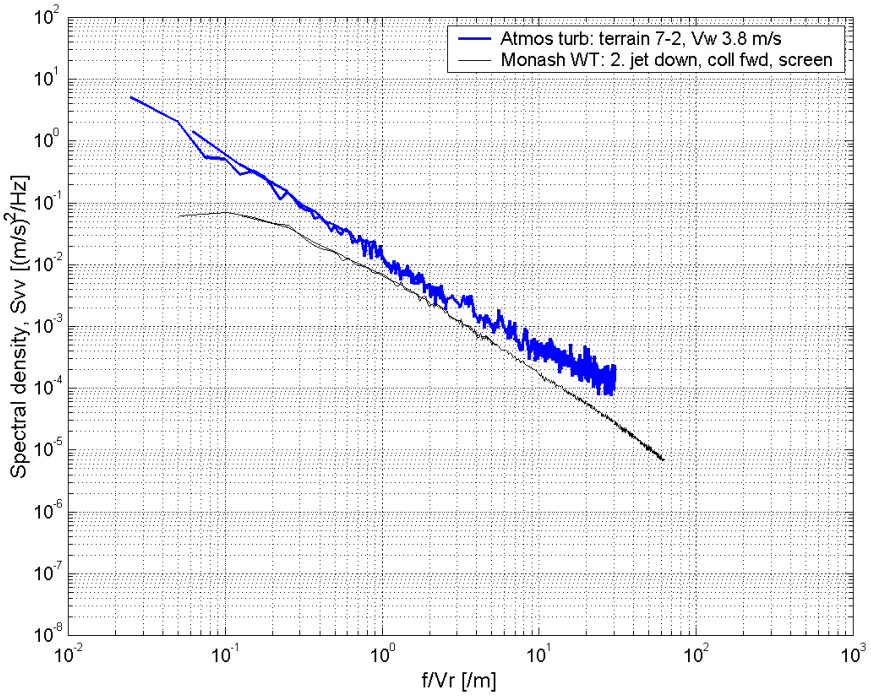

Figure 60: Comparison of v-component spectral levels in a gentle breeze: metropolitan area, terrain 7-2.

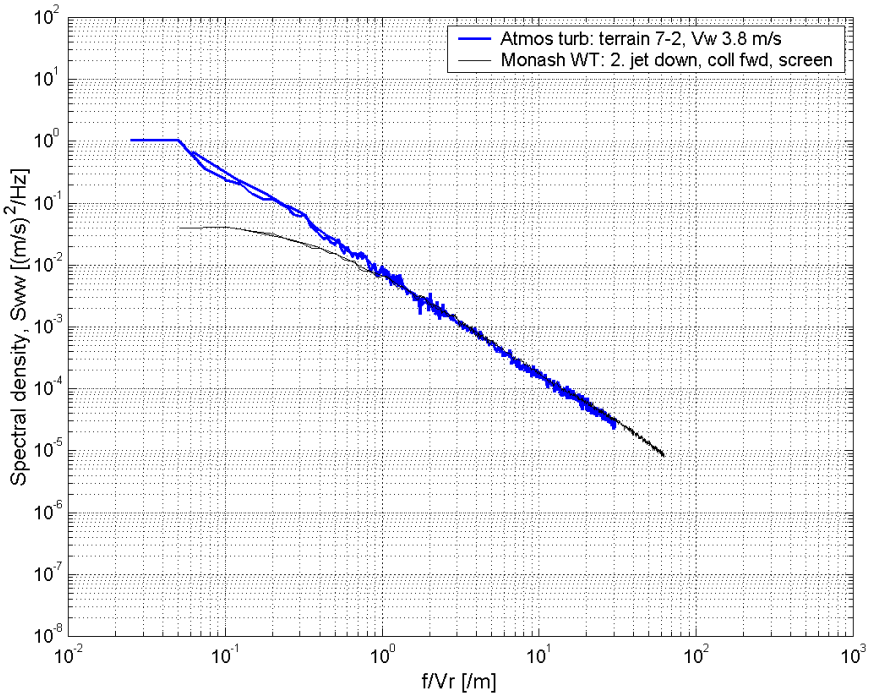

Figure 61: Comparison of w-component spectral levels in a gentle breeze: metropolitan area, terrain 7-2.

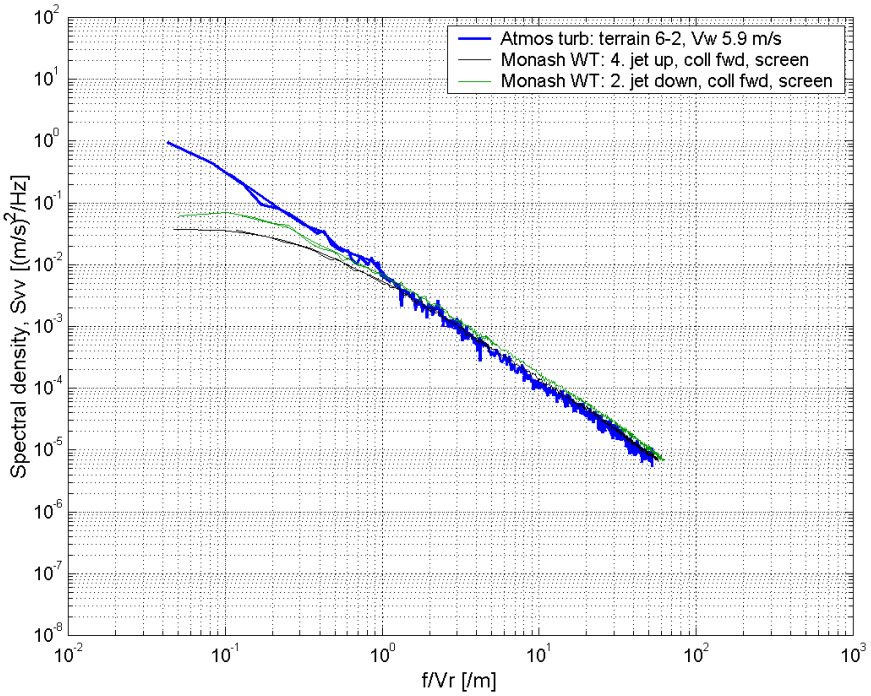

Figure 62: Comparison of v-component spectral levels in a moderate breeze: low suburbs, terrain 6-2.

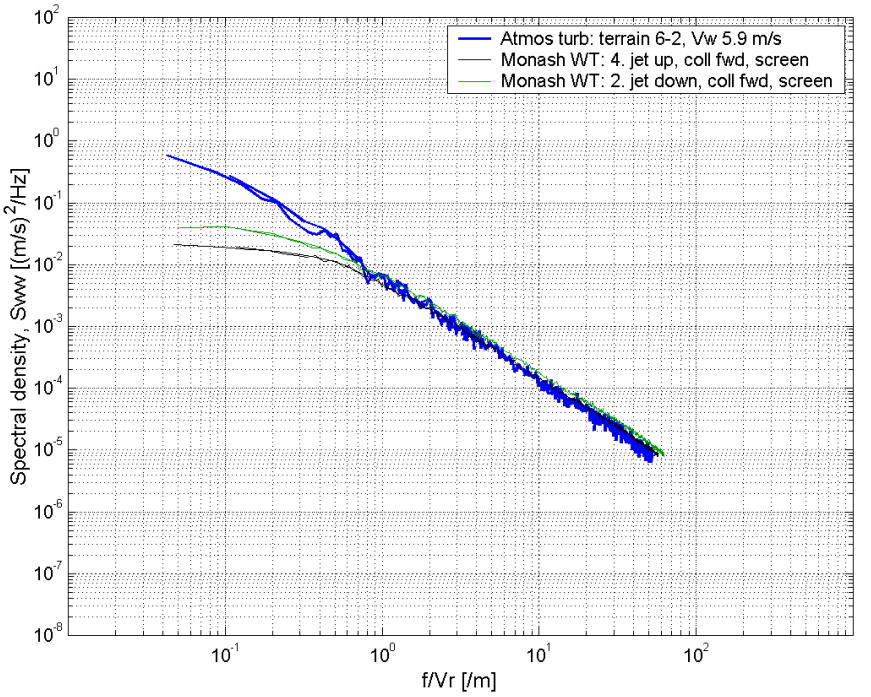

Figure 63: Comparison of w-component spectral levels in a moderate breeze: low suburbs, terrain 6-2.

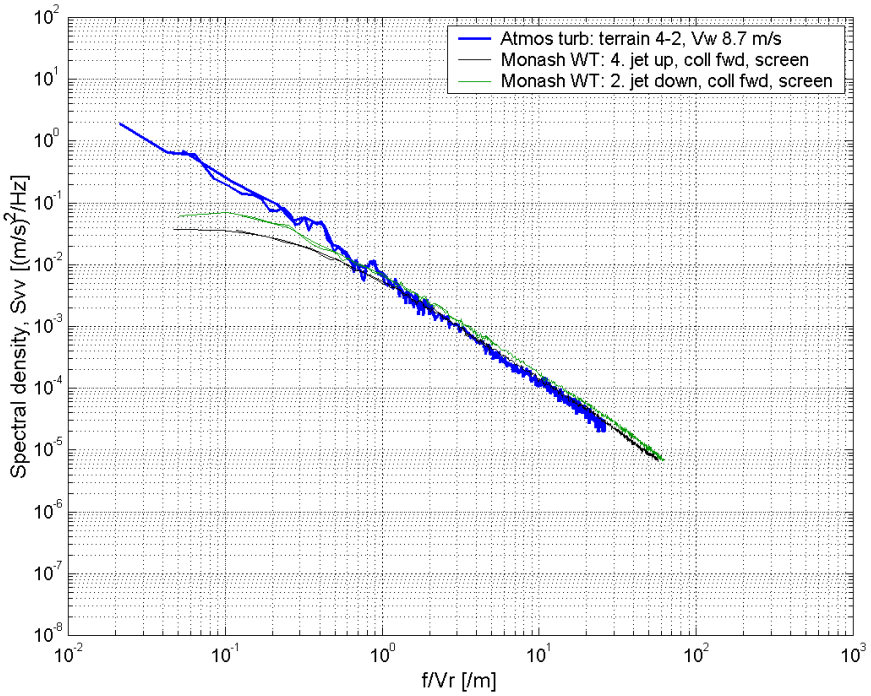

Figure 64: Comparison of v-component spectral levels in a fresh breeze: open farmland, terrain 4-2.

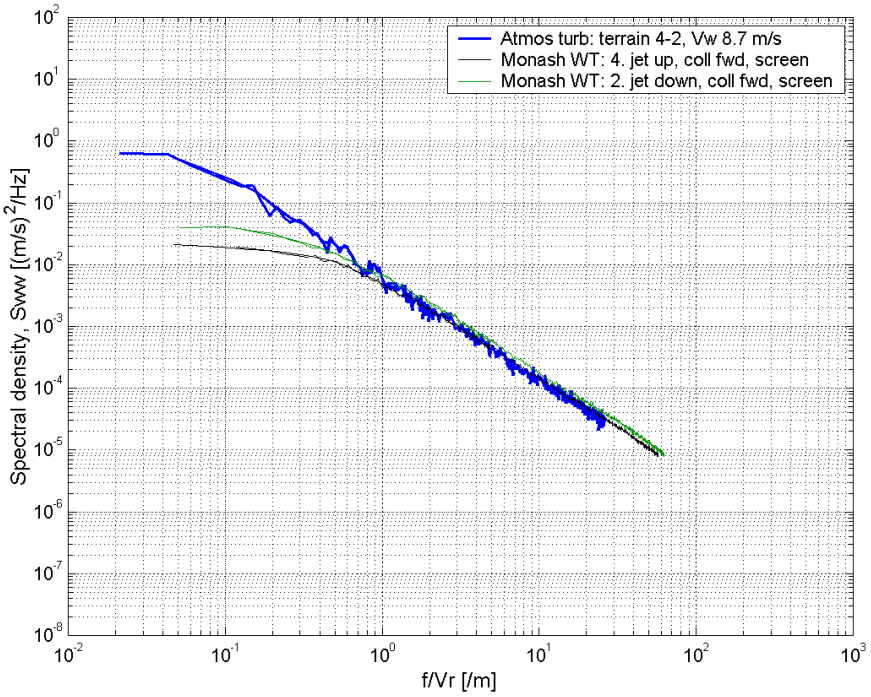

Figure 65: Comparison of w-component spectral levels in a fresh breeze: open farmland, terrain 4-2.